Rapid screening and detection of inter-type viral recombinants using phylo- k -mers

Guillaume E. Scholz, Benjamin Linard, Nikolai Romashchenko, Eric Rivals, Fabio Pardi

Phylogenetics

Rapid screening and detection of inter-type viral recombinants using phylo-k-mers

Guillaume E. Scholz [1,*], Benjamin Linard [1,2], Nikolai Romashchenko [1], Eric Rivals [1] and Fabio Pardi [1,*]

[1] LIRMM, University of Montpellier, CNRS, Montpellier, France and
[2] SPYGEN, 17 Rue du Lac Saint-André, 73370 Le Bourget-du-Lac, France.

* To whom correspondence should be addressed.

Abstract

Motivation: Novel recombinant viruses may have important medical and evolutionary significance, as they sometimes display new traits not present in the parental strains. This is particularly concerning when the new viruses combine fragments coming from phylogenetically-distinct viral types. Here, we consider the task of screening large collections of sequences for such novel recombinants. A number of methods already exist for this task. However, these methods rely on complex models and heavy computations that are not always practical for a quick scan of a large number of sequences.
Results: We have developed SHERPAS, a new program to detect novel recombinants and provide a first estimate of their parental composition. Our approach is based on the precomputation of a large database of "phylogenetically-informed k-mers", an idea recently introduced in the context of phylogenetic placement in metagenomics. Our experiments show that SHERPAS is hundreds to thousands of times faster than existing software, and enables the analysis of thousands of whole genomes, or long sequencing reads, within minutes or seconds, and with limited loss of accuracy.
Availability and Implementation: The source code is freely available for download at https://github.com/phylo42/sherpas
Contact: pardi@lirmm.fr, gllm.scholz@gmail.com
Supplementary information: Supplementary Materials are available online.

1 Introduction

A fundamental task in viral bioinformatics is to recognize when a newly sequenced virus genome or genome fragment is a recombinant —that is, it carries regions from two or more genetically distinct parental strains. Detecting novel recombinant forms has important biological and medical implications, as the new recombinants are sometimes associated with drug resistance (Moutouh *et al.*, 1996), increased virulence (Liu *et al.*, 2002; Suarez *et al.*, 2004), the ability to infect new hosts (Kuiken *et al.*, 2006) or to evade the host's immune system (Streeck *et al.*, 2008). Moreover, for many viral species, recombination is common: for example in HIV the rate of within-host recombination appears to be at least as high as that of point mutations (Neher and Leitner, 2010; Batorsky *et al.*, 2011). Interestingly, a number of artefacts (e.g. caused by PCR amplification or sequence assembly errors) can also result in recombinant sequences, which however never really existed in vivo (Martin *et al.*, 2011; Pérez-Losada *et al.*, 2015). Detecting such artificial recombinants is also important prior to any further sequence analysis.

A virus species is often subdivided into phylogenetically-distinct strains, sometimes called *groups*, *types* or *subtypes* (the nomenclature varies depending on the virus), representing the diversity of the genomes from that virus. For example, HIV-1 is divided into 4 groups (M, N, O and P) and the M group, responsible for the HIV pandemic, is further classified into at least 9 subtypes (A, B, C, D, F, G, H, J, K), some of which have sub-subtypes (Foley *et al.*, 2018). Here, we use the word *strain* to designate any subset of interest for the virus under consideration. Different strains are sometimes associated to important differences, for example in resistance to antiviral drugs (Wainberg and Brenner, 2010) or in disease progression (Kiguoya *et al.*, 2017).

In this paper, we focus on the computational task of recognizing novel recombinants composed of genomic regions coming from different strains (for example from different subtypes in the case of HIV-1). Given a collection of query sequences, we wish to identify inter-strain recombinants, and for each putative recombinant: (1) recognize which strains originated it; (2) partition it into the regions coming from different strains. Fig. 1 shows an example of the type of information that we intend to recover from a query.

A number of tools can already be used precisely for this task. For example, jpHMM (Schultz *et al.*, 2006, 2009) —which partitions each query by "jumping" between profile HMMs constructed for the different strains—, SCUEAL (Kosakovsky Pond *et al.*, 2009) —a likelihood-based genetic algorithm— and the REGA subtyping tool (de Oliveira *et al.*, 2005) —which implements a sliding-window-based phylogenetic bootstrap analysis (bootscanning) for HIV-1. All these approaches use a reference alignment containing several representative sequences from each strain. They either need to align the queries to the reference alignment prior to the analysis (SCUEAL and REGA) or they implicitly construct an alignment during their execution (jpHMM). Sometimes the query alignment phase is followed

by a phylogenetic analysis step (SCUEAL and REGA), which may have to be repeated over many different portions of the alignment. Because of the complexity of the computations involved, the execution of these tools may become tricky when the datasets to analyse contain more than a few thousands queries.

Because rapidly evolving sequencing technologies enable researchers and clinicians to routinely produce increasingly large sequence datasets —potentially containing millions of viral reads— we have developed a fast alignment-free method to detect inter-strain recombinants within large collections of queries, based on the use of phylo-k-mers (Linard *et al.*, 2019) (see Sec. 2.2). The new tool, called SHERPAS (*Screening Historical Events of Recombination in a Phylogeny via Ancestral Sequences*) is able to process thousands of long queries (potentially covering whole viral genomes) within minutes or seconds. It can be used as a tool to screen large sequence datasets for novel recombinants. If necessary, the putative recombinants found by SHERPAS can be subsequently re-analysed with more precise methods such as REGA, SCUEAL or jpHMM.

Beside being orders of magnitude faster than available tools for the discovery of novel recombinants, SHERPAS presents other points of interest. Unlike some popular web interfaces, the code of SHERPAS is distributed freely, which may be an advantage when, for privacy reasons, it is important to process the data in-house (e.g. in a clinical setting). This also makes SHERPAS very flexible: users can choose their own reference alignments, update them as new high-quality sequences become available, and most importantly adapt SHERPAS to any virus for which a reference alignment of sufficient quality can be obtained. Moreover, SHERPAS appears to be relatively robust to the high error rates that characterize Oxford Nanopore sequencers. For these reasons we believe that SHERPAS is appropriate for recombination detection even in the most challenging scenarios, such as in-situ outbreak monitoring, where computational resources and network accessibility may be limited (Quick *et al.*, 2016).

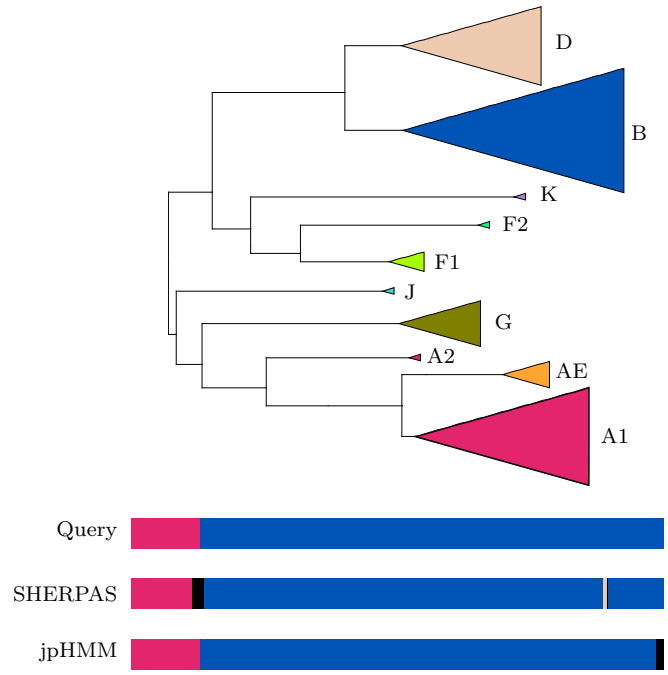

Fig. 1. Illustration of the task of inter-strain recombination detection. Top: Example of what strains may look like in a realistic phylogeny (adapted from part of the reference tree for the HIV-pol dataset). Bottom: Illustration of the composition of a query and of the outputs of two programs. The query combines a small segment of a sequence annotated as A1, and a larger segment of a sequence annotated as B. (Neither of these two sequences were part of the reference alignment used to construct the reference tree.) SHERPAS and jpHMM (both run with default parameters) return the partitions represented by the other two bars. Black segments represent unassigned regions.

2 Algorithm

2.1 Preprocessing and overview

At a preprocessing stage, SHERPAS needs a collection of aligned reference sequences for the virus of interest and a phylogenetic tree built from this alignment. Each reference sequence must be annotated as belonging to exactly one strain, via a .csv file. In the Suppl. Materials (Sec. 3), we discuss a number of properties that we would ideally expect the references (alignment, tree and strains) to satisfy, such as the monophyly of strains and the absence of widespread recombination within the reference alignment. From the reference alignment and tree, a database of phylo-k-mers (the *pkDB*) is then constructed using the pkDB construction step currently implemented in the RAPPAS software (Linard *et al.*, 2019) (see next section). The pkDB construction is a heavy computational step, but it only needs to be executed when a new reference alignment is employed, or when it is updated.

Once these preprocessing steps have been carried out, large datasets of unaligned DNA sequences can be analyzed with the pkDB, as they become available. These sequences —which we refer to as *queries*— can be genomic fragments of moderate size (a few hundreds bp at least) up to entire genomes, including error-prone long reads generated by third-generation sequencing technologies.

The output of SHERPAS is a text file classifying continuous regions within the queries as either unassigned ("N/A") or as belonging to one of the strains. The same format used by jpHMM is adopted.

2.2 The phylo-k-mers

Informally, phylo-k-mers can be described as phylogenetically-informed k-mers (subsequences of length k) that are present with non-negligible probability in unknown/unsampled relatives of the sequences contained in the reference alignment (Linard *et al.*, 2019). Importantly, phylo-k-mers are *inferred* from the reference data (alignment and tree), but not necessarily observed in any of the reference sequences. Typical values for k are currently in the range from 8 to 10. While a detailed mathematical treatment is deferred to the Suppl. Materials (Sec. 1), here we provide an overview.

The inference of phylo-k-mers relies on standard techniques that can calculate the posterior probability of the nucleotide state at (i) any site defined by a column of the reference alignment, and at (ii) any node with a well-defined location with respect to the reference tree. While in traditional applications, such as ancestral sequence reconstruction, the focus is on the internal nodes of the tree, here we are interested in the probabilities at new nodes that are added to the reference tree. These nodes, called *ghost nodes*, represent sequences that have diverged from a given branch, and lie at pre-defined distances from their branch of origin.

Posterior probability calculations are implemented in many programs for likelihood-based phylogenetics (e.g. Guindon and Gascuel (2003); Kozlov *et al.* (2019)), one of which is executed automatically at launch of the phylo-k-mer construction step. For each ghost node u, this step produces a table containing the posterior distribution of the nucleotide at u, at any site of the reference alignment.

The probability of a k-mer w, at a specific ghost node u and at a specific set of k consecutive sites, is then obtained as the product of the posterior probabilities of its constituent nucleotides at their respective sites, in the table for node u. This simple calculation relies on the

assumption of statistical independence among sites, which is standard in phylogenetics (e.g. Felsenstein (2004); Yang (2006)).

A k-mer w is called a *phylo-k-mer* for branch x of the reference tree, if there exists at least one position in the reference alignment and one ghost node associated to x, where the probability of w exceeds a given threshold (controlled by a parameter of the phylo-k-mer construction process). When multiple such positions and ghost nodes exist for a given pair (w, x), the highest probability is the *probability score* of k-mer w at branch x. A k-mer's probability score at x can be interpreted as a measure of how likely x is to be the k-mer's "phylogenetic origin" —that is, the branch from which the k-mer diverged from the rest of the reference tree.

Finally, note that a k-mer w can be a phylo-k-mer for several branches, although with potentially very different probability scores. All such information is stored in the pkDB, which is a look-up table allowing, for a given phylo-k-mer w, the rapid retrieval of all branches and probability scores associated to w.

2.3 Full and reduced pkDBs

Prior to applying the algorithm for recombination detection, outlined below, each branch of the reference tree is assigned at most one strain from the user-specified set of strains, in the following way: Recall that each reference sequence belongs to exactly one of these strains. If all the sequences that descend from a branch belong to the same strain, then this branch gets assigned a label corresponding to that strain, otherwise the branch remains unassigned. Moreover, we call a branch x a *root branch* of strain X if (1) x is assigned to X, and (2) no branch ancestral to x is assigned to X. Note that if a strain X is monophyletic (which we expect to be usually the case), then X has exactly one root branch, the one lying at the root of the clade containing all sequences in X.

From there, two distinct versions of the pkDB can be constructed. The *full* pkDB is the one constructed by the phylo-k-mer inference step currently implemented in RAPPAS, without modification. The *reduced* pkDB is constructed by SHERPAS from the full pkDB, by only keeping the information relative to the branches that are root branches of some strain X. See the Suppl. Materials (Sec. 1.5) for more details. We call SHERPAS-full and SHERPAS-reduced the two variants of SHERPAS using the full pkDB (default) and the reduced pkDB, respectively.

2.4 The sliding window approach

The recombination detection phase in SHERPAS adopts a sliding window approach. Here, a *window* is defined as a contiguous subsequence of the query of a given length. For each window, instead of performing complex phylogenetic analyses, SHERPAS only looks for matches between the k-mers contained in the window and the selected pkDB (full or reduced), and dynamically updates a table of scores associated to the branches encountered in this process. We refer to the Suppl. Materials (Sec. 2) for a detailed description and analysis of the algorithm, and provide the main ideas below.

For each window, the score assigned to a branch is computed using the same weighted vote approach as in RAPPAS's placement algorithm (Linard *et al.*, 2019). This score is a function of the probability scores at that branch, of the k-mers in the window. The scores for the first (leftmost) window are used to initialize a table of scores. For each subsequent window, the table of scores is updated efficiently on the basis of the k-mers that are added to it, and those that are removed from it. The number of k-mers that are added to the new window does not need to coincide with the number of k-mers that are removed from it. This is used to improve the behavior of SHERPAS at the ends of the query: while the leftmost and the rightmost window are relatively small (100 k-mers by default), the window gradually grows as it gets further from the ends of the query, until it reaches its maximum size (300 k-mers by default). By default, the coordinates of two consecutive windows of maximum size only differ by 1 bp.

SHERPAS is also able to process circular queries, which may arise for viruses with circular genomes. In this case, the variable-size approach described above is not executed. Instead, the sliding window retains the same size everywhere. When the sliding window reaches the end of the query, it will extend to the other end of the query, until the sliding window is back to the leftmost window in the query.

Assuming that the signal for classification is strong enough (see the next section for details), the midpoint in each window is classified into the strain that is associated to the highest-scoring branch for the window. This allows SHERPAS to partition the query into segments, each one associated with a strain identified as its origin.

2.5 Signal evaluation and unassigned regions

SHERPAS may leave some parts of a query unassigned, whenever the evidence for the classification into any particular strain is deemed to be too weak. In order to evaluate this, SHERPAS converts the score of a branch into a likelihood score (details of this conversion are provided in the Suppl. Materials, Sec. 2.4). The way this is used depends on the version of the pkDB (full/reduced).

In its full version, the pkDB contains all the branches of the reference phylogeny, including some branches that are not assigned to any strain. If the best scoring branch in a window is one of these unassigned branches, then SHERPAS classifies the window midpoint as unassigned (or "N/A"). If instead the best and second-best scoring branch belong to the same strain, SHERPAS classifies the midpoint in that strain. In all remaining cases, SHERPAS computes the ratio ℓ_1/ℓ_2, where ℓ_1 and ℓ_2 are the likelihoods for the best and second-best branch, respectively. If that ratio is smaller than a user-defined parameter θ_{F}, SHERPAS classifies the window midpoint as unassigned, otherwise it classifies it in the strain of the best scoring branch.

In the reduced version, all branches recorded in the pkDB belong to some strain (usually just one branch per strain). In that case, SHERPAS computes the ratio $\ell_1 / \sum_{i=1}^{N} \ell_i$, where ℓ_1 is the likelihood for the best scoring branch/strain and ℓ_i, $i = 2, \ldots, N$ are the likelihoods of all other branches/strains in the pkDB. Again, if that ratio is smaller than a user-defined parameter $\theta_{\mathrm{R}} \in [0, 1)$, SHERPAS returns the window midpoint as unassigned (or "N/A").

In both SHERPAS-full and SHERPAS-reduced, setting the control parameter θ_F (or θ_R) to a small value is expected to result in a liberal classification, potentially resulting in false positive breakpoints, while setting it to a high value corresponds to a more conservative classification, potentially missing some evidence of recombination. A last optional step that is applied by SHERPAS is the removal of N/A stretches between two segments classified in the same strain (by default, these regions are classified as belonging to that strain).

An interesting observation is that, since by default two consecutive windows only differ by two k-mers, it is very unlikely that their midpoints are both confidently assigned to different strains. Because of this, two genomic regions classified into different strains X and Y are usually separated by a N/A fragment, which can be interpreted as expressing uncertainty about the precise location of the breakpoint between X and Y. In other words, we expect the breakpoint X/Y to lie somewhere within this N/A fragment.

3 Materials and methods

3.1 Experimental protocol overview

Dataset construction. We evaluated the performance of SHERPAS on four datasets of synthetic recombinants, that is, query sequences that are constructed by concatenating fragments of real-world viral sequences. The first three datasets were obtained following the same general procedure: Each dataset is constructed from a different pair of alignments containing real-world sequences reliably annotated as belonging to known strains of a virus of interest (details in Sec. 3.3 to 3.5). One of these alignments is used as the reference alignment for SHERPAS. The sequences in the other alignment are called *pre-queries*. We ensure the two alignments contain no sequence in common. The pre-queries are used to build a large collection of queries by (1) drawing random recombination breakpoints in the alignment containing the pre-queries, (2) cutting the pre-queries at those breakpoints and (3) concatenating the resulting fragments. The fourth dataset was obtained by simulating long-read sequencing errors over the queries of one of the other datasets (Sec. 3.6). For each of the queries, we record the positions of the breakpoints, and the strain of origin of the fragments that are separated by those breakpoints. This recorded information is used as "ground truth" to evaluate the accuracy of the tested methods (see Sec. 3.2).

Software comparison. We compare the performance (accuracy and running times) of SHERPAS over these datasets against that of jpHMM (Schultz *et al.*, 2006, 2009), a natural choice because (1) it is the only tool whose main stated goal is the same as that of SHERPAS (detect *inter*-strain recombinants and partition them according to the strain of origin). Moreover, (2) jpHMM is not specialized for any single virus species, and is distributed with its own reference alignments for a number of viruses, which allows us to compare it to SHERPAS using the same reference alignments. Note that using the same reference alignment (essentially a training set) puts two tools on an equal ground for benchmarking purposes, allowing us to evaluate the relative merits of the algorithms alone —and exclude the influence of the reference data, which is potentially crucial (Pineda-Peña *et al.*, 2013). Also note that, when run with the `-Q blat` option to speed up its execution, jpHMM appears to be at least as fast as SCUEAL and REGA (Pineda-Peña *et al.*, 2013), thus providing a good comparison for running times. Those alternatives to jpHMM were excluded for the following reasons: SCUEAL (Kosakovsky Pond *et al.*, 2009) is specialized for the detection of HIV-1 recombinants, including *intra*-subtype recombinants, and is only distributed with a single reference alignment (for the *pol* gene). The REGA tool (de Oliveira *et al.*, 2005) has only been developed for HIV-1, and does not give access to its code. Since it cannot be run on a local machine, it is not possible to perform fair running-time comparisons with it. All these exclusion criteria also apply to COMET (Struck *et al.*, 2014), a web-based subtyping tool for HIV-1, whose main goal is not recombination analysis.

3.2 Measures of accuracy

To measure the accuracy of SHERPAS and of the other methods, we used two approaches: a site-wise and a mosaic approach.

Site-wise approach. Since the composition of synthetic recombinant queries is known, we can see such composition as a site-wise assignment. It is then possible to compare the assignment of a site by a recombination-detection software with the correct assignment of that site. We use two different measures of the accuracy of a software: we compute the proportion of sites that are assigned to the correct strain, either out of all sites —the **site-wise sensitivity**— or out of all sites that are not assigned to N/A —the **site-wise precision**. We note that this is a slight abuse of vocabulary, as in multi-class classification, precision and sensitivity are class-specific measures. (See the Suppl. Materials, Sec. 4 for a mathematical reconciliation between these definitions.) In the absence of N/A regions, our definitions of site-wise precision and sensitivity give the same value.

Mosaic approach. This is the same approach used by the authors of SCUEAL (Kosakovsky Pond *et al.*, 2009). Any partition of the query into strains is translated into the sequence of strains that appear in it, ignoring the position of the breakpoints and of unassigned regions, when these are present. We call such sequence of strains a *mosaic*. For example the mosaic of the query in Fig. 1 is A1, B. The mosaic of each query is compared to the mosaic reconstructed by the software on that query. Each of these reconstructed mosaics is then classified into one of the following four categories, where the word *subsequence* is defined in the standard way, not implying contiguity (Wikipedia contributors, 2019; Gusfield, 1997). **Match**: the mosaic returned by the software coincides with the correct mosaic. **Superset:** the correct mosaic is a subsequence of the mosaic returned by the software. **Subset:** the mosaic returned by the software is a subsequence of the correct mosaic. **Mismatch:** none of the above. For example, the second mosaic in Figure 1 (returned by SHERPAS) is a superset compared to the correct mosaic (note the presence of the light brown bar towards the right), whereas the third (returned by jpHMM) is a match. For circular queries, the definitions above are modified accordingly.

3.3 HIV-pol dataset

To evaluate the performances of SCUEAL, Kosakovsky Pond *et al.* (2009) generated 10,000 synthetic recombinant queries, combining fragments from 863 pre-queries from the HIV-1 *pol* gene. We used this dataset without modification. The queries are about 1.6 kbp long.

To run SHERPAS on these queries, we built the pkDB using the same reference alignment as SCUEAL. This alignment contains 167 HIV *pol* sequences distributed into 17 strains, which correspond to groups, types, subtypes, chimpanzee SIV sequences, and the circulating recombinant form CRF01_AE. These strains are named A, A1, A2, A3, AE, B, C, D, F1, F2, G, H, J, K, N, O, CPZ. (The inclusion of CPZ and AE is discussed in the Suppl. Materials, Secs. 3.3 and 3.4, respectively.)

The output of SCUEAL on these queries is distributed along with the software, so we did not re-run SCUEAL on this dataset. (Also because SCUEAL is a non-deterministic algorithm.) The queries include intra-strain recombinants and SCUEAL's output includes the detection of intra-strain recombination. In order to make this information comparable to the output of SHERPAS, we ignored intra-strain recombination, and only retained inter-strain recombination information. As a consequence, the mosaic-based accuracy measures that we obtain for SCUEAL (Table 2) are much better than those reported by Kosakovsky Pond *et al.* (2009) (e.g. 93.2% matches vs. 46.6%). In order to interpret the results for jpHMM on this dataset, we note that strains A and N cannot be recognized by jpHMM, which negatively impacts its accuracy measures on this dataset. The impact, however, is limited. (See the Suppl. Materials, Sec. 5.2 for more detail.)

3.4 HBV-genome dataset

Both SHERPAS and the latest version of jpHMM are able to analyze data from viruses with circular genomes, such as the hepatitis B virus (HBV) (Schultz *et al.*, 2012). To experiment with HBV data, we used the reference alignment that is distributed with jpHMM. It contains 339 whole-genome sequences classified into strains A, B, C, D, E, F, G, H (known as *genotypes*). Prior to the construction of the pkDB for SHERPAS, we extended this reference alignment by copying the first 9 columns of the alignment to the end of the alignment. This allows

the construction of phylo-k-mers (with $k = 10$) from positions that overlap with the artificial end of the alignment.

To build a collection of queries, we started with a collection of pre-queries extracted from the database of aligned whole-genome HBV sequences available at the HBVdb website (HBVdb contributors, 2019; Hayer *et al.*, 2013). To construct a query, $2X$ recombination breakpoints are chosen at random, where $X \geq 1$ is geometrically distributed with parameter 0.8, while making sure that no two breakpoints are less than 100 bp apart (as in Kosakovsky Pond *et al.* (2009)). 2000 queries combine fragments from two pre-queries, and 1000 queries are based on three pre-queries. (See the Suppl. Materials, Sec. 5.3, for full details on this procedure.) The parameters used in this procedure were chosen so that the queries loosely reflect the characteristics of inter-genotype HBV recombinants presented in a recent overview (Araujo, 2015). The queries are about 3.2 kbp long.

3.5 HIV-genome dataset

This dataset consist of whole-genome sequences from HIV. Again, we used the reference alignment of jpHMM for HIV to build the pkDB database for SHERPAS. This alignment contains 881 whole-genome sequences, classified in the following 14 strains: A1, A2, AE, B, C, D, F1, F2, G, H, J, K, O, CPZ.

To construct a collection of 3000 synthetic queries, we used pre-queries extracted from Los Alamos HIV sequence database (the "complete Web alignment 2018"). In brief, the main difference with the procedure for the HBV-genome queries is that the number of parental pre-queries and the number of breakpoints are both drawn from (shifted) geometric distributions. Again, the construction procedure was designed to reflect the broad characteristics of known recombinant forms, those listed in the Los Alamos HIV sequence database. Full details of this procedure are described in the Suppl. Materials, Sec. 5.4. The average length of the resulting queries is 8.9 kbp.

3.6 Simulated Nanopore reads from the HIV-genome dataset

To test the robustness of SHERPAS to high error rates typical of long read sequencing technologies, we also built a dataset of reads generated with NanoSim-H, a simulator of Oxford Nanopore reads (Yang *et al.*, 2017; Břinda *et al.*, 2018). For each query in the HIV-genome dataset, we generated a single simulated read using NanoSim-H with minimum and maximum length set to 1000 and 9000, respectively, and rate of unaligned reads set to 0. All other parameters were left to their default values. A total of 3000 simulated reads, with average length about 5.9 kbp, were thus obtained. The reference alignment used for this dataset is the same as that for the HIV-genome dataset. (See the Suppl. Materials, Sec. 5.5 for details.)

3.7 Running the experiments

For each of the datasets described in Sections 3.3 to 3.6, a reference tree was constructed from the reference alignment with PhyML 3.3 (Guindon *et al.*, 2010) using GTR + Γ + I as substitution model. Alignment and tree were given as inputs to a customized version of RAPPAS that built a pkDB using parameters $k = 10$ and threshold parameter 1.5 (called "omega").

We ran SHERPAS with 8 parameters combinations: SHERPAS-reduced for $\theta_R \in \{0.90, 0.99\}$ and window size in $\{300, 500\}$, and SHERPAS-full for $\theta_F \in \{1, 100\}$ and window size again in $\{300, 500\}$. Using two values for each parameter allows us to gauge their impact on the accuracy of SHERPAS. We also ran jpHMM using its default behavior for HIV and HBV, with and without the option `-Q blat` to speed-up its execution. See Sec. 3.1 for motivation regarding the choice of jpHMM for comparisons. For the HIV-pol dataset (Sec. 3.3) the results of running SCUEAL are distributed together with the software (Kosakovsky Pond *et al.*, 2009), so we included them in our comparisons.

The commands used for all these operations and links to files used —including the pkDBs constructed by RAPPAS— are reported for reproducibility in the Suppl. Materials (Sec. 5). All experiments were run on the same PC with 32GB RAM and using a single core operating at 3.6GHz. Running times were measured using the Unix command `time` (recording user CPU time).

			jpHMM		SHERPAS	
	Mbp	#br.	default	`-Q blat`	F	R
HIV-pol	16.2	332(23)	12964m 46s	1533m 22s	2m 40s	32s
HBV-g	9.6	676(8)	-	673m 24s	2m 35s	11s
HIV-g	26.7	1760(20)	4997m 48s	2367m 36s	20m 44s	51s
HIV-LR	17.7	1760(20)	7414m 17s	-	12m 29s	33s

Table 1. Running times of jpHMM and SHERPAS on the four datasets. Column "Mbp" reports the total size of the query dataset in Mbp. Column "#br." reports the number of branches for which the full pkDB (reduced pkDB) stores information. "R" and "F" distinguish between SHERPAS-reduced and SHERPAS-full, respectively. "HBV-g" and "HIV-g" refer to the HBV-genome and HIV-genome datasets, respectively. "HIV-LR" refers to the dataset of simulated long reads. All times are measured in minutes (m) and seconds (s).

4 Results

4.1 Running times

Table 1 shows the running times of SHERPAS-full, SHERPAS-reduced and of two ways of executing jpHMM, that is, with and without the `-Q blat` option to speed-up its execution. We do not include the time necessary to construct the pkDBs with RAPPAS, as we assume that the pkDB has been obtained prior to the analysis. (To this end, SHERPAS is distributed with the 3 pkDBs used in the experiments reported here.) Moreover, the numerical parameters of SHERPAS (the θ thresholds and the window size) have very little impact on its running time. For this reason, we only report runtimes for default parameters. The running times for jpHMM could not be obtained in two cases for the following reasons: (1) for the HBV-genome dataset, we must run jpHMM with the `-C` option for circular queries, which automatically activates the `-Q blat` option; (2) for the simulated Nanopore HIV reads, the `-Q blat` option resulted in the program failing to execute, probably because of the difficulty of aligning error-rich reads.

SHERPAS is orders of magnitude faster than jpHMM. Compared to jpHMM with the `-Q blat` option, SHERPAS-full is hundreds of times faster, while SHERPAS-reduced is thousands of times faster. Datasets that took days for jpHMM `-Q blat` to analyse, can be analyzed by SHERPAS in a matter of minutes, or even seconds.

The running time of SHERPAS essentially depends on two characteristics of the dataset. First, it scales linearly with the amount of data to analyse (number of queries and their lengths). Second, it is also related to the number of branches for which some information is stored in the pkDB. In the full version, this number is proportional to the size of the reference tree, while in the reduced version it is equal to the number of root branches. These numbers are reported in the first two columns of Table 1. See the Suppl. Materials (Sec. 2.6) for a detailed complexity analysis of the algorithms implemented in SHERPAS.

Consistent with the expectations above, the speed-up obtained with SHERPAS-reduced relative to SHERPAS-full is related to the strength of the reduction in the number of branches in the pkDB: the speed-up is moderate for HIV-pol (from 332 to 23 branches), but much

Method	thr	w	site-wise N/A	site-wise sens	site-wise prec	mosaic m	mosaic sup	mosaic sub	mosaic mm
SCUEAL	-	-	0.0	98.5	98.5	93.2	3.0	1.9	1.9
jpHMM	-	-	0.0	97.4	97.4	90.0	0.0	7.0	2.9
jpHMM-Qb	-	-	0.0	97.4	97.5	90.2	0	7.0	2.8
SHERPAS R	0.9	500	7.5	89.8	97.1	83.6	8.5	6.3	1.6
SHERPAS R	0.9	300	8.8	89.4	98.0	81.9	12.6	4.0	1.5
SHERPAS R	0.99	500	17.0	81.2	97.9	82.6	3.0	13.1	1.3
SHERPAS R	0.99	300	21.0	78.2	98.8	82.3	3.6	12.9	1.2
SHERPAS F	1	500	4.4	93.5	97.8	81.9	12.0	5.3	0.8
SHERPAS F	1	300	3.0	95.3	98.2	78.2	19.0	2.2	0.7
SHERPAS F	100	500	7.0	91.6	98.6	89.0	3.3	7.3	0.3
SHERPAS F	100	300	5.3	93.7	98.9	88.4	7.4	3.7	0.5

Table 2. Accuracies observed on the HIV-pol dataset. jpHMM-Qb stands for jpHMM with the `-Q blat` (fast) option. "R" and "F" distinguish between SHERPAS-reduced and SHERPAS-full, respectively. Columns "thr" and "w" report the threshold and window-size used by SHERPAS. Column "N/A" reports the percentage of sites that are not assigned to any strain. Columns "sens" and "prec" report site-wise sensitivity and precision (in percentage), respectively. Columns "m", "sup", "sub" and "mm" report the percentages of mosaic matches, supersets, subsets and mismatches, respectively. (See Sec. 3.2 for definitions.)

more pronounced for HBV-genome (from 676 to 8 branches), and for the two whole-genome HIV datasets (from 1760 to 20 branches). As for the differences across different datasets, it is not surprising that the dataset that results in the longest running time for SHERPAS is HIV-genome: its set of queries has the largest aggregate size, and the number of branches in the full pkDB is by far the largest. Running times for HIV-LR (the simulated Nanopore reads dataset) are lower than those for HIV-genome because the simulated reads are in general shorter than the whole genome.

4.2 HIV-pol dataset

Table 2 compares the accuracy of inter-strain recombination detection methods (see Sec. 3.7) on the HIV-pol dataset. SCUEAL and jpHMM achieve high accuracies overall on this dataset. Here, SCUEAL and jpHMM use different reference alignments, and two strains (A and N) present in some of the queries cannot be recognized by jpHMM (see Sec. 3.3). We also observed that many of the pre-queries that Kosakovsky Pond *et al.* (2009) used to construct the queries in this dataset are in fact part of the reference alignment for HIV used by jpHMM. For these reasons, it is not a good idea to draw conclusions about the relative performance of SCUEAL and jpHMM here.

Overall, the accuracies displayed by SHERPAS on this dataset are not as good as those of the other methods, especially in terms of site-wise sensitivity and mosaic measures. The low sensitivity is due to the high incidence of unassigned regions, which is particularly pronounced for SHERPAS-reduced and high values of the thresholds. On the other hand, for SHERPAS-full, a high value of the threshold ($\theta_F = 100$) results in a better site-wise precision than SCUEAL and jpHMM, and in mosaic measures that are almost as good as those of SCUEAL and jpHMM (frequency of mosaic matches: 88.4%-89% vs. 90%-93.2%).

We also observe that on this dataset SHERPAS-full is generally more accurate than SHERPAS-reduced. This is not surprising, as SHERPAS-reduced uses far less pre-computed information (a much smaller pkDB) than SHERPAS-full. As for the effect of window size, smaller windows consistently result in higher site-wise precision, and lower frequencies of mosaic matches. This appears to be due to the fact that a smaller window "switches" more easily between different strains and therefore has a tendency to produce finer classifications, but more fragmented mosaics. This is corroborated by the observation that the frequency of superset mosaics is consistently higher for windows of size 300 than for windows of size 500.

Method	thr	w	site-wise N/A	site-wise sens	site-wise prec	mosaic m	mosaic sup	mosaic sub	mosaic mm
jpHMM	-	-	0.0	98.5	98.5	91.4	0.4	6.8	1.4
SHERPAS R	0.9	500	1.6	93.7	95.3	80.2	5.1	14.0	0.7
SHERPAS R	0.9	300	2.5	94.6	97.0	81.4	11	6.6	1.0
SHERPAS R	0.99	500	3.5	92.6	96.0	81.2	2.2	16.5	0.1
SHERPAS R	0.99	300	5.0	92.9	97.8	86.6	3.7	9.4	0.3
SHERPAS F	1	500	2.1	93.5	95.5	76.0	8.7	14.4	0.8
SHERPAS F	1	300	1.5	95.3	96.8	74.7	19.3	5.0	1.0
SHERPAS F	100	500	4.8	92.0	96.6	80.2	1.3	18.3	0.2
SHERPAS F	100	300	3.8	94.1	97.8	84.4	7.5	7.4	0.8

Table 3. Accuracies observed on the HBV-genome dataset. jpHMM stands for jpHMM launched with the `-C` option for circular queries. Note that this option automatically activates the `-Q blat` (fast) option. All other abbreviations are as in Table 2.

4.3 HBV-genome dataset

The results in Table 3 show that, again, jpHMM has a very high overall accuracy, which is rarely matched by SHERPAS. Some of the observations made for HIV-pol can be re-iterated here: again, the site-wise sensitivity of SHERPAS is markedly lower than that of jpHMM, and again, as expected, increasing the thresholds deteriorates sensitivity, and improves mosaic accuracy.

Interestingly, on this dataset there does not seem to be any consistent difference between the accuracies of SHERPAS-full and SHERPAS-reduced. This may have something to do with the nature of the reference tree for HBV, where the 8 strains are monophyletic and well-delimited by relatively long root branches. (Which is not the case for all the strains in HIV-1.) This may imply that for HBV, the phylo-k-mers inferred for the root branches represent well their respective strains. It is also interesting to note that on this dataset, setting the window size to 300 usually leads to better results than 500, an observation that is not generally true for the other datasets.

4.4 HIV-genome dataset

The results for the HIV-genome dataset, shown in Table 4, show a slightly different pattern from the other datasets. On the one hand, jpHMM and SHERPAS-full have similar site-wise accuracy measures. Unlike in the previous datasets, the sensitivity of SHERPAS-full is higher than that of jpHMM in 3 cases out of 4. On the other hand, the frequency of mosaic matches for SHERPAS is now substantially lower than that of jpHMM.

These seemingly contradictory observations can be explained by inspecting the outputs of SHERPAS and jpHMM on the queries in this dataset. The Suppl. Materials (Annex C) contain an illustration of the outputs of SHERPAS-full and jpHMM on the first 100 queries out of the 3000 in this dataset. An important observation is that the partition produced by SHERPAS often includes short erroneous fragments (that is, that were not present in the correct partition of the query). For example, among the first 10 queries shown in the Suppl. Materials, 5 queries present such short erroneous fragments (queries 2, 3, 4, 6, 9; in some cases the erroneous fragment is so short that it is difficult to observe without zooming). The output of SHERPAS in Fig. 1 (corresponding to query 56) is also an example of this phenomenon: note the short erroneous fragment from strain D.

A consequence of this behavior of SHERPAS is that, although its output is usually close to the correct partition, the mosaics it

Method	thr	w	site-wise N/A	site-wise sens	site-wise prec	mosaic m	mosaic sup	mosaic sub	mosaic mm
jpHMM	-	-	3.6	95.6	99.2	77.8	4.2	16.6	1.4
jpHMM-Qb	-	-	4.0	95.4	99.3	78.2	4.0	17.0	0.8
SHERPAS R	0.9	500	3.4	94.5	97.9	48.2	37.3	6.1	8.4
SHERPAS R	0.9	300	5.5	92.5	97.9	27.4	63.0	1.9	7.7
SHERPAS R	0.99	500	6.0	92.7	98.6	65.8	15.3	13.4	5.5
SHERPAS R	0.99	300	8.6	90.5	99.0	56.7	27.0	9.8	6.5
SHERPAS F	1	500	2.1	96.1	98.2	46.3	43.6	4.3	5.8
SHERPAS F	1	300	1.6	96.6	98.2	24.2	71.5	0.7	3.6
SHERPAS F	100	500	3.5	95.3	98.8	67.8	19.2	9.5	3.5
SHERPAS F	100	300	2.7	96.4	99.1	54.3	39.6	2.9	3.2

Table 4. Accuracies observed on the HIV-genome dataset. All abbreviations are as in Table 2.

Method	thr	w	site-wise N/A	site-wise sens	site-wise prec	mosaic m	mosaic sup	mosaic sub	mosaic mm
jpHMM	-	-	15.0	38.7	45.5	0.7	49.8	0.4	49.1
SHERPAS R	0.9	500	16.7	65.2	78.4	2.7	71.2	0.6	25.5
SHERPAS R	0.9	300	25.2	56.3	75.2	1.1	75.1	0.2	23.6
SHERPAS R	0.99	500	28.7	59.8	83.9	9.4	55.0	2.7	32.9
SHERPAS R	0.99	300	38.3	49.3	79.9	5.0	56.0	1.6	37.4
SHERPAS F	1	500	21.8	71.8	91.9	12.3	58.4	3.9	25.4
SHERPAS F	1	300	21.8	69.3	88.7	3.2	75.9	0.4	20.5
SHERPAS F	100	500	25.7	70.3	94.6	34.1	30.2	16.8	18.9
SHERPAS F	100	300	21.8	73.8	94.4	22.3	51.3	6.3	20.0

Table 5. Accuracies observed on the dataset of simulated Nanopore HIV reads. For jpHMM only the results of launching it with its default options for HIV are reported, as the use of the `-Q blat` (fast) option resulted in the program failing to execute. All abbreviations are as in Table 2.

produces are often supersets of the correct mosaics. This phenomenon was also present in the other datasets, as can be seen in the frequencies of supersets, which are always higher than in the other methods (see again Tables 2 and 3). However, here this becomes more visible because the queries are about 3 to 5 times longer than in the other datasets, meaning that the probability of observing such erroneous short fragments in one query increases significantly. As we discuss in Sec. 5.1, when using SHERPAS to screen for recombinants, supersets should be regarded as far less serious errors than subsets or mismatches. From Table 4, it is easy to check that here the aggregate frequency of subsets and mismatches is higher for jpHMM (about 18%) than in all 4 runs of SHERPAS-full.

The lower sensitivity of jpHMM relatively to the other datasets is due to its behavior at the two ends of queries spanning a whole HIV genome. As can be seen in the Suppl. Materials (Annex C), jpHMM often leaves the ends of a HIV-genome query as unassigned (N/A). This is likely due to the difficulty of alignment and of profile-based modeling in those peripheral regions.

Like in the HIV-pol dataset, we note that SHERPAS-full tends to be slightly more accurate than SHERPAS-reduced, in terms of site-wise measures. Using a window of size 300 instead of 500, strongly reduces the frequency of mosaic matches, which is again due to a higher frequency of short erroneous fragments. However, it consistently reduces the aggregate frequency of subsets and mismatches (not shown) which may be important for screening purposes (Sec. 5.1).

4.5 Simulated Nanopore reads from the HIV-genome dataset

The results in Table 5 show that the simulated Nanopore reads pose a significant challenge to jpHMM and SHERPAS. This is not surprising, given the high error rates that characterize these reads. We refer to Yang *et al.* (2017) and its Suppl. Materials for an in-depth analysis of these error rates.

Strikingly, however, jpHMM is much more negatively affected by the simulated Nanopore sequencing errors than SHERPAS. Note that if a classifier was to choose randomly one of the 14 strains at every site, its sensitivity and precision would be $1/14 = 7.1\%$, but if it was to classify every query as a non-recombinant sequence belonging to the most frequent strain (B) its sensitivity and precision would be 41.9% (this is the proportion of sites from strain B in the queries). Thus, jpHMM's site-wise accuracy measures are only partially better than those of random classifiers. On the other hand the site-wise precision of SHERPAS, especially in the full version, is only marginally affected (cf. Table 4). The site-wise sensitivity is lowered, which is due to the fact that error-rich regions are often unassigned. SHERPAS is also more accurate than jpHMM in terms of mosaic measures (cf. the frequencies of matches and mismatches).

Finally, once again SHERPAS-full is consistently more accurate than SHERPAS-reduced. Interestingly, on this dataset, using a smaller window generally results in a deterioration of accuracy. However, this is not true if the goal is to minimize the aggregate frequency of subsets and mismatches (see Sec. 5.1).

5 Discussion

5.1 Uses of SHERPAS

SHERPAS is a tool for the detection and analysis of inter-strain recombinants in a large collection of query sequences. It relies on the availability of a reference multiple sequence alignment, which is used to "learn" to recognize sequences from the different strains. It accomplishes a bioinformatics task considerably different from that of detecting the presence of recombinant sequences within a multiple sequence alignment — a task that can be tackled with other methods, such as those implemented in the RDP software (Martin *et al.*, 2015, 2017). An important difference between the two tasks is that here we make a clear distinction between reference sequences (known in advance and well-characterized) and the novel sequences to analyse, the queries. The latter do not need to be aligned, which opens the possibility of treating a much larger amount of sequence data. SHERPAS can be used for any dataset of viral sequences for which a reference alignment of sufficient quality and size can be obtained. In fact SHERPAS, like SCUEAL, could also be used to detect recombinant bacterial sequences (Kosakovsky Pond *et al.*, 2009), although we have not experimented with such data.

By default, SHERPAS uses the full pkDB, with $\theta_F = 100$ and window size 300. If the user chooses to run SHERPAS-reduced, the default parameters are $\theta_R = 0.99$ and again window size 300. These default settings were chosen while trying to achieve a good balance among all accuracy measures, and assuming a volume of data that is not prohibitively large. However, users should be aware that the choice of settings will depend on the nature of the data and the goal of the analysis.

For example, SHERPAS may be used as a first screen to detect potential recombinants in a large set of sequences. The putative recombinants can then be analysed further with more accurate but slower software, such as REGA (de Oliveira *et al.*, 2005; Pineda-Peña *et al.*, 2013), SCUEAL (Kosakovsky Pond *et al.*, 2009) or jpHMM (Schultz *et al.*, 2006, 2009). In this case, the primary goal is not high accuracy, but rather to lower the odds of missing evidence of recombination in a query. In terms of inferred mosaics, this means lowering the frequencies of subsets and mismatches. In Tables 2 – 5, the parameter combinations that minimize the occurrence of subsets

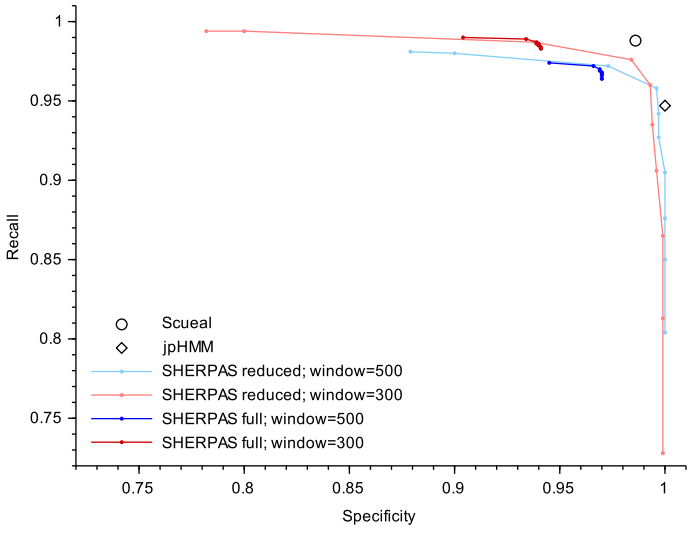

Fig. 2. Trade-off between recall and specificity for the binary classification of HIV-pol queries. Recall and specificity are plotted for SCUEAL (circle), jpHMM (diamond) and SHERPAS (colored lines). The four colored lines correspond to the different combinations of a pkDB version (full/reduced) and window size (500,300) for SHERPAS. Each point in a colored line corresponds to a different value of the threshold, with the lowest values of the threshold (1 for SHERPAS-full and 0 for SHERPAS-reduced) resulting in the leftmost points. See the Suppl. Materials (Sec. 5.6) for full details. Note that all rates fall in the interval $[0.72, 1]$, which is why the curves are not depicted in the full $[0, 1]$ range.

and mismatches for SHERPAS-full and SHERPAS-reduced are the ones with the lowest tested thresholds and window size 300. Note that these combinations consistently produce fewer aggregate subsets and mismatches than jpHMM.

To provide further insight into the ability of detecting evidence of recombination, we re-analyzed the queries in the HIV-pol dataset, which include a substantial number of sequences that are not inter-strain recombinants. We then considered SHERPAS as a binary classifier for inter-strain recombination, classifying a sequence as a "positive" if at least one breakpoint is detected, and a "negative" otherwise. This allows us to observe how changing settings in SHERPAS (full vs. reduced database, threshold and window size) affects its ability of recovering true positives (known as the *recall* of the classifier), and how much specificity has to be traded to improve this ability. The results of this experiment, shown in Fig. 2, confirm that SHERPAS can indeed achieve high recall with the use of low thresholds (not the default one), and small windows, although users must be aware that this entails a loss of specificity. A full description and discussion about this experiment can be found in the Suppl. Materials (Sec. 5.6).

5.2 Scaling-up

Another important factor influencing how SHERPAS should be run is the amount of data to analyse. The query datasets that we used here were of relatively manageable sizes, to facilitate comparisons with slower software. Should the data to analyse be substantially more abundant (e.g. millions of reads), running SHERPAS in reduced mode may become more appealing, or even necessary in some cases. This is especially true if the reference tree is large, as in this case the speedup for SHERPAS-reduced is more pronounced (see Sec. 4.1). Moreover, for some datasets or applications, the accuracy of SHERPAS-reduced may be comparable to that of SHERPAS-full (see, e.g., Sec. 4.3 and Fig. 2).

Because the running times of SHERPAS scale linearly with the amount of data to analyse, running SHERPAS on few millions queries is feasible in a matter of days (using SHERPAS-full) or in a matter of hours (using SHERPAS-reduced; see Table 1). To the best of our knowledge, none of the recombination detection tools currently available are scalable to datasets of that size. Although our experiments focused on comparing SHERPAS to jpHMM —for the reasons detailed in Sec. 3.1— previous comparisons of running times between jpHMM and phylogeny-based tools for recombination detection (namely REGA and SCUEAL) showed that jpHMM was at least as fast as those tools (see Pineda-Peña *et al.* (2013), Table 4), when run with the fast `-Q blat` option, meaning that the running time advantage of SHERPAS likely extends to the other available tools.

5.3 Accuracy

Consistent with previous literature (Schultz *et al.*, 2006; Kosakovsky Pond *et al.*, 2009; Schultz *et al.*, 2009), we evaluated the predictive accuracy of SHERPAS using large datasets of semi-artificial recombinant sequences, which combine fragments of real HIV and HBV sequences (the *pre-queries*) via artificially-introduced breakpoints. In the absence of large datasets of real sequences for which the true recombinant structure is known with certainty, this is a good way to evaluate a new method for recombination detection. (Note that we ensure that none of the pre-queries belongs to the reference alignment for the tested methods.) Using sequences that are fully simulated using a fixed evolutionary model (Kosakovsky Pond *et al.*, 2009) is also a viable option, but the choice of the simulation parameters can have an important impact on the results, and the advantage over using semi-artificial sequences is unclear.

The experiments were designed to assess accuracy loss in SHERPAS compared to jpHMM (Schultz *et al.*, 2006, 2009). The choice of jpHMM is motivated in Sec. 3.1. The other goal of our experiments was to explore the influence of the parameters of SHERPAS, including the use of full/reduced pkDB. Using two possible values for all parameters allows us to gauge their impact. The two window sizes (300 and 500 bp) were chosen on the basis of common practices of sliding window approaches (e.g. the REGA tool employs a window of 400 bp).

Possibly the most interesting result here is the inferior performance of jpHMM compared to SHERPAS on the simulated Nanopore reads dataset. We suspect that the reason for this is that profile HMMs may be strongly affected by large indels (which are common in these reads) and by errors that do not correspond well to their emission probabilities (which were estimated on error-free datasets by Schultz *et al.* (2006)). SHERPAS, on the other hand, appears to be able to exploit the information coming from the error-free stretches of sequences that lie between errors in the reads. Further work, beyond the scope of the present paper, would be needed to investigate these hypotheses.

5.4 Future work and limitations

SHERPAS-full implicitly computes the most probable branch of origin of any window within a query. This means that it can be used for precise phylogenetic placement of the segments composing the query (Matsen *et al.*, 2010; Berger *et al.*, 2011; Barbera *et al.*, 2019; Linard *et al.*, 2019), or even to detect *intra*-strain recombinants. We plan to add these functionalities in future versions of SHERPAS.

Second, the use of a sliding window has a few well-known disadvantages (Kosakovsky Pond *et al.*, 2009). Specifically, it makes it hard to precisely locate breakpoints (Schultz *et al.*, 2006), and choosing its size involves a trade-off between resolution and informativeness. In the future, we plan to implement algorithms that are not window-based in SHERPAS (using, e.g., dynamic programming). However, this will potentially entail a cost in terms of computational efficiency.

Third, here we focused on the problem of recognizing cases of *homologous* recombination, which occurs when the new sequence combines parental fragments with different origins, but joined at homologous sites. Non-homologous or *illegitimate* recombination is also known to occur in viruses, and results in genomes displaying structural changes (e.g. with large insertions, deletions, duplications etc.) (Crawford-Miksza and Schnurr, 1996; Scheel *et al.*, 2013; Galli and Bukh, 2014). Some preliminary experiments (not shown) suggest that SHERPAS is also able to recognize and correctly partition non-homologous recombinants. Note that phylogeny-based tools such as SCUEAL and REGA align the query to the reference sequences prior to the analysis, a problematic step when the query contains, for example, genomic duplications or translocations. In the future, we plan to conduct an in-depth study of this novel functionality of SHERPAS.

Fourth, SHERPAS was developed to detect novel recombinants, but not to recognize widespread and well-known recombinants — known as *circulating recombinant forms* (CRFs). If some of the query sequences are CRFs, SHERPAS should detect that they are inter-strain recombinants, and partition them accordingly. Although we have done so for one CRF (CRF01_AE) in HIV-1, including CRFs in the reference alignment and defining one strain per CRF is risky, as the reference tree will not be an accurate description of the true history. This point is discussed in depth in the Suppl. Materials (Sections 3.2 and 3.3), where we also explain how users may solve this problem by modifying the reference alignment following an idea already exploited for example, by Kosakovsky Pond *et al.* (2009) and D. Martin (personal communication). Automatic treatment of CRFs is a possible extension that we plan to add to SHERPAS.

Finally, every step involved in SHERPAS's analyses can be in principle parallelized, including the construction of the phylo-k-mer database. This would further improve the scalability of our approach.

5.5 Conclusion

SHERPAS achieves a reasonable accuracy compared to state-of-the-art inter-strain recombination detection tools for viruses, but is orders of magnitude more efficient. This advantage derives from the fact that SHERPAS does not need to align the query sequences, and from the relative simplicity of its classification algorithm. To the best of our knowledge, it is the first software that can estimate the recombinant structure of thousands of long sequences (up to whole genomes) within minutes or even seconds. It also appears to be relatively robust to high error rates typical of long read sequencing technologies. SHERPAS paves the way to systematic screening of recombinants in large datasets of long reads or assembled genome sequences.

Acknowledgements

We thank Philippe Roumagnac for useful discussions and guidance, and the VIROGENESIS consortium (http://www.virogenesis.eu/) for stimulating this work — in particular Pieter Libin, Kristof Theys and Anne-Mieke Vandamme.

Funding and conflicts of interest

This work was publicly funded through ANR (The French National Research Agency) under the *Investissements d'avenir* programme with the reference ANR-16-IDEX-0006. B.L. is employed by Spygen, a company specialising in aquatic and terrestrial biodiversity monitoring using environmental DNA. N.R. is supported by a doctoral fellowship from the French *Ministère de l'Enseignement supérieur, de la Recherche et de l'Innovation*. We also received support from *Institut Français de Bioinformatique* (ANR-11-INBS-0013).

References

Araujo, N. M. (2015). Hepatitis B virus intergenotypic recombinants worldwide: an overview. *Infection, Genetics and Evolution*, **36**, 500–510.

Barbera, P. *et al.* (2019). EPA-ng: massively parallel evolutionary placement of genetic sequences. *Systematic Biology*, **68**(2), 365–369.

Batorsky, R. *et al.* (2011). Estimate of effective recombination rate and average selection coefficient for HIV in chronic infection. *Proceedings of the National Academy of Sciences*, **108**(14), 5661–5666.

Berger, S. A. *et al.* (2011). Performance, accuracy, and web server for evolutionary placement of short sequence reads under maximum likelihood. *Systematic Biology*, **60**(3), 291–302.

Břinda, K. *et al.* (2018). Karel-brinda/nanosim-h: Nanosim-h 1.1.0.4. *Zenodo*.

Crawford-Miksza, L. K. and Schnurr, D. P. (1996). Adenovirus serotype evolution is driven by illegitimate recombination in the hypervariable regions of the hexon protein. *Virology*, **224**(2), 357–367.

de Oliveira, T. *et al.* (2005). An automated genotyping system for analysis of HIV-1 and other microbial sequences. *Bioinformatics*, **21**(19).

Felsenstein, J. (2004). *Inferring Phylogenies*, volume 2. Sinauer associates Sunderland, MA.

Foley, B. *et al.* (2018). *HIV Sequence Compendium 2018*. Theoretical Biology and Biophysics Group, Los Alamos National Laboratory, NM, LA-UR 18-25673.

Galli, A. and Bukh, J. (2014). Comparative analysis of the molecular mechanisms of recombination in hepatitis C virus. *Trends in Microbiology*, **22**(6), 354–364.

Guindon, S. and Gascuel, O. (2003). A simple, fast and accurate algorithm to estimate large phylogenies by maximum likelihood. *Systematic Biology*, **52**, 696–704.

Guindon, S. *et al.* (2010). New algorithms and methods to estimate maximum-likelihood phylogenies: assessing the performance of PhyML 3.0. *Systematic Biology*, **59**(3), 307–321.

Gusfield, D. (1997). *Algorithms on Strings, Trees and Sequences*. Cambridge University Press.

Hayer, J. *et al.* (2013). HBVdb: a knowledge database for hepatitis B virus. *Nucleic Acids Research*, **41**(D1), D566–D570.

HBVdb contributors (2019). Dataset for nucleotide sequence genomes of genotype all. https://hbvdb.ibcp.fr/HBVdb/HBVdbDataset?view=/data/nucleic/alignments/all_Genomes.clu&seqtype=0. Accessed: December 2019.

Kiguoya, M. W. *et al.* (2017). Subtype-specific differences in gag-protease-driven replication capacity are consistent with intersubtype differences in HIV-1 disease progression. *Journal of Virology*, **91**(13), e00253–17.

Kosakovsky Pond, S. L. *et al.* (2009). An evolutionary model-based algorithm for accurate phylogenetic breakpoint mapping and subtype prediction in HIV-1. *PLoS Computational Biology*, **5**(11), e1000581.

Kozlov, A. M. *et al.* (2019). RAxML-NG: a fast, scalable and user-friendly tool for maximum likelihood phylogenetic inference. *Bioinformatics*, **35**(21), 4453–4455.

Kuiken, T. *et al.* (2006). Host species barriers to influenza virus infections. *Science*, **312**(5772), 394–397.

Linard, B. *et al.* (2019). Rapid alignment-free phylogenetic identification of metagenomic sequences. *Bioinformatics*, **35**(18), 3303–3312.

Liu, S.-L. *et al.* (2002). Selection for human immunodeficiency virus type 1 recombinants in a patient with rapid progression to AIDS. *Journal of Virology*, **76**(21), 10674–10684.

Martin, D. P. *et al.* (2011). Analysing recombination in nucleotide sequences. *Molecular Ecology Resources*, **11**(6), 943–955.

Martin, D. P. *et al.* (2015). RDP4: Detection and analysis of recombination patterns in virus genomes. *Virus Evolution*, **1**(1).

Martin, D. P. *et al.* (2017). Detecting and analyzing genetic recombination using rdp4. *Bioinformatics*, pages 433–460.

Matsen, F. A. *et al.* (2010). pplacer: linear time maximum-likelihood and bayesian phylogenetic placement of sequences onto a fixed reference tree. *BMC Bioinformatics*, **11**(1), 538.

Moutouh, L. *et al.* (1996). Recombination leads to the rapid emergence of HIV-1 dually resistant mutants under selective drug pressure. *Proceedings of the National Academy of Sciences*, **93**(12), 6106–6111.

Neher, R. A. and Leitner, T. (2010). Recombination rate and selection strength in HIV intra-patient evolution. *PLoS Computational Biology*, **6**(1).

Pérez-Losada, M. *et al.* (2015). Recombination in viruses: mechanisms, methods of study, and evolutionary consequences. *Infection, Genetics and Evolution*, **30**, 296–307.

Pineda-Peña, A.-C. *et al.* (2013). Automated subtyping of HIV-1 genetic sequences for clinical and surveillance purposes: performance evaluation of the new rega version 3 and seven other tools. *Infection, Genetics and Evolution*, **19**, 337–348.

Quick, J. *et al.* (2016). Real-time, portable genome sequencing for Ebola surveillance. *Nature*, **530**(7589), 228–232.

Scheel, T. K. *et al.* (2013). Productive homologous and non-homologous recombination of hepatitis C virus in cell culture. *PLoS Pathogens*, **9**(3).

Schultz, A.-K. *et al.* (2006). A jumping profile hidden markov model and applications to recombination sites in HIV and HCV genomes. *BMC Bioinformatics*, **7**(1), 265.

Schultz, A.-K. *et al.* (2009). jpHMM: improving the reliability of recombination prediction in HIV-1. *Nucleic Acids Research*, **37**(suppl_2), W647–W651.

Schultz, A.-K. *et al.* (2012). jpHMM: recombination analysis in viruses with circular genomes such as the hepatitis B virus. *Nucleic Acids Research*, **40**(W1), W193–W198.

Streeck, H. *et al.* (2008). Immune-driven recombination and loss of control after HIV superinfection. *The Journal of Experimental Medicine*, **205**(8), 1789–1796.

Struck, D. *et al.* (2014). COMET: adaptive context-based modeling for ultrafast HIV-1 subtype identification. *Nucleic Acids Research*, **42**(18).

Suarez, D. L. *et al.* (2004). Recombination resulting in virulence shift in avian influenza outbreak, Chile. *Emerging Infectious Diseases*, **10**(4), 693.

Wainberg, M. A. and Brenner, B. G. (2010). Role of HIV subtype diversity in the development of resistance to antiviral drugs. *Viruses*, **2**(11), 2493–2508.

Wikipedia contributors (2019). Subsequence — Wikipedia, the free encyclopedia. [Online; accessed 5-March-2020].

Yang, C. *et al.* (2017). NanoSim: nanopore sequence read simulator based on statistical characterization. *GigaScience*, **6**(4).

Yang, Z. (2006). *Computational Molecular Evolution*. Oxford University Press.

Supplementary Materials to

Rapid screening and detection of inter-type viral recombinants using phylo-k-mers

Contents

1 Phylo-k-mers, formalized **3**

1.1 The reference data and their preprocessing . . . 3

1.2 Probability of a k-mer at a position in the reference tree and alignment . . . 4

1.3 Phylo-k-mers and their probability score . . . 5

1.4 The full pkDB . . . 6

1.5 The reduced pkDB . . . 7

2 The algorithm, formalized **7**

2.1 The algorithm at a glance . . . 7

2.2 The main procedure . . . 8

2.3 Heap property and update . . . 9

2.4 Converting scores into likelihoods . . . 10

2.5 Producing the output . . . 11

2.6 Complexity analysis . . . 11

3 Assumptions on the reference data **14**

3.1 Accuracy of the reference tree . . . 14

3.2 Absence of recombination . . . 14

3.3 Dealing with circulating recombinant forms . . . 15

3.4 Monophyly of the strains . . . 16

4 Site-wise measures of accuracy **17**

5 Dataset construction, data availability, and reproducibility **19**

5.1 Preprocessing 19

5.2 HIV-pol 19

5.3 HBV-genome 20

5.4 HIV-genome 21

5.5 HIV Nanopore reads dataset 23

5.6 Experiment on the specificity/recall trade-off 23

References **25**

A Annex: Marginal posterior distributions of ancestral states **27**

B Annex: Approximate relationship between branch scores and likelihoods **28**

C Annex: Some illustrated outputs **30**

1 Phylo-k-mers, formalized

For completeness, here we describe in detail what phylo-k-mers are, and the main ideas behind their construction. The material presented in Section 1 not novel, as it was introduced informally in the original publication about RAPPAS [11]. The treatment here is somewhat more formal, which should help readers interested in the details of the technique, or as a first step towards understanding its theoretical foundations.

1.1 The reference data and their preprocessing

The input data for the construction of phylo-k-mers are a *reference alignment* A_0, a *nucleotide substitution model* (e.g. GTR+Γ), and a rooted *reference tree* T_0 describing the evolutionary process that led to the sequences in A_0 (i.e. there is a one-to-one correspondence between the leaves of T_0 and the sequences aligned in A_0). By default, the branch lengths of T_0 and the parameters θ of the substitution model are re-estimated using A_0 at launch of the phylo-k-mer building process.

Both references (alignment and tree) are then preprocessed for the construction of phylo-k-mers. Improved ways to do this are the subject of ongoing research. Here we describe the way this is performed currently by default. We denote the set of nodes, leaves and branches (edges) of any tree T by $V(T)$, $L(T)$ and $E(T)$, respectively. Note that $L(T) \subset V(T)$.

First, we remove from A_0 all columns that contain more than a certain fraction of gaps "–" (0.99 by default). The rationale for this step is that ancestral reconstruction techniques do not account for gaps, and highly gappy columns have been observed to be deleterious for phylo-k-mer construction. We call the resulting alignment the *reduced reference alignment*, and denote it by A.

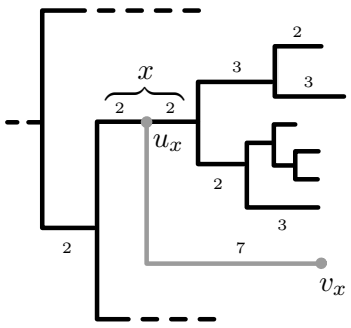

Figure 1: **Injection of two ghost nodes on a branch of the reference tree.** Depicted in black is the reference tree T_0. Branches are labelled by their lengths. Branches without labels have length 1. In gray, two ghost nodes u_x, v_x injected over branch x: u_x is placed on the midpoint of x, giving rise to two new branches of length 2; v_x is a new leaf, connected to u_x via the new branch (u_x, v_x). Since the lengths of the paths from u_x to its 6 descendants in T_0 are 7, 8, 6, 7, 7, 7, the length of the new branch is set to their average, i.e. 7. To get the extended reference tree, this process is repeated for each $x \in E(T_0)$.

As for the reference tree, a number of nodes and branches are added to T_0, leading to what we call the *extended reference tree* T. For each branch x in T_0, two new nodes u_x and v_x are introduced, as shown in Figure 1: node u_x is placed at the midpoint of branch x, and a new branch (u_x, v_x) leading to a new leaf v_x is also added. The length of this new branch is set to the average length among all paths from u_x to the leaves in $L(T_0)$ that descend from u_x. This length is the only aspect that depends on the position of the root of T_0 in the phylo-k-mer building process. Note that $V(T_0) \subset V(T)$. Nodes that are in $V(T)$ but not $V(T_0)$ are called *ghost nodes*.

1.2 Probability of a k-mer at a position in the reference tree and alignment

We consider the reduced reference alignment as a matrix $A = (a_{u,i})$, where $a_{u,i} \in \{\mathtt{A}, \mathtt{C}, \mathtt{G}, \mathtt{T}, -\}$ is the nucleotide or gap in the sequence at leaf $u \in L(T_0)$ aligned to site $i \in \{1, \ldots, m\}$, where m is the number of columns in A. Note that gaps are usually interpreted and treated as missing data in phylogenetics. Aside from gaps, the contents of A represent all sequence data that have been actually observed from the reference tree.

Here, we wish to model nucleotides at the nodes in $V(T) \setminus L(T_0)$, i.e. the nodes in the extended reference tree from which no data has been observed. In order to represent these unobserved nucleotides, we define, for every $u \in V(T)$ and every site i, the random variable

$$A'_{u,i} = \text{nucleotide at site } i \text{ of the sequence at node } u.$$

Note that the only possible realizations of this random variable are in $\{\mathtt{A}, \mathtt{C}, \mathtt{G}, \mathtt{T}\}$ and that whenever $u \in L(T_0)$ and $a_{u,i} \neq -$, we must have $A'_{u,i} = a_{u,i}$. Thus, the A' variables specify a random "extension" of alignment A. For the calculations that follow, the only relevant $A'_{u,i}$ variables are those where u is a ghost node.

The observed data in A and the substitution model specified by θ determine the marginal posterior distribution of $A'_{u,i}$, i.e. the probabilities, for every $a \in \{\mathtt{A}, \mathtt{C}, \mathtt{G}, \mathtt{T}\}$

$$\mathbb{P}[A'_{u,i} = a \mid A, \theta]. \tag{1}$$

Calculating these probabilities can be performed with standard techniques of ancestral state reconstruction, which for completeness we briefly summarize in Annex A.

Because the probabilities above depend on the particular nucleotide substitution model that the user wishes to adopt, and because substitution models are a subject of active research, their calculation is best performed by well-maintained and up-to-date software packages for likelihood-based phylogenetic calculations, such as RAxML-NG [9] and PhyML [6]. The choice of the software to use as well as the nucleotide substitution model and its parameters θ, can be controlled with suitable options of the phylo-k-mer construction software (currently a module within RAPPAS). The result of this step is a large collection of tables containing all the marginal posterior probabilities of $A'_{u,i}$ that are relevant for the calculations that follow. See Figure 2 for an example of such a table, and its use.

Now let $S_{u,i}$ be the random sequence $A'_{u,i}A'_{u,i+1}\ldots A'_{u,i+k-1}$, that is the k-mer at sites $i, i+1, \ldots, i+k-1$ in the sequence at node u. Using the assumption of independent evolution at different sites, we calculate the probability distribution of $S_{u,i}$ as follows:

$$\mathbb{P}[S_{u,i} = a_1 a_2 \ldots a_k \mid A, \theta] = \prod_{j=1}^{k} \mathbb{P}[A'_{u,i+j-1} = a_j \mid A, \theta]. \tag{2}$$

The assumption of independence between sites, although unrealistic, is standard practice in phylogenetics, and is also needed for computing the probabilities in (1).

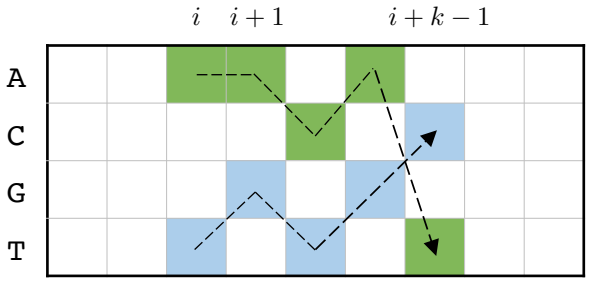

Figure 2: **Computing the probability of a k-mer at k consecutive sites in A.** Software for likelihood-based phylogenetics can be used to produce, for any given ghost node u, a table of marginal posterior probabilities of the four nucleotides at u and at all sites in A, i.e. the probabilities in (1). The table for a specific node u is depicted here with nucleotides corresponding to rows and sites corresponding to columns. Given this table, the probability of any k-mer at u and any k consecutive sites in A can be computed using (2). For example, the probability of 5-mer `AACAT` (resp. `TGTGC`) at u and sites i to $i + 4$ is obtained by multiplying the table entries highlighted in green (resp. blue).

1.3 Phylo-k-mers and their probability score

In the previous section, we have explained the simple ideas behind calculating the probability $\mathbb{P}[S_{u,i} = w \mid A, \theta]$ for any k-mer w, any node $u \in V(T)$, and any site $i \in \{1, \ldots, m - k + 1\}$. Also recall that each branch $x \in E(T_0)$ is associated to a subset of ghost nodes in $V(T)$ (by default $\{u_x, v_x\}$, see Section 1.1). Let G_x denote this subset.

For any k-mer w and any branch of the original reference tree $x \in E(T_0)$, we then define the *probability score* of w at x as

$$\widetilde{\mathbb{P}}[w|x] = \max_{u \in G_x} \max_{i \in \{1,\ldots,m-k+1\}} \mathbb{P}[\, S_{u,i} = w \mid A, \theta\,]. \tag{3}$$

In other words, $\widetilde{\mathbb{P}}[w|x]$ is probability of w at the best placement for w within A and among the nodes in G_x. The $\widetilde{\mathbb{P}}[w|x]$ scores play a central role to determine the phylogenetic origin of a sequence in both SHERPAS and RAPPAS [11]. Because of this, it is helpful to pause here and offer a few informal interpretations of what they mean.

1. The simplest way to interpret $\widetilde{\mathbb{P}}[w|x]$ is as an approximation of the probability of k-mer w being present in a sequence that has diverged from the reference tree T_0 at branch x. Note, however, that if we were to compute such probability, it would make more sense to take a weighted average over $u \in G_x$ instead of the first maximum, and to take $\mathbb{P}[\,$there exists i such that $S_{u,i} = w \mid A, \theta\,]$ instead of the second maximum.

2. We can also view $\widetilde{\mathbb{P}}[w|x]$ as a quantity proportional to the maximum likelihood score of the phylogenetic tree that is obtained from T_0 by inserting w at the end of a new branch attached to x (as in Figure 1). Taking the maximum over $i \in \{1, \ldots, m-k+1\}$ corresponds to finding a maximum likelihood alignment of k-mer w to A, constrained to having no indel breaking up the k-mer. Taking the maximum over $u \in G_x$ corresponds to finding a maximum likelihood configuration within a small set of possible configurations for the branch lengths surrounding the attachment point of w to x. (E.g. when $G_x = \{u_x, v_x\}$, as in Figure 1, placing w at u_x corresponds to setting the new pendant branch length to 0, while placing it at v_x corresponds to setting it to 7.)

In short, all that matters for SHERPAS and other algorithms using the $\widetilde{\mathbb{P}}[w|x]$ scores is that they represent a probabilistic measure of how likely x is to be the phylogenetic origin of k-mer w. Note that this implies that scores coming from different k-mers must be combined using products, or equivalently by using sums of their logarithms.

A *phylo-k-mer* is defined as a k-mer w for which there exists at least one branch $x \in E(T_0)$ with $\widetilde{\mathbb{P}}[w|x]$ larger than a given threshold, currently set to $(\omega/4)^k$, where ω is a user-set parameter (1.5 by default).

The phylo-k-mer database construction step relies on algorithms that generate all such phylo-k-mers, and stores them together with a list of (1) all the branches in $E(T_0)$ for which $\widetilde{\mathbb{P}}[w|x]$ is larger than the threshold, and (2) their respective probability scores $\widetilde{\mathbb{P}}[w|x]$ (see next section for more details). A number of alternative algorithms for this step have been the subject of recent research which will be described in an upcoming publication (N. Romashchenko et al., pers. comm.).

1.4 The full pkDB

The *full phylo-k-mer database* (*pkDB*) is a data structure containing all phylo-k-mers and their associated information. It is a look-up table B that, given a phylo-k-mer w, returns the list of pairs

$$B(w) = \Big[(x_1, s_1), (x_2, s_2), \ldots, (x_{|B(w)|}, s_{|B(w)|})\Big]$$

where the x_i are branches of the reference tree (hence the use of the letter B) and

$$s_i = \log \widetilde{\mathbb{P}}[w|x_i].$$

Unless otherwise stated, all logarithms are base 10.

The pkDB also contains all the relevant information regarding the parameters that were used to generate the phylo-k-mers, most notably the threshold on their scores. In the following we call Thr_B the threshold for log-probability scores, meaning that all s_i in a $B(w)$ list are such that $s_i > \mathsf{Thr}_B$.

The value of the threshold is taken into account in the calculations performed by SHERPAS: anytime a branch x does not appear in $B(w)$, SHERPAS assumes $\log \widetilde{\mathbb{P}}[w|x] = \mathsf{Thr}_B$.

1.5 The reduced pkDB

The *root branches* of the reference tree are those that lie at the root of a maximal subtree whose leaves all belong to the same strain. (See the main text for an equivalent definition.)

The *reduced pkDB* B' is obtained from the full pkDB B by removing all pairs (x_i, s_i) where x_i is not a root branch. That is, if $B(w) = \left[(x_1, s_1), (x_2, s_2), \ldots, (x_{|B(w)|}, s_{|B(w)|})\right]$ and $x_{i_1}, x_{i_2}, \ldots, x_{i_l}$ are the root branches among $x_1, x_2, \ldots, x_{|B(w)|}$, then

$$B'(w) = \left[(x_{i_1}, s_{i_1}), (x_{i_2}, s_{i_2}), \ldots, (x_{i_l}, s_{i_l})\right].$$

In the following, for simplicity we denote by B the pkDB used, regardless of whether the full or reduced version is used.

2 The algorithm, formalized

2.1 The algorithm at a glance

Below, we provide a detailed description of the algorithm underlying SHERPAS, complementing the high-level description in the main text. In order to understand the pseudocode that follows, here we introduce the main important ideas, namely the mathematical scores that SHERPAS computes.

At any point during the execution of SHERPAS, only a subset of the branches of the reference tree are "active". These are the branches that are associated by the pkDB to at least one k-mer in the current window. We will denote this subset of branches by L, for consistency with the algorithm used by RAPPAS for placement [11].

As the sliding window moves along, SHERPAS updates L, and for every branch x currently in L, it also keeps a score $S[x]$ equal to the sum of all the log-probabilities associated to x by the k-mers in the current window. To express this mathematically, let W denote the sequence of k-mers in the current window. That is, $W = (w_1, w_2, \ldots, w_{|W|})$, where each w_i is a k-mer that overlaps by $k-1$ characters with w_{i-1} and w_{i+1}, for $i \in \{2, \ldots, |W| - 1\}$. Then,

$$S[x] = \sum_{i=1}^{|W|} \log \widetilde{\mathbb{P}}[w_i|x] \tag{4}$$

Recall that if x does not appear in any pair in $B(w_i)$, SHERPAS assumes $\log \widetilde{\mathbb{P}}[w_i|x] = \mathsf{Thr}_B$ where Thr_B is the threshold for log-probability scores, used for the construction of the pkDB (see Section 1.4).

To determine the recombinant structure of the query sequence, for every window SHERPAS inspects the branch or branches in L that have the highest score $S[x]$. In order to find these branches efficiently, L is implemented as a binary max-heap [2], a data structure that partially orders the branches it contains on the basis of their scores $S[x]$, and that is efficient to update. Every time a branch changes score or is added or removed from L, the max-heap is updated using a well-known procedure that for completeness we report in Sec. 2.3.

2.2 The main procedure

Let $W_0, W_1, \ldots, W_N$ denote the windows considered by SHERPAS during its execution. We set $W_0 = \emptyset$ for mathematical convenience. The way the other windows are defined depends on whether the query is circular or not. If the sequence is not circular, the first window W_1 contains the first 100 k-mers of the sequence. Then two k-mers are added from one window to the next, until the size of a window coincides with the standard size (300 by default). As that size is attained, at each step the first k-mer of the current window W_i is removed, and the k-mer following the last k-mer in W_i is added, to get the next window W_{i+1}. Finally, when the end of the query is reached, the first two k-mers of the current window are removed at each step, until we get a final window W_N of size 100.

If the query sequence represents a full circular genome, the size of all the windows are the same, and each window is obtained from the previous one by removing the first k-mer and adding the next one. However, a pre-processing step modifies the query, to reflect its circularity, as follows: The last $(|W| + k - 1)/2$ base pairs of the sequence are added to its beginning, and the first $(|W| + k - 1)/2$ base pairs are added to its end. Note that $|W| + k - 1$ equals the length of the sliding window in base pairs.

The pseudocode below describes the algorithm employed by SHERPAS to treat one query. The following notation and terminology is adopted:

- The set of *candidate branches* E is the set of all branches for which some information is stored in the pkDB. For SHERPAS-full, $E = E(T_0)$, i.e. E is the set of all branches in the reference tree, whereas for SHERPAS-reduced, E is the set of root branches.
- $+=$ denotes increment of its left-hand side by its right-hand side.
- $W_i \setminus W_{i-1}$ denotes the sequence of k-mers that are newly added to W_i. Note that, unless $i = 1$, there are at most two k-mers in $W_i \setminus W_{i-1}$, but usually (when $|W_i| = |W_{i-1}|$) there is exactly one k-mer here.
- $W_{i-1} \setminus W_i$ denotes the sequence of k-mers that are removed when transitioning from W_{i-1} to W_i. Again there are at most two k-mers here (usually exactly one).
- $\biguplus B(w), w \in W$ denotes the concatenation of the lists $B(w)$, for all k-mers w in W.
- L is the data structure containing the branches that are currently active, that is, associated by the pkDB to at least one k-mer in the current window.

- $C[\,]$ is a table of counts, where $C[x]$ contains the number of k-mers in the current window that are associated by the pkDB to branch x.

Algorithm 1: SHERPAS, main algorithm (treatment of one query)

Input: A query with (ordered) windows $W_1, \ldots, W_N$, a pkDB B, a set of candidate branches E, a threshold θ

Output: For each window W_i, a strain P_i associated to W_i

set $C[x] = 0$ *for all branches* $x \in E$
set $L = \emptyset$, $W_0 = \emptyset$
for $i = 1$ *to* N **do**
  set $B_a = \biguplus B(w_a), w_a \in W_i \setminus W_{i-1}$ // B_a = branches added
  set $B_r = \biguplus B(w_r), w_r \in W_{i-1} \setminus W_i$ // B_r = branches removed
  for *all pairs* (x, s) *in* B_a **do**
    if $C[x] = 0$ **then**
      add x *at the end of* L
      set $S[x] = |W_{i-1}| \cdot \mathsf{Thr}_B$ //Set $S[x]$ to its minimum possible value
    $C[x]$ += 1
    $S[x]$ += $s - \mathsf{Thr}_B$
    UPDATE(L, x)
  for *all pairs* (x, s) *in* B_r **do**
    $C[x]$ += (-1)
    $S[x]$ += $\mathsf{Thr}_B - s$
    if $C[x] = 0$ **then**
      set $S[x] = -\infty$ // This causes the removal of x from L
    UPDATE(L, x)
  if $|W_i| \neq |W_{i-1}|$ **then**
    for *all branches* $x \in L$ **do**
      $S[x]$ += $\mathsf{Thr}_B \cdot (|W_i| - |W_{i-1}|)$ // Minimum possible value correction
  set P_i = GET_STRAIN(L, θ)
return $P_1, \ldots, P_N$

Sub-procedures UPDATE and GET_STRAIN are described in subsections 2.3 and 2.5, respectively.

2.3 Heap property and update

As mentioned in Sec. 2.1, L is a binary max-heap. We adopt here the standard practice to implement L as an array whose first element is $L[1]$ and whose last element is $L[|L|]$ [2]. Each of its elements $L[j]$ is a branch in E, and we ensure that L satisfies the *heap property*, that is, for all $j \in \{2, \ldots, |L|\}$, we have $S[L[\lfloor j/2 \rfloor]] \geq S[L[j]]$. We use this structure because it is computationally fast to update it when the score of an element of L changes (Algorithm 2), and because it ensures that at any time the following two properties are satisfied:

(i) The best-scoring branch is $L[1]$.

(ii) The second best-scoring branch is either $L[2]$ or $L[3]$, whichever has the greatest score.

In terms of computational complexity, each update is carried out in $O(\log |L|)$ time, and finding the two best scoring branches (which is what SHERPAS-full does) takes $O(1)$ time.

Algorithm 2: UPDATE(L, x) (subprocess of Algorithm 1)

Input: An array L satisfying the heap property for a score vector S. An element x of L whose score $S[x]$ was modified.

Output: The list L that satisfies the heap property for the new value of $S[x]$.

```
set j as the position of x in L
if S[x] = −∞ then
    set L[j] = L[|L|]
    remove the last element of L from L
set hp = 0
while hp = 0 do
    set p = ⌊j/2⌋
    set l = 2j, r = 2j + 1
    if S[L[j]] > S[L[p]] then
        swap the contents of L[j] and L[p]
        set j = p
    else if (l ≤ |L| and S[L[l]] > S[L[j]]) or (r ≤ |L| and S[L[r]] > S[L[j]]) then
        if l = |L| or S[L[l]] ≥ S[L[r]] then
            set b = l
        else
            set b = r
        swap the contents of L[j] and L[b]
        set j = b
    else
        set hp = 1
return L
```

2.4 Converting scores into likelihoods

To compare the scores of different branches, these scores must first be converted into numbers that can be interpreted as likelihoods or probabilities. Recall the definition of $S[x]$:

$$S[x] = \sum_{i=1}^{|W|} \log \widetilde{\mathbb{P}}[w_i|x]$$

Because $\widetilde{\mathbb{P}}[w_i|x]$ is defined as the product of the probabilities of the nucleotides in w_i at a given placement, the log-probability of each nucleotide in the sum above is usually counted k times (the only exception being the nucleotides near the ends of the window). Thus it makes sense

to: (i) divide $S[x]$ by k, and then (ii) convert the resulting log-probability into a probability. This leads to the following definition:

$$\ell_x = b^{S[x]/k}, \tag{5}$$

where b is the base of the logarithm (10 in current databases). We interpret ℓ_x as an approximation of the likelihood of x being the phylogenetic origin of the sequence in W.

A more detailed justification for definition (5) is developed in Annex B, where the assumptions behind the argument above are made explicit.

2.5 Producing the output

For any given window, procedure GET_STRAIN(L, θ) associates a classification (either a strain or N/A, which stands for *not assigned*) to that window on the basis of the contents of L. This involves converting the scores of the two best-scoring branches (SHERPAS-full) or all branches (SHERPAS-reduced) in L into likelihoods ℓ_x, in the way described in Sec. 2.4.

Algorithm 3: GET_STRAIN(L, θ) (subprocess of Algorithm 1)

Input: A max-heap L of branches for window W_i and a threshold θ
Output: A classification for window W_i

```
if full pkDB in use then
    set x_1 and x_2 to the best-scoring and the second best-scoring branch in L, resp.
    if x_1 and x_2 are assigned to the same strain or ℓ_{x_1}/ℓ_{x_2} ≥ θ then
        return the strain assigned to x_1
    else
        return N/A
else // reduced pkDB in use
    set r = ℓ_{L[1]} / Σ_{i=1}^{|L|} ℓ_{L[i]}
    if r ≥ θ then return the strain assigned to L[1]
    else return N/A
```

Given the output $P_1, \ldots, P_N$ of Algorithm 1, SHERPAS infers the breakpoints as follows. If for some $1 \leq i \leq N-1$, we have $P_i \neq P_{i+1}$, a breakpoint between a segment of origin P_i and a segment of origin P_{i+1} is placed between the middle point of the window W_i and the middle point of window W_{i+1}. Note that by construction of the windows, these two positions are always consecutive.

By default, if an unassigned (N/A) segment is inferred between two segments associated to the same strain X, the segment is then reassigned to strain X, and the breakpoints at its ends are removed. Note that this option can be deactivated by the user (see SHERPAS GitHub page).

2.6 Complexity analysis

We start by analyzing the computational complexity of processing a single query.

Each k-mer in the query is processed at most twice: once when it is added for the first time to the sliding window, and once when it is removed from it. Processing a k-mer means first retrieving $B(w)$ from the pkDB, and then, for each pair (x, s) in $B(w)$, updating $S[x]$, $C[x]$ and L (see again Algorithm 1 for notation). Assuming that k is a constant, the retrieval and inspection of each element in $B(w)$ takes $O(|B(w)|)$ time. The same holds for the update of $S[\cdot]$ and $C[\cdot]$, as each element of $B(w)$ involves $O(1)$ operations of update. As for the update of L following the change of one $S[x]$, very often this will involve no change, as the change in $S[x]$ is usually very small and thus it does not require any swap within the max-heap. However, the worst-case time complexity of updating L is $O(\log |L|)$. Since this needs to be repeated for many branches appearing in $B(w)$, the worst-case time complexity of processing a single k-mer w is $O(|B(w)| \log |L|)$. Now note that L can only contain candidate branches taken from E, and therefore $|L| \leq |E|$. The worst-case time complexity of processing a single k-mer w is therefore

$$O(|B(w)| \log |E|)$$

The above analysis covers the time spent executing most of the code within the **for** $i = 1$ to N loop in Algorithm 1, but it does not cover the part of the code within **if** $|W_i| \neq |W_{i-1}|$, nor the time spent executing GET_STRAIN. Whenever $|W_i| \neq |W_{i-1}|$ is true, SHERPAS updates the score of $O(|L|) = O(|E|)$ branches. But $|W_i| \neq |W_{i-1}|$ is only true for a constant number of windows (about 200 with default parameters), which means that the overall contribution to the running time of SHERPAS of this **if** clause is $O(|E|)$.

Finally, GET_STRAIN runs in $O(1)$ time for SHERPAS-full and $O(|E|)$ time for SHERPAS-reduced, because the calculation of the likelihood ratio requires reading the scores of 3 branches and $|L|$ branches for SHERPAS-full and SHERPAS-reduced, respectively. Now note that GET_STRAIN is called once for each window and that the number of windows is $O(|Q|)$, where $|Q|$ is the number of k-mers in the query Q. Therefore, the total contribution of GET_STRAIN to the running time of SHERPAS is $O(|Q|)$ and $O(|Q||E|)$ for SHERPAS-full and SHERPAS-reduced, respectively.

If we let $w_1, w_2, \ldots, w_{|Q|}$ be the sequence of k-mers that make up Q, then we can put together the observations of the last three paragraphs, and obtain an overall time complexity of

$$\begin{aligned} O(|E| + \sum_{i=1}^{|Q|} |B(w_i)| \log |E|) \quad & \text{for SHERPAS-full} \\ O(|Q||E| + \sum_{i=1}^{|Q|} |B(w_i)| \log |E|) \quad & \text{for SHERPAS-reduced} \end{aligned}$$

These expressions can be simplified: let $\bar{B}_Q$ denote the average size of $B(w)$ across all k-mers in Q. In other words, we have $|Q|\bar{B}_Q = \sum_{i=1}^{|Q|} |B(w_i)|$. This allows us to rewrite the complexities above:

$$\begin{aligned} O(|E| + |Q|\bar{B}_Q \log |E|) \quad & \text{for SHERPAS-full} \\ O(|Q||E| + |Q|\bar{B}_Q \log |E|) \quad & \text{for SHERPAS-reduced} \end{aligned}$$

Now note that while $\bar{B}_Q$ is usually very close to $|E|$ in SHERPAS-reduced (they are both small numbers), the same cannot be said in general for SHERPAS-full, where depending on

the pkDB (and to a lesser extent on the query Q), we may have $\bar{B}_Q \ll |E|$ (in which case we say that the pkDB is *sparse*) or $\bar{B}_Q \approx |E|$ (the pkDB is *dense*). Moreover, the number of candidate branches $|E|$ is very different for SHERPAS-full and SHERPAS-reduced. For SHERPAS-full, $|E| = O(|T_0|)$, where $|T_0|$ is any measure of the size of the reference tree (e.g. $|T_0| = |E(T_0)|$). For SHERPAS-reduced, $|E| = |R_0|$, where R_0 denotes the set of root branches in T_0. Because of these observations, we conclude the following worst-case time complexities for a single query Q:

$$\begin{aligned} O(|T_0|+|Q|\bar{B}_Q \log|T_0|) &\quad \text{for SHERPAS-full and a sparse pkDB} \\ O(|Q||T_0|\log|T_0|) &\quad \text{for SHERPAS-full and a dense pkDB} \\ O(|Q||R_0|\log|R_0|) &\quad \text{for SHERPAS-reduced, with } |R_0| \ll |T_0|. \end{aligned}$$

As for memory complexity, SHERPAS uses $O(|E|)$ space to store all the information on candidate branches, including $S[\cdot], C[\cdot]$ and L. In practice, most of the memory employed by SHERPAS is used to store the pkDB, which is proportional to $\sum_w |B(w)|$ and therefore also $O(|E|)$, with a very large multiplicative constant proportional to the number of phylo-k-mers. Although in theory $O(|Q|)$ space is used to store the query and the partial results $P_1, \ldots, P_N$, in practice this is dominated by the $O(|E|)$ term. Therefore the space complexity for SHERPAS is $O(|E|)$.

To extend the analyses above for multiple queries, for running times it suffices to add together the complexities for the single queries. Memory complexity remains $O(|E|)$.

3 Assumptions on the reference data

Below we discuss a number of assumptions that, ideally, the reference data should satisfy. As we will illustrate in the subsections below, many of these assumptions were violated to some extent in the experiments we report in the paper. This means that some negative effects that these violations may have on the accuracy of SHERPAS may already be accounted by the results that we reported. This makes us optimistic about the robustness of SHERPAS to such violations.

3.1 Accuracy of the reference tree

Like any other method based on a phylogenetic model, SHERPAS was developed assuming that the input phylogenetic tree is an accurate reflection of the evolutionary history of the sequences in the reference alignment. Violations of this assumption will result in phylo-k-mers having scores that do not reflect optimally their phylogenetic origin.

Although we have not investigated it extensively, we believe that SHERPAS should exhibit some robustness to the use of a reference tree containing a few errors. In fact, we believe that the trees that we used in our experiments are likely to contain a few differences with the reality, most notably because some ancestors of the reference sequences have probably undergone recombination. In this case *no* reference tree is an accurate description of the reality. We discuss the issue of hidden recombination in the next section.

The position of the root in the reference tree also has an influence on the pkDB construction step and on the scores of the phylo-k-mers. We refer the reader to the Supplementary Materials of the RAPPAS paper [11], where this point was discussed at length. For the purpose of recombination detection, the user should make sure that the root is placed outside the clades that are monophyletic with respect to the strains (see Sec. 3.4). Aside from that, it is definitely a good idea to place the root of the reference tree in a realistic position, but we do not think this will have a major influence on the accuracy of SHERPAS. In our experiments for HIV, we placed the root of the reference tree on the branch directly ancestral to strain O, which is probably not the correct position of the root for the reference tree.

3.2 Absence of recombination

A standard assumption of phylogeny-based methods for recombination detection is that the reference alignment is recombination-free, that is, none of the sequences in the alignment, nor their ancestors, have undergone recombination events. See for example the discussion on this point in the paper about SCUEAL [8]. However, other tools are inherently robust to the inclusion of some types of recombinants, as their models do not depend on a particular phylogenetic tree. For example this is the case for jpHMM. Being phylogeny-based, SHERPAS is closer to SCUEAL in this respect. However, we can expect that minor violations to the assumption that the alignment is recombination-free can be tolerated. We discuss the possible effect of a number of possible violations below.

First, it is likely that even in the reference alignments used by many phylogeny-based methods, sequences that are "pure" for one strain are in fact *intra*-strain recombinants. These recombinants —which are difficult to detect, as they involve recombination events between similar

sequences— are believed to be relatively frequent, for example in HIV [7] and HBV [12]. Including intra-strain recombinants in the reference alignment is probably not only inevitable, but also relatively innocuous for SHERPAS. This is because the errors it causes in the reference phylogeny will presumably only involve branches that are internal to one strain. These errors are likely to have a limited effect on the scores of some phylo-k-mers, and they should not cause the misclassification of a window in an incorrect strain. Note that most of our experiments with SHERPAS were done using the same reference alignments as jpHMM, which to the best of our knowledge were not screened to exclude intra-subtype recombinants.

Second, sometimes entire strains may be composed of recombinant sequences. This occurs when a recombination event was ancestral to a common ancestor of all the sequences in the strain. This is believed to be the case for *circulating recombinant forms* (CRFs), which are recombinant forms that have been observed in several unrelated individuals. A naïve approach to include sequences of a particular CRF in a reference alignment is to define a strain coinciding with that CRF. This is what we have done in the two HIV datasets for CRF01_AE, which is believed to be a recombinant between subtype A and a now extinct (or unsampled) subtype E. Setting a strain to a CRF allows users to recognize novel recombinants between that CRF and other strains.

However, the naïve approach above comes at a risk: the true evolutionary history of the reference sequences involves at least one reticulation ancestral to the CRF, meaning that the reference tree —whatever it is— will definitely not be correct in the part ancestral to that CRF. We do not know how strong the effect of using such an incorrect tree is, but it is probably more important than the effect of including intra-strain recombinants. For this reason, with the exception of CRF01_AE, we have avoided the inclusion of CRFs in the reference alignment, and we advise users to do the same. In the HIV-genome dataset we have noticed that SHERPAS appears to have some difficulties distinguishing CRF01_AE from strain A1 (this can be observed for example in queries 18, 51, 65 in Section C below), which is related to the fact that the relative position of CRF01_AE and the A strains within the reference tree is probably erroneous for at least part of the reference alignment. In the next subsection we discuss how an advanced user may include CRFs in the reference alignment in a clever way, which addresses in a satisfactory way the problems above.

Third, some sequences may be erroneously annotated as belonging to one strain, but in fact they are *inter*-strain recombinants. Compared to the other cases discussed above, these are definitely the recombinants that may cause the most serious disruption to the accuracy of SHERPAS —and of other methods too, including jpHMM and SCUEAL. **Users should always make sure that the reference alignment only contains sequences that are "pure" with respect to the input strains.** In our experiments, we have always used the reference alignments that were distributed with either jpHMM or SCUEAL.

3.3 Dealing with circulating recombinant forms

Including CRFs in the reference alignment and assigning them to strains labelled by the CRF identifier is attractive from a practical point of view because it may allow users of SHERPAS to (1) recognize if a sequence is a CRF and (2) detect novel recombinants between a CRF and another strain. However, as explained above, the naïve way of doing so is probably not a good idea, as the reference tree will contain some large-scale differences with the reality.

If tasks (1) and (2) are important to a user, there is a relatively simple way of solving this problem, which we explain below.

This idea was already explained, among others, by Sergei Kosakovsky Pond and coauthors [8] and Darren Martin (personal communication). It exploits the fact that, because CRFs have been the object of several analyses, their recombinant structure is well-known, including the (sometimes approximate) position of breakpoints. This means that any CRF sequence can be decomposed into subsequences that are "pure" with respect to their strains. For example in HIV-1, the sequences tagged as CRF03_AB have mosaic structure ABA with the central B segment starting at site 2688 and ending at site 8649 [10]. In this case, every sequence x from CRF03_AB should be decomposed into the following two sequences prior to their inclusion in the reference alignment: x_A, which is identical to x, except for positions 2688-8649 which are replaced by a long stretch of gaps; and x_B, a sequence that has gaps up to position 2687, then coincides with x from position 2688 to 8649, and finally has gaps up to the last position of x. These two sequences can then be assigned to strain CRF03_AB. Note that x_A and x_B have different phylogenetic origins within the reference tree, with x_A likely to be found near subtype A and x_B likely to be found near subtype B. In fact all the sequences obtained as x_A from some sequence x from CRF03_AB should form a clade, and the same holds for all sequences obtained as x_B.

In general, if we subdivide each reference sequence from a CRF into its non-recombinant components, then it is not a problem anymore to represent the evolution of the reference sequences with a phylogenetic tree. The strain corresponding to a CRF will be partitioned in as many sub-strains as there are parental sequences for that CRF, and generally each of these sub-strains will form a separate clade in the reference tree. Since SHERPAS is able to deal with strains that are polyphyletic (see next section), it can be used on the pkDB constructed above without modification.

3.4 Monophyly of the strains

Since strains are usually defined either using phylogenetic criteria or by adopting appropriate thresholds for intra-strain similarity, we expect them to be usually monophyletic, meaning that each strain should correspond to a separate clade in the reference tree. In fact it is always a good idea for users of SHERPAS to check that most strains are monophyletic after they reconstructed, or downloaded, the reference tree. A few exceptions to this rule are acceptable, for example when (1) an "artificial" strain is designed to contain all reference sequences that are not in a strain of interest, or (2) the user knows that the strain is not monophyletic, yet it makes sense to define it as a single strain. As an example of (2), in our experiments on HIV, we used a strain named CPZ to include all SIV (simian immunodeficiency virus) sequences from chimpanzees, which are expected to be polyphyletic. For another example of why (2) may be useful, see Sec. 3.3 above.

Because of the possible exceptions to monophyly, SHERPAS was designed to tolerate the inclusion of polyphyletic strains. However, this will have some subtle effects on the behavior of SHERPAS, which may differ depending on the version (full/reduced) of the pkDB used. Specifically, the presence of polyphyletic strains increases the number of branches that are unassigned (not assigned to any strain) in SHERPAS-full and increases the number of root branches in SHERPAS-reduced. Although our experiments did include a few polyphyletic

strains (3 in HIV-pol and 2 in HIV-genome, including CPZ), we do not have enough perspective to describe their effect on the analysis. Because of this, we believe that they should be used with caution.

4 Site-wise measures of accuracy

Here we show some simple mathematical relationships between the site-wise sensitivity and precision defined in the Materials and Methods of the paper, and strain-specific definitions of sensitivity and precision, which are standard in multi-class classification literature.

Let n be the number of strains. For ease of notation, we associate each strain to one integer from 1 to n, whereas we associate integer $n+1$ to the "unassigned" status.

We define the *confusion matrix* as an $n \times (n+1)$ matrix $M = (m_{ij})$, where m_{ij} is the number of sites whose correct strain is i and that were classified as j.

The following two definitions are standard in multi-class classification.

- The *sensitivity for strain* i ($1 \leq i \leq n$) is the proportion of sites that are classified as i, out of all sites whose correct strain is i. That is, in terms of the confusion matrix:

$$\text{sensitivity}_i = \frac{m_{ii}}{\sum_{j=1}^{n+1} m_{ij}}.$$

- The *precision for strain* i ($1 \leq i \leq n$) is the proportion of sites whose correct strain is i, out of all sites that are classified as i. That is, in terms of the confusion matrix:

$$\text{precision}_i = \frac{m_{ii}}{\sum_{j=1}^{n} m_{ji}}.$$

The following two definitions are the ones that we gave in the paper.

- The *site-wise sensitivity* is the proportion of sites that are classified in their correct strain, out of all sites. That is, in terms of the confusion matrix:

$$\text{site-wise sensitivity} = \frac{\sum_{i=1}^{n} m_{ii}}{\sum_{i=1}^{n} \sum_{j=1}^{n+1} m_{ij}}.$$

- The *site-wise precision* is the proportion of sites that are classified in their correct strain, out of all sites that are classified in some strain other than $n+1$. That is, in terms of the confusion matrix:

$$\text{site-wise precision} = \frac{\sum_{i=1}^{n} m_{ii}}{\sum_{i=1}^{n} \sum_{j=1}^{n} m_{ij}}.$$

The two pairs of definitions above are linked in an intuitive way by the following two propositions.

Proposition 1. *The site-wise sensitivity is the weighted average of the strain-specific sensitivities, where the weight for strain i is proportional to the number of sites whose correct strain is i.*

Proof. The weight w_i for class i is proportional to $\sum_{j=1}^{n+1} m_{ij}$. Since the sum of weights in a weighted average is 1, we have:

$$w_i = \frac{1}{S} \sum_{j=1}^{n+1} m_{ij},$$

where

$$S = \sum_{i=1}^{n} \sum_{j=1}^{n+1} m_{ij}.$$

Then, the weighted average in the statement is given by:

$$\begin{aligned} \sum_{i=1}^{n} w_i \cdot \text{sensitivity}_i &= \sum_{i=1}^{n} \left(\frac{1}{S} \sum_{j=1}^{n+1} m_{ij} \right) \cdot \frac{m_{ii}}{\sum_{j=1}^{n+1} m_{ij}} \\ &= \frac{1}{S} \sum_{i=1}^{n} m_{ii} \\ &= \text{site-wise sensitivity.} \end{aligned}$$

□

Proposition 2. *The site-wise precision is the weighted average of the strain-specific precisions, where the weight for strain i is proportional to the number of sites that are classified as i.*

Proof. The weight w_i' for class i is proportional to $\sum_{j=1}^{n} m_{ji}$. Since the sum of weights in a weighted average is 1, we have:

$$w_i' = \frac{1}{S'} \sum_{j=1}^{n} m_{ji},$$

where

$$S' = \sum_{i=1}^{n} \sum_{j=1}^{n} m_{ji}.$$

Then, the weighted average in the statement is given by:

$$\begin{aligned} \sum_{i=1}^{n} w_i' \cdot \text{precision}_i &= \sum_{i=1}^{n} \left(\frac{1}{S'} \sum_{j=1}^{n} m_{ji} \right) \frac{m_{ii}}{\sum_{j=1}^{n} m_{ji}} \\ &= \frac{1}{S'} \sum_{i=1}^{n} m_{ii} \\ &= \text{site-wise precision.} \end{aligned}$$

□

5 Dataset construction, data availability, and reproducibility

Here we describe a number of details about the construction of the datasets behind the experiments presented in the main text. We also provide the information necessary for their reproducibility. All relevant files that do not belong to a third party can either be downloaded from the SHERPAS GitHub repository at https://github.com/phylo42/sherpas or from the Dryad dataset distributed with this paper (link provided on the GitHub README page).

5.1 Preprocessing

The operations necessary prior to the execution of SHERPAS —i.e. the construction of the reference tree, of the phylo-k-mer database, and of the sequences-to-strains mapping— were the same for all the datasets. We briefly describe them here.

Reference trees were constructed from the reference alignments (dataset-specific, see below) using PhyML 3.3.20180214 [5] using GTR+Γ+I as nucleotide substitution model. A discrete Γ distribution with 4 rate categories (the default in PhyML) was used to model rate variation across sites. The proportion of invariant sites was estimated from the alignment, as well as the shape parameter α (the latter is done by default by PhyML). The resulting reference trees are included in the Dryad dataset. PhyML was run with the following command:

```
phyml -i <reference_alignment> -m GTR -v e
```

The pkDBs were constructed using RAPPAS2 v0.1.3a, using parameter $k = 10$ (which is not the default value) and threshold parameter $\omega = 1.5$ (the default). (See also Sec. 1.3 above for the meaning of the ω parameter.) The resulting pkDBs are included in the Dryad dataset (`.rps` files). RAPPAS2 was run with the following command:

```
python3 rappas2.py build -s nucl -b <path_to_phyml> -w <output_directory>
       -r <reference_alignment> -t <reference_tree> -m GTR -k 10
```

Finally, the `.csv` files mapping reference sequences to strains were constructed manually, using the information contained in the name of each sequence, to infer the strain it belongs to. These files are also included in the Dryad dataset.

5.2 HIV-pol

References. The reference alignment that we used for SHERPAS is the one provided with SCUEAL (167 sequences), and is available at https://github.com/spond/SCUEAL/blob/master/data/pol2009.nex. (Accessed October 2019.)

Queries. The 10,000 synthetic queries and the output of SCUEAL for these queries are accessible here: http://www.hyphy.org/pubs/SCUEAL/SCUEAL%20Files_files/Shuffled.zip. (Accessed October 2019.) Note that none of the queries contains fragments from strains A3, AE, O, CPZ, although these strains are present in the reference alignment. All other strains in the reference alignment are present in some queries.

Running SHERPAS. The reference tree reconstructed from the reference alignment, the .csv file recording the classification of the sequences in the reference alignment, and the .rps file encoding the pkDB for this dataset are available in the `pkDB-HIV-pol` directory within the Dryad dataset.

SHERPAS was executed with the following command:

```
SHERPAS -o out/ -d pkDB-HIV-pol/DB_k10_o1.5.rps
        -q HIV_pol/queries.fasta -g pkDB-HIV-pol/ref-groups.csv
```

Running jpHMM. jpHMM was executed with default parameters for HIV sequences, with the following command:

```
./jpHMM -s HIV_pol/queries.fasta -v HIV
```

It was also executed with the `-Q blat` option for speed-up. Out of the several files produced by jpHMM, the output file that was used to read the predictions made by jpHMM is `recombination.txt`.

Note that on this dataset the reference alignment used by jpHMM does not coincide with that used by the other methods. Moreover, as discussed in the main text, strains A and N cannot be recognized by jpHMM, which has a slightly negative impact on jpHMM's accuracy measures on this dataset.

In order to understand how strong this impact is, we also analyzed the results of jpHMM under the assumptions that returning A1 or A2 is correct when A is the true strain, and that CPZ is correct when N is the true strain. In this case, jpHMM returns 92.9% matches, 0% supersets and 6.9% subsets, and its sensitivity and precision equal 99.3%.

5.3 HBV-genome

References. We used the reference alignment that is distributed with jpHMM. It can be downloaded at `http://jphmm.gobics.de/download.html`, and is located at `jpHMM/input/HBV_alignment.fas`. (Accessed December 2019.) This alignment contains 339 whole-genome sequences classified into strains A, B, C, D, E, F, G, H. Prior to the construction of the pkDB for SHERPAS, we extended this reference alignment by copying the first $k - 1 = 9$ columns of the alignment to the end of the alignment. This allows the construction of phylo-k-mers (with $k = 10$) from positions that overlap with the artificial end of the alignment.

Queries. We downloaded the dataset for nucleotide sequence genomes of "genotype all" from the HBVdb website at `https://hbvdb.ibcp.fr/HBVdb/HBVdbDataset?view=/data/nucleic/alignments/all_Genomes.clu&seqtype=0`. (Accessed December 2019.) This alignment contained 7273 sequences, from which we removed 794 sequences marked as recombinant and 273 sequences that belonged to the jpHMM reference alignment. We also removed 1664 sequences that were estimated to be recombinant by both jpHMM and SHERPAS (in fact some of these turn out to be known recombinants [12]).

The remaining 4542 sequences are the pre-queries that were used as a basis to build 3000 recombinant queries. Out of these 3000 queries, 2000 combine fragments from two pre-queries, and 1000 are based on three pre-queries. To generate each query, we proceeded as follows. First, the 2 or 3 pre-queries are chosen at random from the 4542, making sure that they belong to different strains. Second, we picked $2X$ random coordinates within the alignment of pre-queries, where $X \geq 1$ is chosen following a geometric distribution with parameter $p = 0.8$. The coordinates are chosen uniformly at random, making sure that no two coordinates are less that 100 positions apart (circularity-wise). This is the same minimal distance that was applied to build the dataset of queries for HIV-pol [8]. Third, each query is built by combining segments extracted from the selected pre-queries and delimited by the random coordinates.

The parameters that we used in the construction procedure above were chosen so as to loosely reflect the characteristics of inter-genotype HBV recombinants presented in a recent overview [1]. For example, about 80% of the recombinants involving 2 genotypes in Fig. 2 of that review only have 2 breakpoints, hence the choice of $p = 0.8$.

The queries are available here: https://github.com/phylo42/sherpas/blob/master/examples/HBV_all/queries-3000.fasta.

Running SHERPAS. The reference tree reconstructed from the reference alignment, the .csv file recording the classification of the sequences in the reference alignment, and the .rps file encoding the pkDB for this dataset are available in the `pkDB-HBV-full` directory within the Dryad dataset (link above).

SHERPAS was executed using the option `-c` (for circular queries) with the following command:

```
SHERPAS -o out/ -d pkDB-HBV-full/DB_k10_o1.5.rps
        -q HBV_all/queries-3000.fasta -g pkDB-HBV-full/ref-groups.csv -c
```

Running jpHMM. jpHMM was executed using the option `-C` (for circular queries):

```
./jpHMM -s HBV_all/queries-3000.fasta -v HBV -C
```

Note that the `-C` option automatically activates the `-Q blat` option. Out of the several files produced by jpHMM, the output file that was used to read the predictions made by jpHMM is `recombination.txt`.

5.4 HIV-genome

References. The reference alignment was obtained as part of the jpHMM package which can be downloaded here: http://jphmm.gobics.de/download.html, and is located at `jpHMM/input/HIV_alignment.fas`. (Accessed December 2019.) This alignment contains 881 whole-genome sequences, classified in the following 14 strains: A1, A2, AE, B, C, D, F1, F2, G, H, J, K, O, CPZ.

Queries. We downloaded the Los Alamos Web alignment 2018 available at https://www.hiv.lanl.gov/content/sequence/NEWALIGN/align.html (accessed January 2020), using the following parameters. *Alignment type*: Web alignment (all complete sequences). *Year*: 2018. *Organism*: HIV-1/SIVcpz. *DNA/Protein*: DNA. *Region*: genome. *Subtype*: ALL. *Format*: FASTA. *Alignment ID*: 118AG1. This alignment consisted of 4004 sequences, from which we removed 1328 sequences that do not belong to any of the 14 strains above (CRFs other than CRF01_AE, see Sec. 3.3 above), and also removed 803 sequences that are present in the jpHMM reference alignment. Finally, we removed 27 sequences that were identified as recombinant by both jpHMM and SHERPAS.

We constructed 3000 synthetic recombinant sequences from the remaining 1846 pre-queries. For each of the 3000 sequences, we started by drawing $X \geq 1$ and $Y \geq 1$ from geometric distributions with parameters 0.2 and 0.8 respectively, discarding any pair with $X < Y$. X and $Y + 1$ represent the number of breakpoints in the query and the number of pre-queries involved, respectively. We picked X coordinates within the alignment of pre-queries using a uniform distribution, making sure that no two coordinates are less that 100 sites apart and no coordinate is less than 100 sites away from one end of the query. We also drew $Y + 1$ pre-queries at random, making sure that at least two of these pre-queries are from different strains. Finally, we built a query sequence by inserting, between each pair of consecutive coordinates, the corresponding segment in one of the selected pre-queries, making sure that the pre-queries chosen for any two consecutive intervals are different. The length of the resulting queries is on average 8.9 kbp, and it ranges from 5.5 kbp to 9.9 kbp. The longest queries are obtained from pre-queries whose length is close to 1 Mbp (which are common e.g. in group O or when sampled from chimpanzees).

The queries are available at https://github.com/phylo42/sherpas/blob/master/examples/HIV_all/queries-C.fasta.

Running SHERPAS. The reference tree reconstructed from the reference alignment, the .csv file recording the classification of the sequences in the reference alignment, and the .rps file encoding the pkDB for this dataset are available in the `pkDB-HIV-full` directory within the Dryad dataset (link above).

SHERPAS was executed with the following command:

```
SHERPAS -o out/ -d pkDB-HIV-full/DB_k10_o1.5.rps
        -q HIV_all/queries-C.fasta -g pkDB-HIV-full/ref-groups.csv
```

Running jpHMM. jpHMM was executed with default parameters for HIV sequences:

```
./jpHMM -s HIV_all/queries-C.fasta -v HIV
```

It was also executed with the `-Q blat` option for speed-up. Out of the several files produced by jpHMM, the output file that was used to read the predictions made by jpHMM is `recombination.txt`.

5.5 HIV Nanopore reads dataset

References. The reference alignment, the reference tree and the pkDB are the same as in the HIV-genome dataset.

Queries. We ran NanoSim-H (v1.1.0.4) on the queries from the HIV-genome dataset using the following command:

```
nanosim-h HIV_all/queries-C.fasta -n 100000 -o reads-C.fasta -u 0.0 --max-
    len 9000 --min-len 1000
```

This generates 100,000 reads, each one from a random query of the HIV-genome dataset. For each one of these sequences, we picked the first (in order of appearance) read in the forward strand that comes from that sequence. The resulting queries are available at https://github.com/phylo42/sherpas/blob/master/examples/HIV_all/reads-C.fasta.

Running SHERPAS and jpHMM. The same commands as for the HIV-genome dataset were used here (replace the name of the file containing the queries). The execution of jpHMM with the `-Q blat` option aborted.

5.6 Experiment on the specificity/recall trade-off

Measures of accuracy. Given a binary classifier $\mathcal{C}$ for the detection of inter-strain recombinant sequences, and a collection of query sequences, we define:

TP (*true positives*): the number of queries that are both inter-strain recombinants and classified as such by $\mathcal{C}$.

FP (*false positives*): the number of queries that are erroneously classified by $\mathcal{C}$ as inter-strain recombinants.

FN (*false negatives*): the number of queries that are inter-strain recombinants, but not classified as such by $\mathcal{C}$.

TN (*true negatives*): the number of queries that are neither inter-strain recombinants, nor classified as such by $\mathcal{C}$.

Recall (also known as *true positive rate* or *sensitivity*): out of all inter-strain recombinant queries, the proportion that are recognized as such by $\mathcal{C}$. That is, Recall $= \frac{\mathrm{TP}}{\mathrm{TP+FN}}$.

Specificity (also known as *true negative rate*): out of all queries that are *not* inter-strain recombinants, the proportion that are not classified as inter-strain recombinants. That is, Specificity $= \frac{\mathrm{TN}}{\mathrm{TN+FP}}$.

Dataset. Among the 10,000 queries in the HIV-pol dataset, there are 2374 queries that are not inter-strain recombinants. Thus this dataset provides a way to compute not only the recall of a classifier, but also its specificity. Moreover, on this dataset, the results of running SCUEAL were made available by the authors [8], which allows us to compare the results of SHERPAS to those of jpHMM *and* SCUEAL. Since jpHMM is not designed to recognize sequence fragments labelled as A or N, for this experiment we removed all queries from the initial 10,000 that were obtained from sequences from these two strains. This ensures that all classifiers compete on an equal ground, and leaves us with 7652 queries, of which 5317 are inter-strain recombinants.

Classifiers. For all tested programs, a query is classified as an inter-strain recombinant if and only if the partition produced by the program contains regions from 2 or more different strains. jpHMM was run with and without the `-Q blat` option, but the results were virtually indiscernible. SHERPAS-full was run for all combinations of window size in $\{300, 500\}$ and threshold parameter $\theta_F \in \{1, 2, 5, 10, 20, 50, 100, 200, 500, 1000\}$. SHERPAS-reduced was run for all combinations of window size in $\{300, 500\}$ and threshold parameter $\theta_R \in \{0, 0.5, 0.75, 0.9, 0.95, 0.975, 0.99, 0.995, 0.9975, 0.999\}$.

Discussion of the results. Results of this experiment are reported in Fig. 2 of the main text. A number of observations can be made here. First, while SCUEAL and jpHMM result in good (Pareto-optimal) combinations of specificity and recall, it is interesting to note that on this dataset jpHMM has better (100%) specificity, while SCUEAL has better recall. Previously reported results on other datasets do not appear to confirm this observation [13], but this is not surprising because those results were on a different but related classification problem, namely typing whole sequences, i.e. assigning them to their strain of origin. Moreover SCUEAL implements a non-deterministic optimization heuristic, with better results expected if SCUEAL is left to run for longer times.

As for SHERPAS, window size has a clear effect, with small windows favoring recall, and larger windows favoring specificity. This is consistent with the results in Tables 2 – 5 in the main text, where smaller window sizes are generally associated with more fragmented mosaics. Interestingly the threshold θ_R has a very strong control over the trade-off between recall and specificity in SHERPAS-reduced, with small values of θ_R causing very high recall, and large θ_R causing very high specificity. This is not the case for SHERPAS-full, where θ_F only has a limited effect on specificity and recall.

This difference in the behaviors of SHERPAS-reduced and SHERPAS-full can be understood by considering again the way these algorithms use their respective thresholds (see Sec. 2.5 above, and Algorithm 3). Consider the case where a region of the query has weak evidence for belonging to strain X. While θ_R entirely controls whether X is present in the partition produced by SHERPAS-reduced, θ_F only plays a role in determining the output of SHERPAS-full if the two best-scoring branches are from different strains. If the two best-scoring branches in SHERPAS-full are both from X, then X will be present in the output partition, irrespective of the value of the threshold. This is why the specificity for SHERPAS-full cannot be increased up to 100% by increasing its threshold.

Coming back to the question that motivated this experiment —namely the use of SHERPAS as a first screening tool for inter-strain recombinants— finally note that very high recall can be

achieved with both SHERPAS-reduced and SHERPAS-full by using small window sizes and low thresholds. On this dataset, these parameter settings result in recall that is substantially higher than jpHMM, and at least as good as SCUEAL (up to 99.0% for SHERPAS-full, and up to 99.4% for SHERPAS-reduced, vs. 98.8% for SCUEAL), for a fraction of their running times.

References

[1] Natalia M Araujo. Hepatitis B virus intergenotypic recombinants worldwide: an overview. *Infection, Genetics and Evolution*, 36:500–510, 2015.

[2] Thomas H Cormen, Charles E Leiserson, Ronald L Rivest, and Clifford Stein. *Introduction to Algorithms*. MIT press, 2009.

[3] Joseph Felsenstein. Maximum likelihood and minimum-steps methods for estimating evolutionary trees from data on discrete characters. *Systematic Biology*, 22(3):240–249, 1973.

[4] Joseph Felsenstein. Evolutionary trees from DNA sequences: a maximum likelihood approach. *Journal of Molecular Evolution*, 17(6):368–376, 1981.

[5] Stéphane Guindon, Jean-François Dufayard, Vincent Lefort, Maria Anisimova, Wim Hordijk, and Olivier Gascuel. New algorithms and methods to estimate maximum-likelihood phylogenies: assessing the performance of PhyML 3.0. *Systematic Biology*, 59(3):307–321, 2010.

[6] Stéphane Guindon and Olivier Gascuel. A simple, fast and accurate algorithm to estimate large phylogenies by maximum likelihood. *Systematic Biology*, 52:696–704, 2003.

[7] Ireen E Kiwelu, Vladimir Novitsky, Lauren Margolin, Jeannie Baca, Rachel Manongi, Noel Sam, John Shao, Mary F McLane, Saidi H Kapiga, and M Essex. Frequent intra-subtype recombination among HIV-1 circulating in Tanzania. *PLoS One*, 8(8), 2013.

[8] S. L. Kosakovsky Pond, D. Posada, E. Stawiski, C. Chappey, A. F. Poon, G. Hughes, E. Fearnhill, M. B. Gravenor, A. J. Leigh Brown, and Frost S. D. An evolutionary model-based algorithm for accurate phylogenetic breakpoint mapping and subtype prediction in HIV-1. *PLoS Computational Biology*, 5(11):e1000581, 2009.

[9] Alexey M Kozlov, Diego Darriba, Tomáš Flouri, Benoit Morel, and Alexandros Stamatakis. RAxML-NG: a fast, scalable and user-friendly tool for maximum likelihood phylogenetic inference. *Bioinformatics*, 35(21):4453–4455, 2019.

[10] Kirsi Liitsola, Kirsi Holm, Aleksei Bobkov, Vadim Pokrovsky, Tatjana Smolskaya, Pauli Leinikki, Saladin Osmanov, and Mika Salminen. An AB recombinant and its parental HIV type 1 strains in the area of the former soviet union: low requirements for sequence identity in recombination. *AIDS Research and Human Retroviruses*, 16(11):1047–1053, 2000.

[11] Benjamin Linard, Krister Swenson, and Fabio Pardi. Rapid alignment-free phylogenetic identification of metagenomic sequences. *Bioinformatics*, 35(18):3303–3312, 2019.

[12] Anna L McNaughton, Peter A Revill, Margaret Littlejohn, Philippa C Matthews, and M Azim Ansari. Analysis of genomic-length HBV sequences to determine genotype and subgenotype reference sequences. *Journal of General Virology*, 101(3):271–283, 2020.

[13] Andrea-Clemencia Pineda-Peña, Nuno Rodrigues Faria, Stijn Imbrechts, Pieter Libin, Ana Barroso Abecasis, Koen Deforche, Arley Gómez-López, Ricardo J Camacho, Tulio de Oliveira, and Anne-Mieke Vandamme. Automated subtyping of HIV-1 genetic sequences for clinical and surveillance purposes: performance evaluation of the new rega version 3 and seven other tools. *Infection, Genetics and Evolution*, 19:337–348, 2013.

[14] Ziheng Yang. *Computational Molecular Evolution*. Oxford University Press, 2006.

A Annex: Marginal posterior distributions of ancestral states

Ancestral state reconstruction is a wide subject in phylogenetics. As explained in Section 1.2, constructing phylo-k-mers and calculating their probability scores relies on a specific technique for ancestral reconstruction: the calculation of the marginal posterior distribution of $A'_{u,i}$. (Recall that $A'_{u,i}$ represents the random nucleotide at node u in the extended reference tree, homologous to site i in alignment A.)

Here, we describe how this calculation is performed by standard software for phylogenetic inference (e.g. PhyML [6]) using the notation introduced in Section 1.2. More information can be found in many phylogenetics textbooks (e.g. [14, Chapter 4.4]).

Let $A_{*,i}$ denote the ith column of A. Because of the assumption of independent evolution at different sites, the probability that we seek to calculate only depends on the data in $A_{*,i}$. That is,

$$\mathbb{P}[A'_{u,i} = a \mid A, \theta] \quad = \quad \mathbb{P}[A'_{u,i} = a \mid A_{*,i}, \theta]. \tag{6}$$

The first ingredient to derive the probability above is the probability of the data in $A_{*,i}$, given $A'_{u,i} = a$, that is

$$\mathbb{P}[A_{*,i} \mid A'_{u,i} = a, \theta]. \tag{7}$$

This is sometimes referred to as a *partial likelihood* and can be obtained for every $a \in \{\mathtt{A}, \mathtt{C}, \mathtt{G}, \mathtt{T}\}$ by using Felsenstein's pruning algorithm [3, 4] on the extended reference tree T rooted in u.

The other ingredient is the prior distribution of $A'_{u,i}$, which is simply given by

$$\mathbb{P}[A'_{u,i} = a \mid \theta] = \pi_a \tag{8}$$

where $(\pi_{\mathtt{A}}, \pi_{\mathtt{C}}, \pi_{\mathtt{G}}, \pi_{\mathtt{T}})$ is the stationary distribution implied by the substitution model. (E.g. for the Jukes-Cantor model all $\pi_a = 1/4$, while for many other models the π_a are parameters included in θ.)

Given the probabilities in (7) and (8), the probability in (6) can be obtained as

$$\mathbb{P}[A'_{u,i} = a \mid A_{*,i}, \theta] = \frac{\mathbb{P}[A'_{u,i} = a, A_{*,i} \mid \theta]}{\mathbb{P}[A_{*,i} \mid \theta]} = \frac{\mathbb{P}[A'_{u,i} = a \mid \theta] \cdot \mathbb{P}[A_{*,i} \mid A'_{u,i} = a, \theta]}{\sum_{a' \in \{\mathtt{A},\mathtt{C},\mathtt{G},\mathtt{T}\}} \mathbb{P}[A'_{u,i} = a' \mid \theta] \cdot \mathbb{P}[A_{*,i} \mid A'_{u,i} = a', \theta]}.$$

B Annex: Approximate relationship between branch scores and likelihoods

Here we show that, under many simplifying assumptions, the quantity

$$\ell_x = b^{S[x]/k} \tag{9}$$

is approximately proportional to the likelihood of x being the phylogenetic origin of the sequence in the current window W. Since the assumptions are very strong, we only expect this relationship to hold in the limit, as the assumptions get closer and closer to being verified. Even if the assumptions are never verified in practice, this result provides a justification for the way SHERPAS converts scores into likelihoods. The text below shows the details of the reasoning behind (9) and its assumptions.

Let $a_1 a_2 \ldots a_{m_W}$ be the nucleotide sequence in the current window W, where $m_W = |W|+k-1$. We use here the notation introduced in Section 2.1, where the ith k-mer in W is $w_i = a_i a_{i+1} \ldots a_{i+k-1}$.

Our first assumption is that $a_1 a_2 \ldots a_{m_W}$ unequivocally aligns to a stretch of contiguous sites, going from site $s_W + 1$ to site $s_W + m_W$. In fact we also assume that k is long enough for every k-mer w_i to align unequivocally to the k sites starting from $s_W + i$.

Now recall that $x \in E(T_0)$ denotes a branch of the reference tree and define tree T_x as the tree that is obtained from T_0 by attaching a ghost branch to the midpoint of x, where v_x is the new ghost leaf (see Figure 1). Finally, we place sequence $a_1 a_2 \ldots a_{m_W}$ at leaf v_x.

We can then define the likelihood of x being the phylogenetic origin of W as the likelihood of tree T_x, which we can then develop following standard phylogenetic calculations based on rooting T_x at leaf v_x. Using the notation introduced in Section 1.2 and Annex A, we get:

$$\begin{aligned}
\mathrm{Lik}(T_x) &= \prod_{j=1}^{m_W} \mathbb{P}[\, A_{*,s_W+j} \mid A'_{v_x,s_W+j} = a_j \,,\, \theta \,] \cdot \pi_{a_j} \\
&= \prod_{j=1}^{m_W} \mathbb{P}[\, A'_{v_x,s_W+j} = a_j \mid A_{*,s_W+j} \,,\, \theta \,] \cdot \mathbb{P}[A_{*,s_W+j} \mid \theta] \\
&= \mathrm{const} \cdot \prod_{j=1}^{m_W} \mathbb{P}[A'_{v_x,s_W+j} = a_j \mid A_{*,s_W+j}, \theta]
\end{aligned}$$

where const is a constant that does not depend on x. The result above simply states that, as we vary x, the likelihood of T_x is directly proportional to the posterior probability of having $a_1 a_2 \ldots a_{m_W}$ at leaf v_x and at sites $s_W + 1$ to $s_W + m_W$.

Now define $p_j(x)$ as the posterior probability of having a_j at leaf v_x and site s_W+j, i.e. $p_j(x) = \mathbb{P}[A'_{v_x,s_W+j} = a_j \mid A_{*,s_W+j}, \theta]$. This allows us to express $\mathrm{Lik}(T_x)$ compactly:

$$\mathrm{Lik}(T_x) = \mathrm{const} \cdot \prod_{j=1}^{m_W} p_j(x) \tag{10}$$

Now consider $\widetilde{\mathbb{P}}[w_i|x]$, defined in (3) as $\widetilde{\mathbb{P}}[w_i|x] = \max_{u \in G_x} \max_j \mathbb{P}[\, S_{u,j} = w_i \mid A, \theta \,]$. Since w_i aligns to the k sites starting from $s_W + i$, and assuming that the probabilities associated

to different nodes $u \in G_x$ are approximately equal, we have that

$$\widetilde{\mathbb{P}}[w_i|x] \approx \mathbb{P}[\, S_{v_x, s_W+i} = w_i \mid A, \theta\,] = \prod_{h=0}^{k-1} \mathbb{P}[A'_{v_x, s_W+i+h} = a_{i+h} \mid A, \theta].$$

Recall that, because sites are assumed to be independent, the posterior probabilities at a site only depend on the data at that same site. This implies

$$\widetilde{\mathbb{P}}[w_i|x] \approx \prod_{h=0}^{k-1} \mathbb{P}[A'_{v_x, s_W+i+h} = a_{i+h} \mid A_{*, s_W+i+h}, \theta] = \prod_{h=0}^{k-1} p_{i+h}(x).$$

Now combine the equation above to the definition of SHERPAS's scores (Eqn. (4), page 7):

$$S[x] = \log \prod_{i=1}^{|W|} \widetilde{\mathbb{P}}[w_i|x] \;\approx\; \log \prod_{i=1}^{|W|} \prod_{h=0}^{k-1} p_{i+h}(x)$$
$$= \log \Big(p_1(x)^1 \cdot p_2(x)^2 \cdots p_k(x)^k \cdot p_{k+1}(x)^k \cdots p_{|W|}(x)^k \cdot p_{|W|+1}(x)^{k-1} \cdots p_{|W|+k-2}(x)^2 \cdot p_{|W|+k-1}(x)^1 \Big)$$

By changing the first and last $k-1$ terms in the product above, so that all terms have exponent k or 0, we obtain the following bounds:

$$\log \prod_{j=1}^{m_W} p_j(x) \lesssim \frac{S[x]}{k} \lesssim \log \prod_{j=k}^{|W|} p_j(x) \tag{11}$$

Compare this result to (10) and note that both the lower and the upper bound in (11) can be interpreted as log-likelihoods (albeit for slightly different sequences). By exponentiating we get the following approximate relationship:

$$b^{\frac{S[x]}{k}} \approx \text{const}' \cdot \text{Lik}(T_x),$$

which is what we set out to show.

C Annex: Some illustrated outputs

To provide readers with a feeling of how similar the results of SHERPAS and jpHMM are, here we show an illustration of the outputs of SHERPAS-full (with default parameters) and jpHMM on the first 100 queries out of the 3000 in the HIV-genome dataset.

For each query, three bars show respectively: (top) the true composition of the query, with different strains represented by different colors; (mid) the output of SHERPAS-full, (bottom) the output of jpHMM. Black regions are those that are left unassigned (N/A) by the recombination detection tool. Each colored fragment is drawn to scale. Below the three bars, we also report the color coding for the strains present in at least one of the three bars.

It is helpful to look at these results together with those reported in Table 4 in the main text.

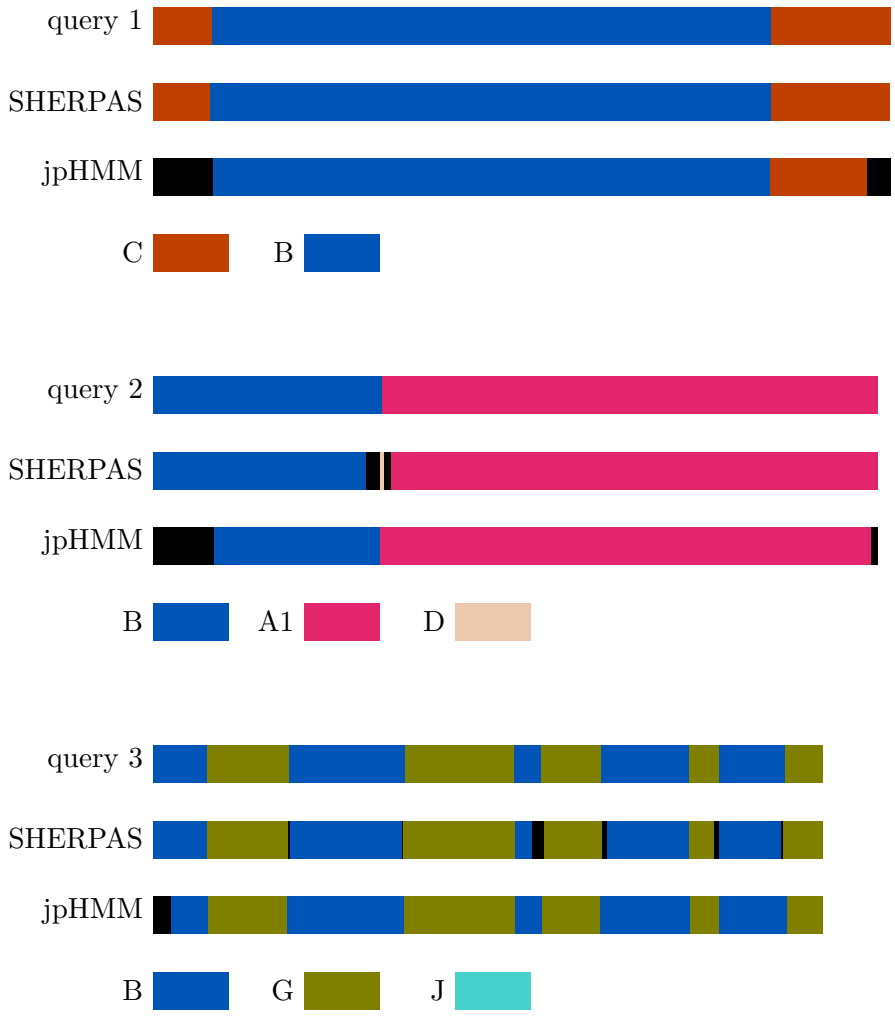

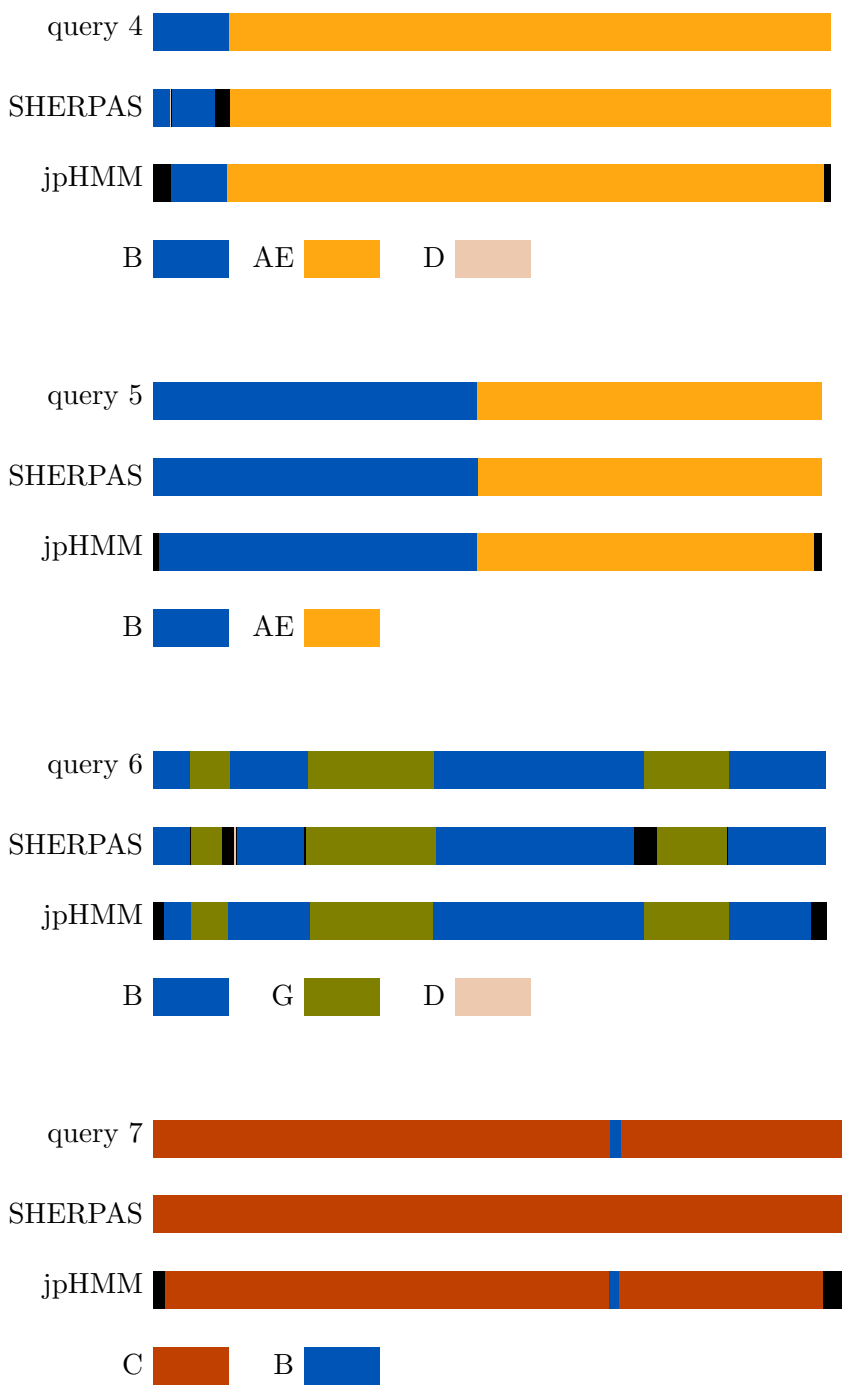
query 4
SHERPAS
jpHMM
B
AE
D
query 5
SHERPAS
jpHMM
B
AE
query 6
SHERPAS
jpHMM
B
G
D
query 7
SHERPAS
jpHMM
C
B

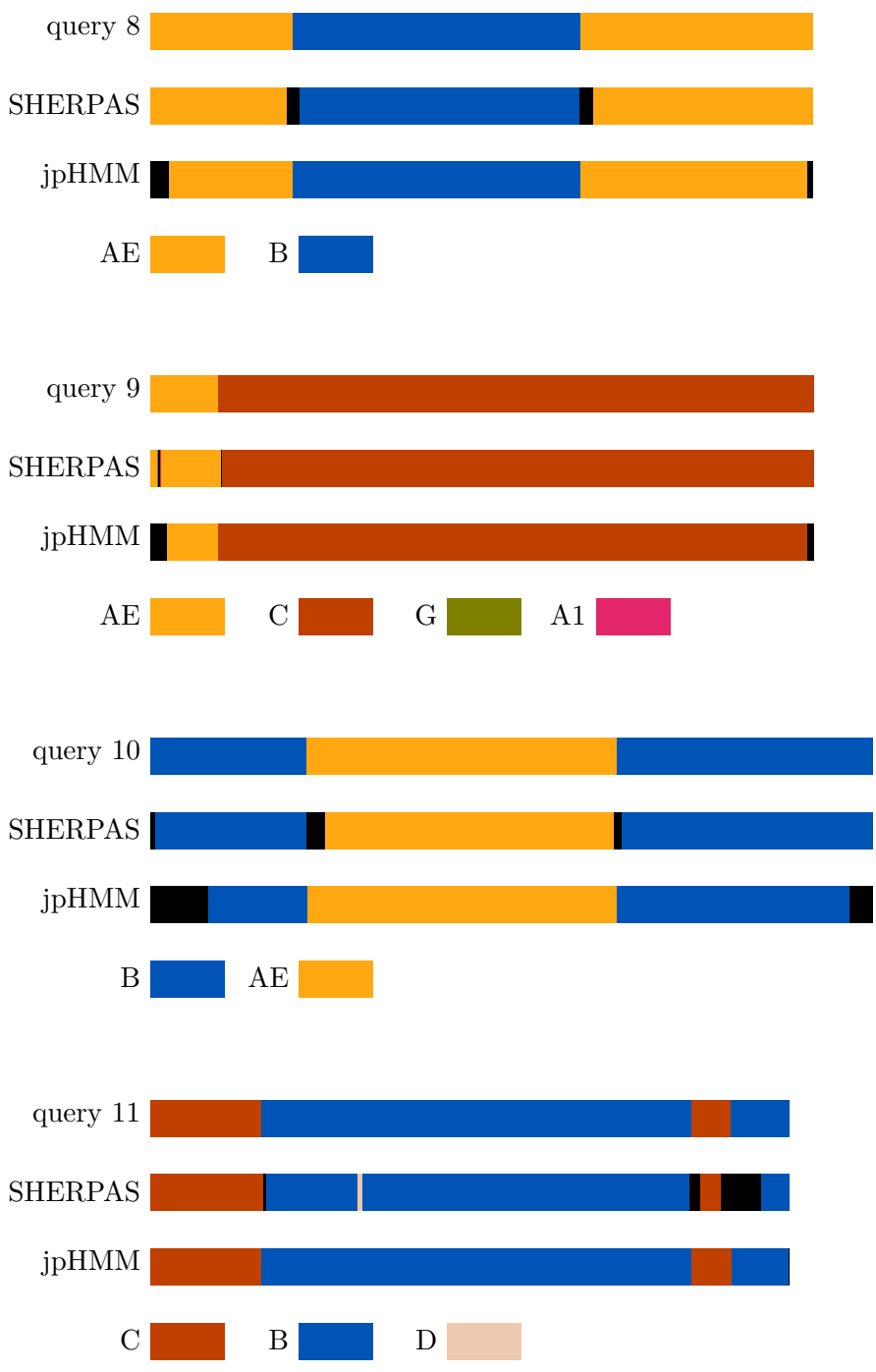
query 8
SHERPAS
jpHMM
AE
B
query 9
SHERPAS
jpHMM
AE
C
G
A1
query 10
SHERPAS
jpHMM
B
AE
query 11
SHERPAS
jpHMM
C
B
D

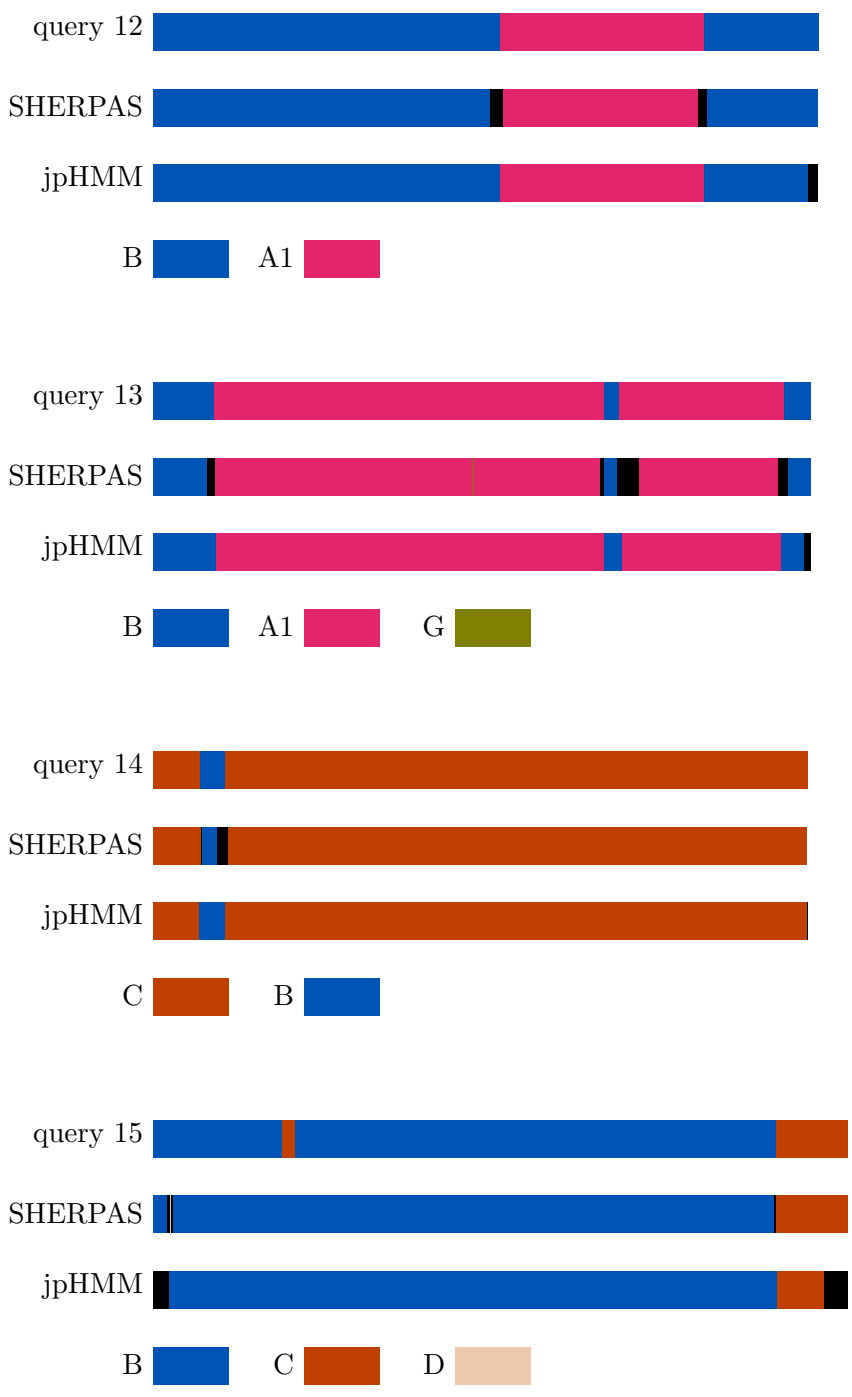
query 12
SHERPAS
jpHMM
B
A1
query 13
SHERPAS
jpHMM
B
A1
G
query 14
SHERPAS
jpHMM
C
B
query 15
SHERPAS
jpHMM
B
C
D

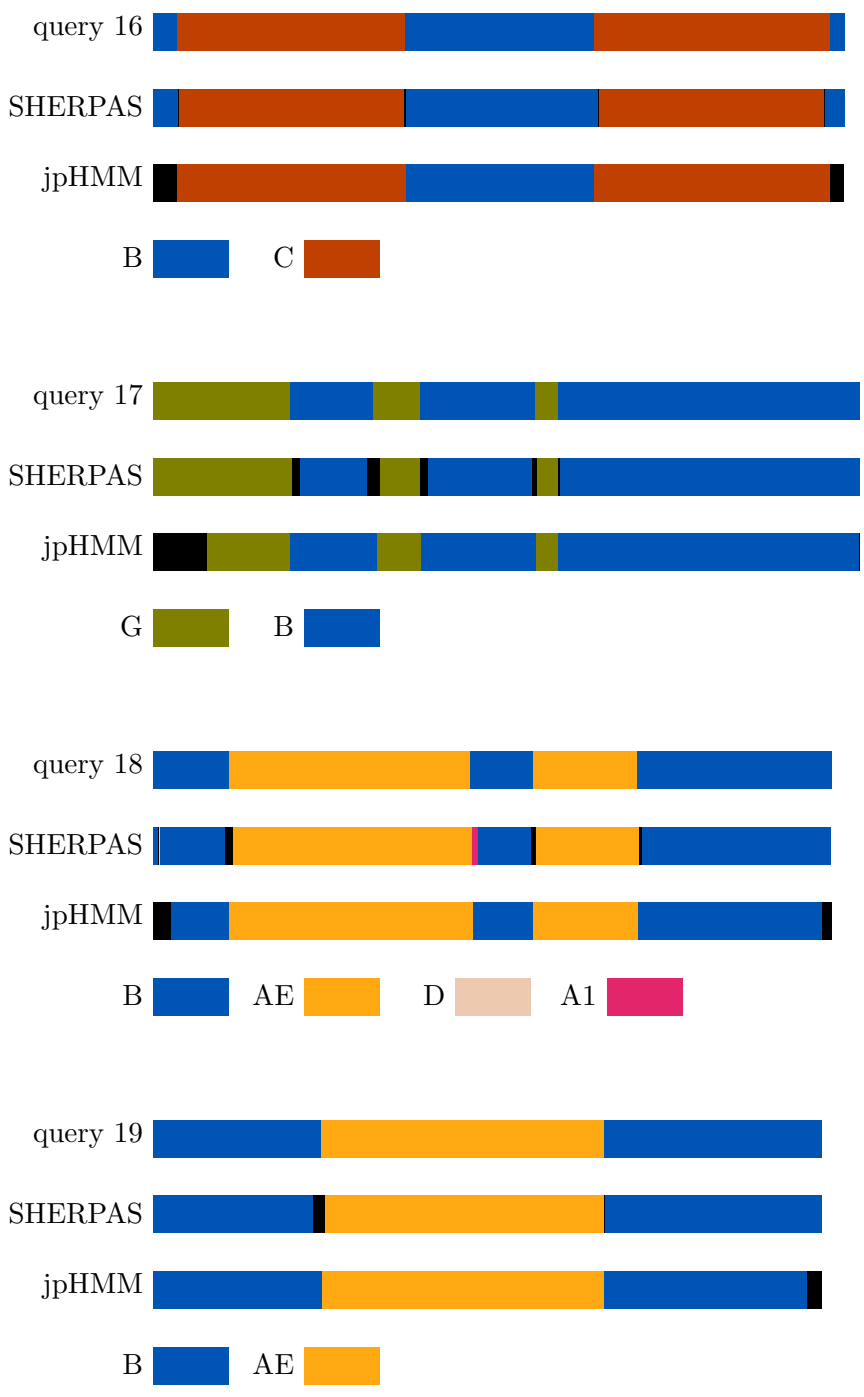
query 16
SHERPAS
jpHMM
B
C
query 17
SHERPAS
jpHMM
G
B
query 18
SHERPAS
jpHMM
B
AE
D
A1
query 19
SHERPAS
jpHMM
B
AE

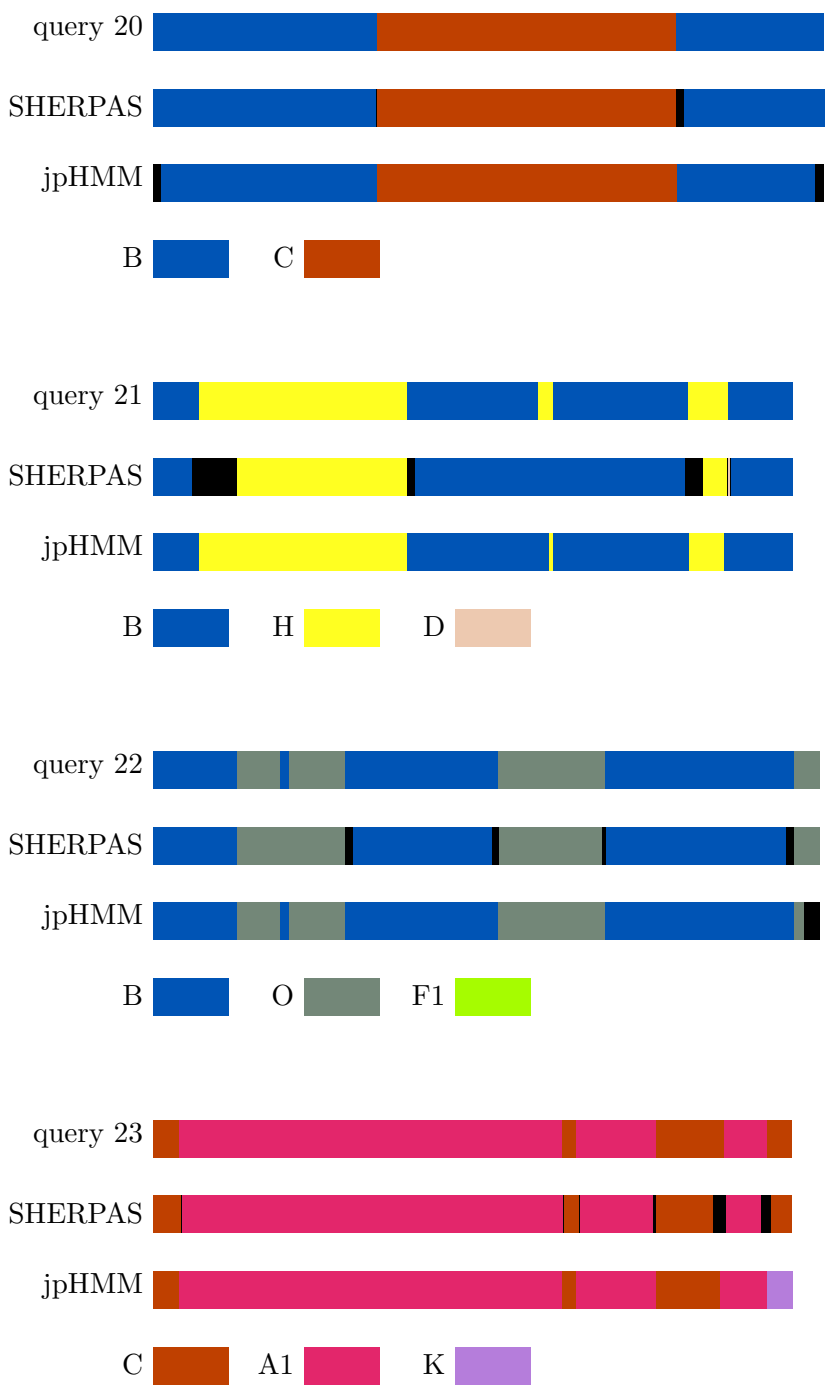
query 20
SHERPAS
jpHMM
B
C
query 21
SHERPAS
jpHMM
B
H
D
query 22
SHERPAS
jpHMM
B
O
F1
query 23
SHERPAS
jpHMM
C
A1
K

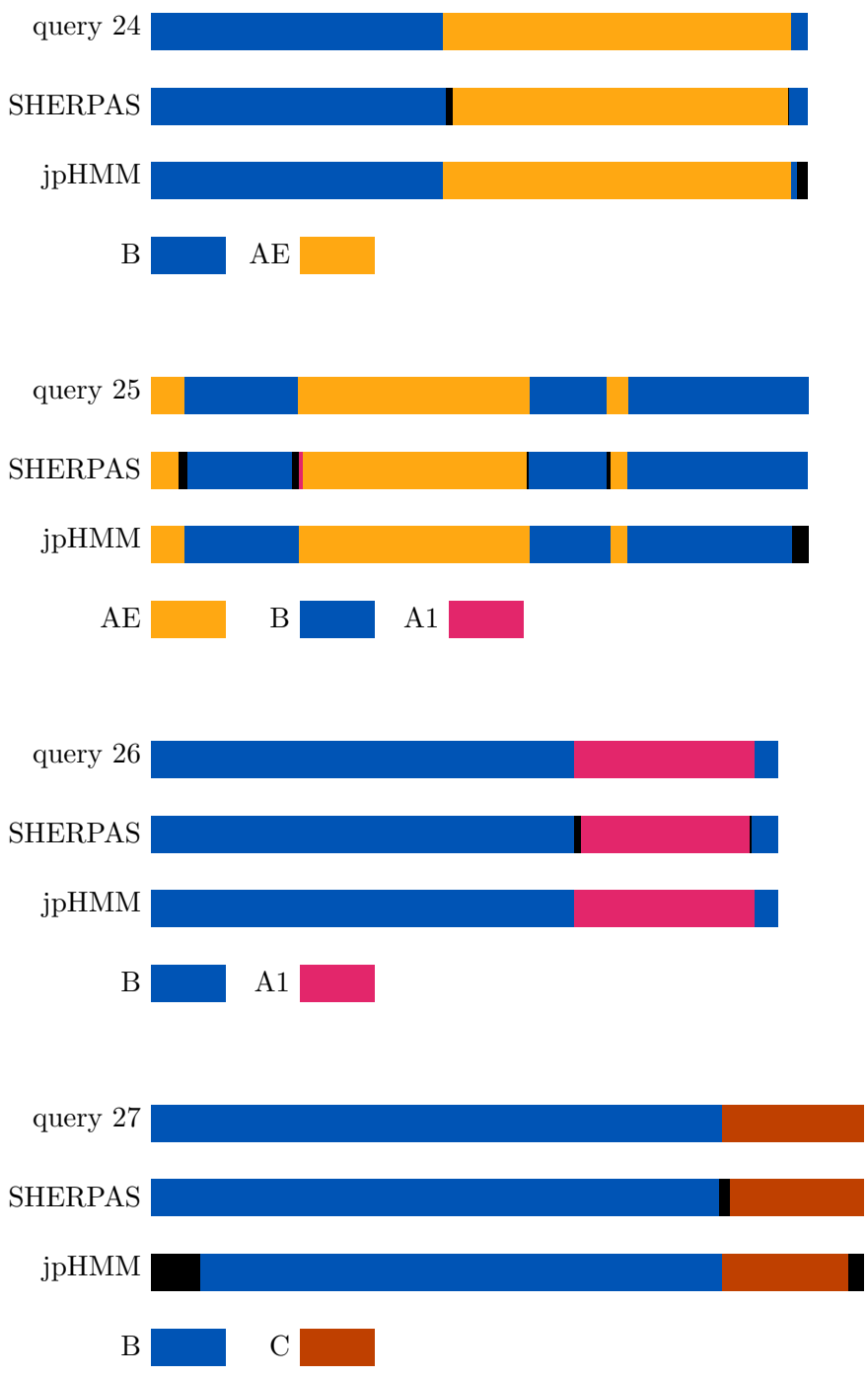
query 24
SHERPAS
jpHMM
B
AE
query 25
SHERPAS
jpHMM
AE
B
A1
query 26
SHERPAS
jpHMM
B
A1
query 27
SHERPAS
jpHMM
B
C

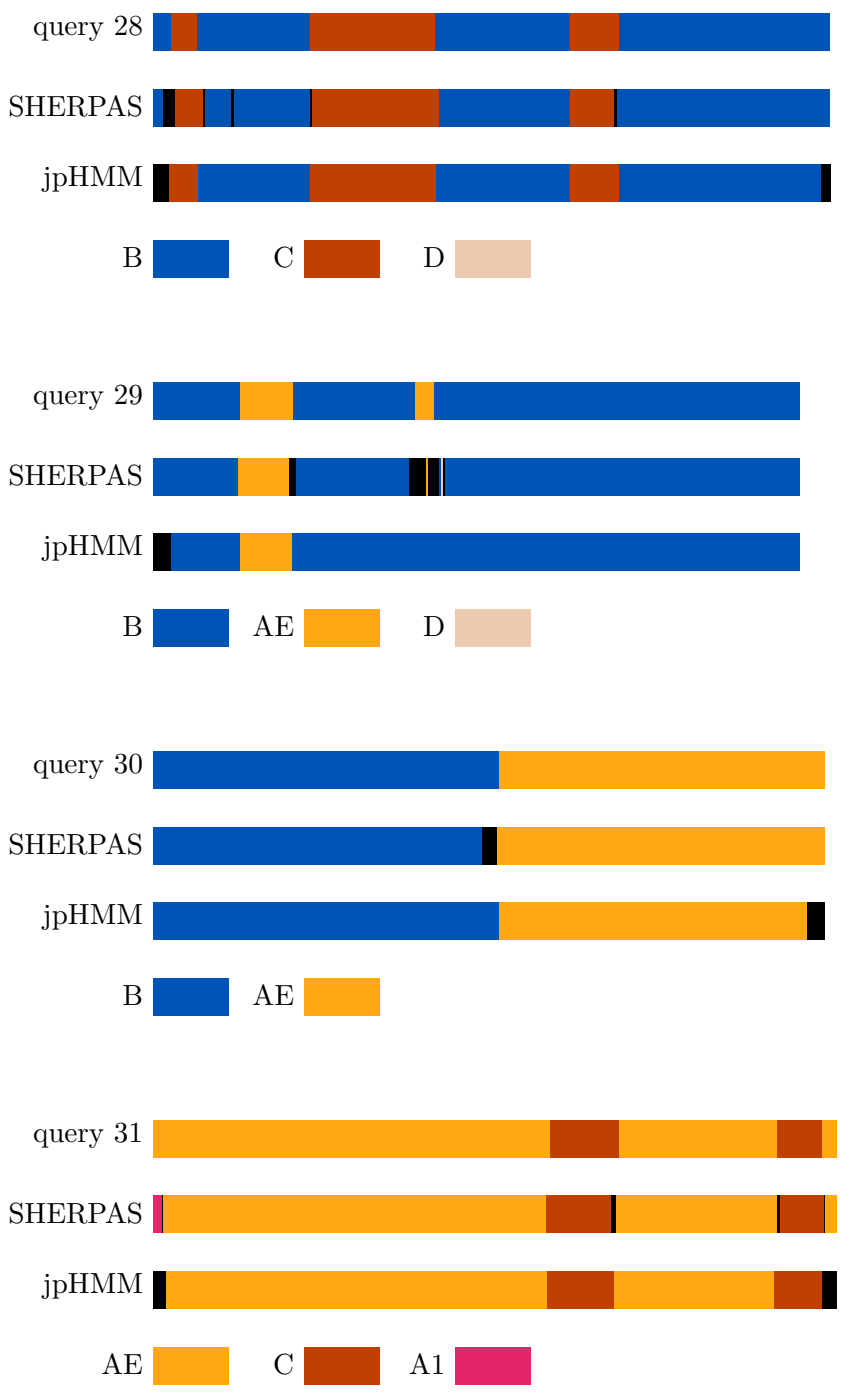
query 28
SHERPAS
jpHMM
B
C
D
query 29
SHERPAS
jpHMM
B
AE
D
query 30
SHERPAS
jpHMM
B
AE
query 31
SHERPAS
jpHMM
AE
C
A1

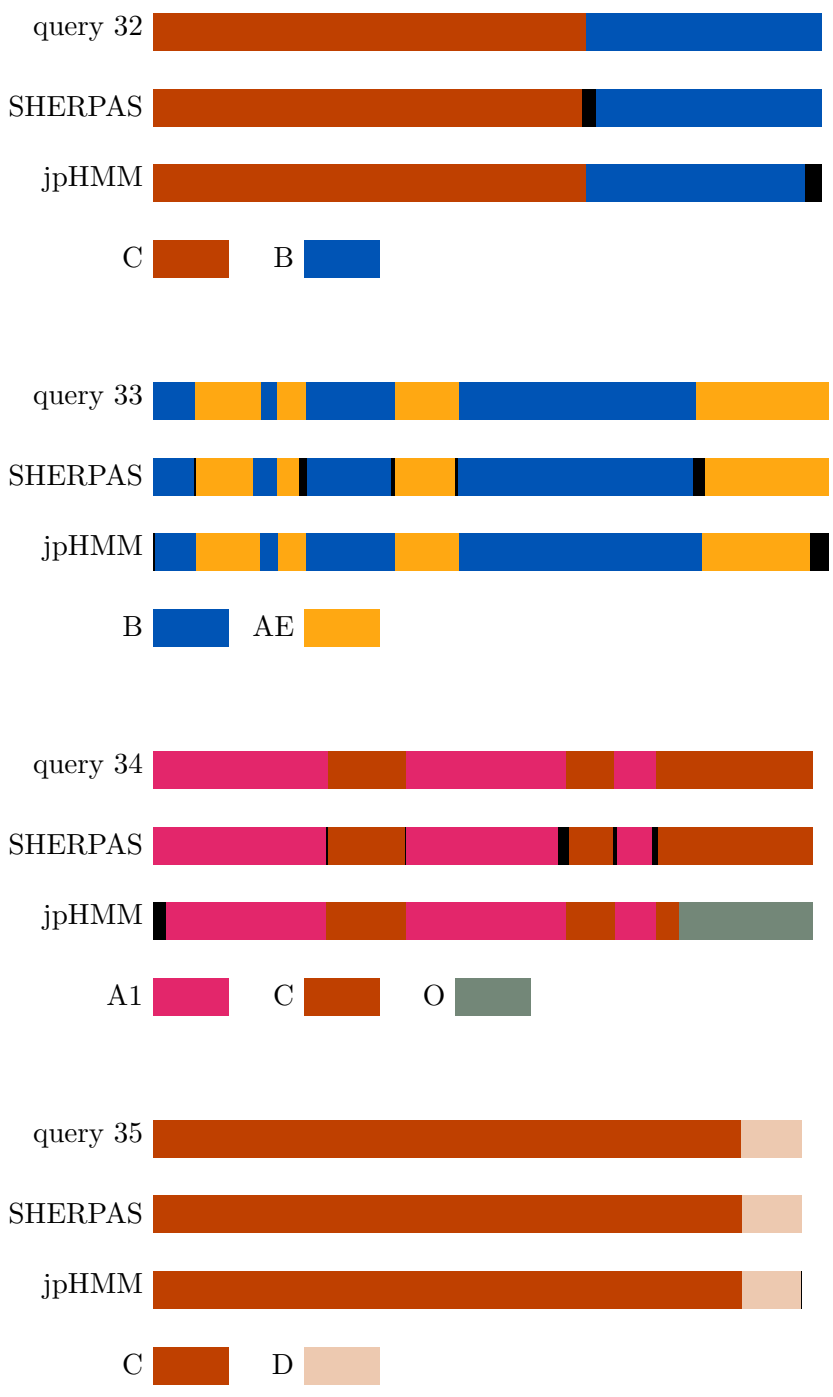
query 32
SHERPAS
jpHMM
C
B
query 33
SHERPAS
jpHMM
B
AE
query 34
SHERPAS
jpHMM
A1
C
O
query 35
SHERPAS
jpHMM
C
D

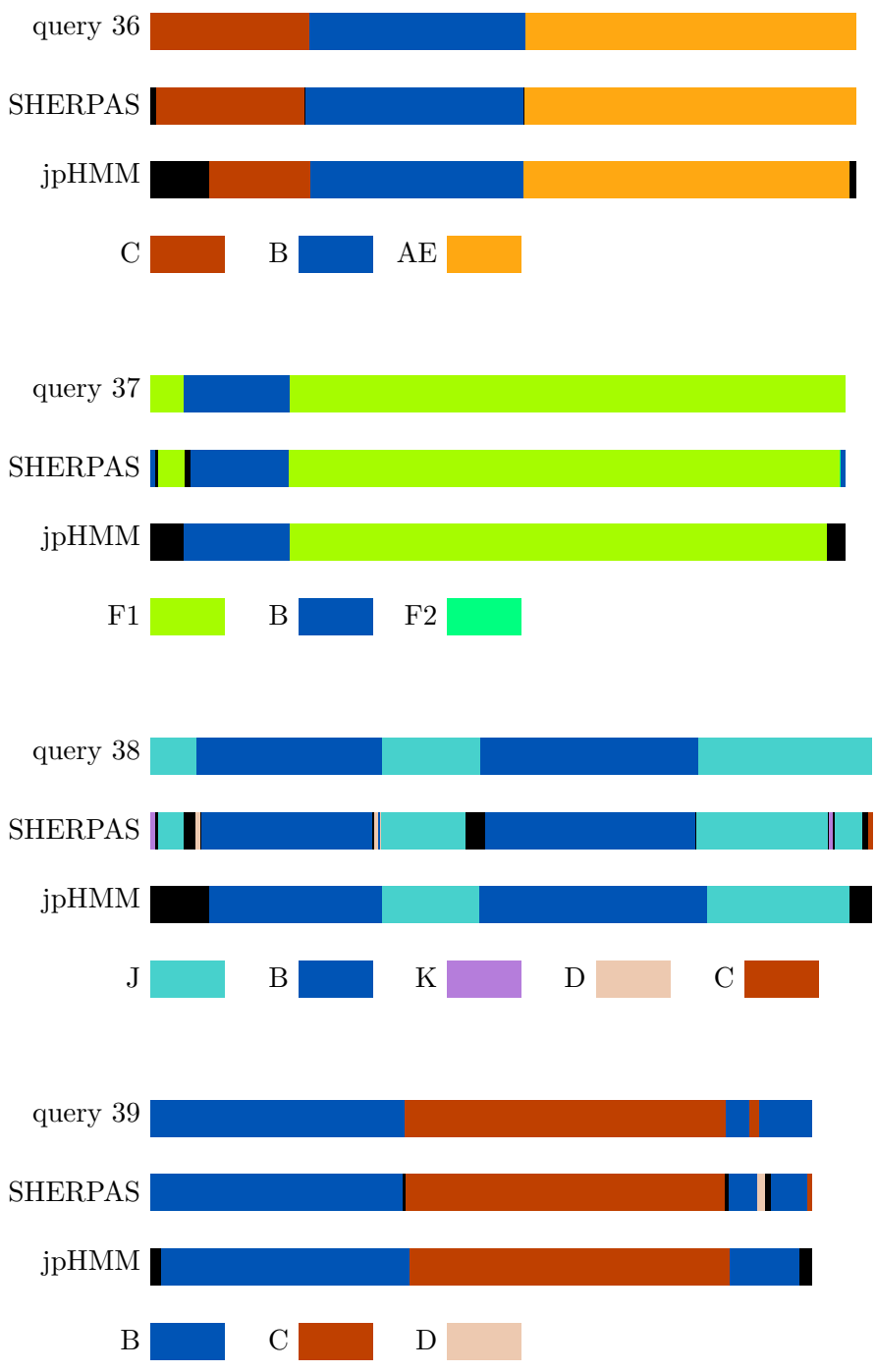
query 36
SHERPAS
jpHMM
C
B
AE
query 37
SHERPAS
jpHMM
F1
B
F2
query 38
SHERPAS
jpHMM
J
B
K
D
C
query 39
SHERPAS
jpHMM
B
C
D

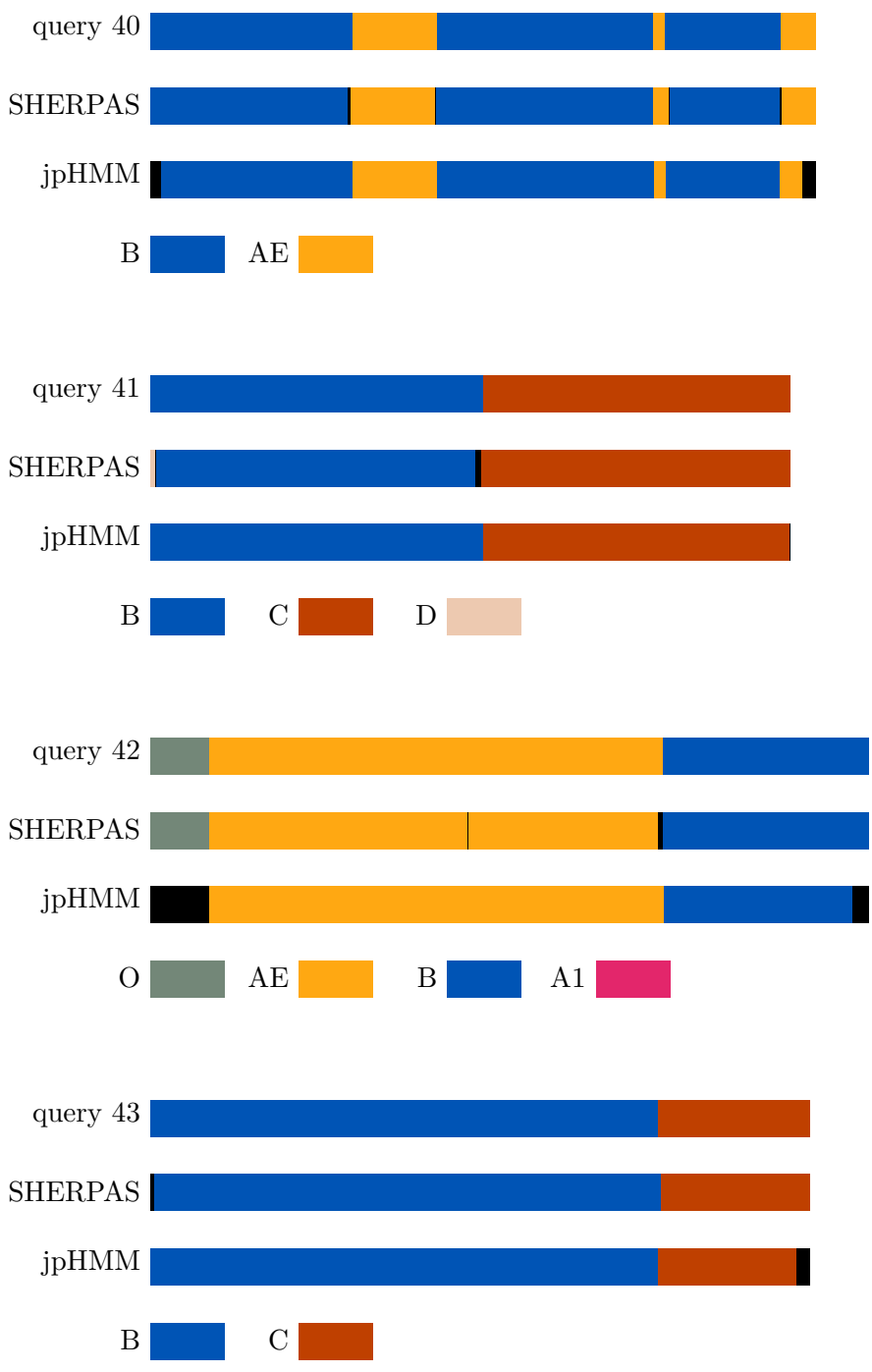
query 40
SHERPAS
jpHMM
B
AE
query 41
SHERPAS
jpHMM
B
C
D
query 42
SHERPAS
jpHMM
O
AE
B
A1
query 43
SHERPAS
jpHMM
B
C

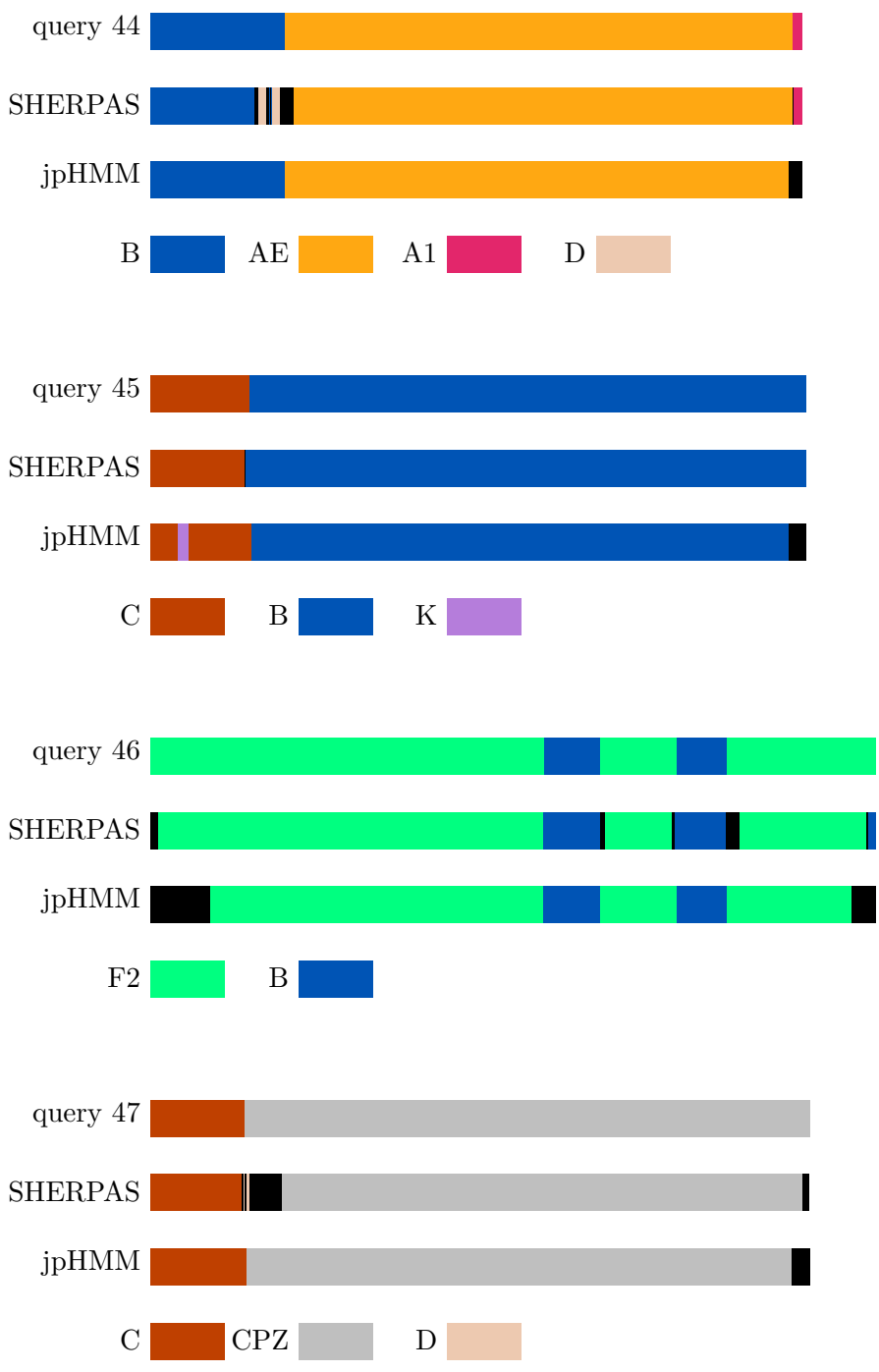
query 44
SHERPAS
jpHMM
B
AE
A1
D
query 45
SHERPAS
jpHMM
C
B
K
query 46
SHERPAS
jpHMM
F2
B
query 47
SHERPAS
jpHMM
C
CPZ
D

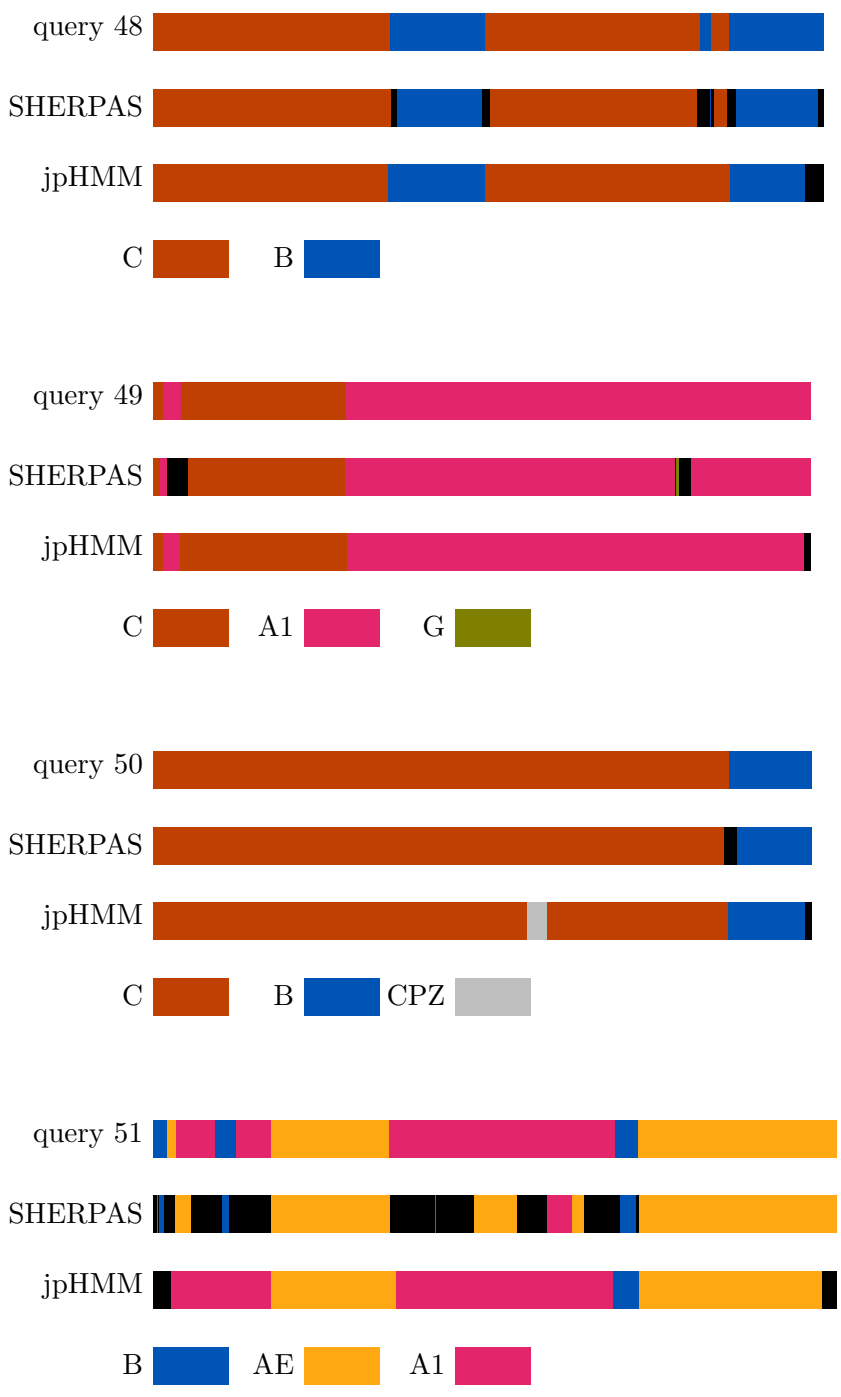
query 48
SHERPAS
jpHMM
C
B
query 49
SHERPAS
jpHMM
C
A1
G
query 50
SHERPAS
jpHMM
C
B
CPZ
query 51
SHERPAS
jpHMM
B
AE
A1

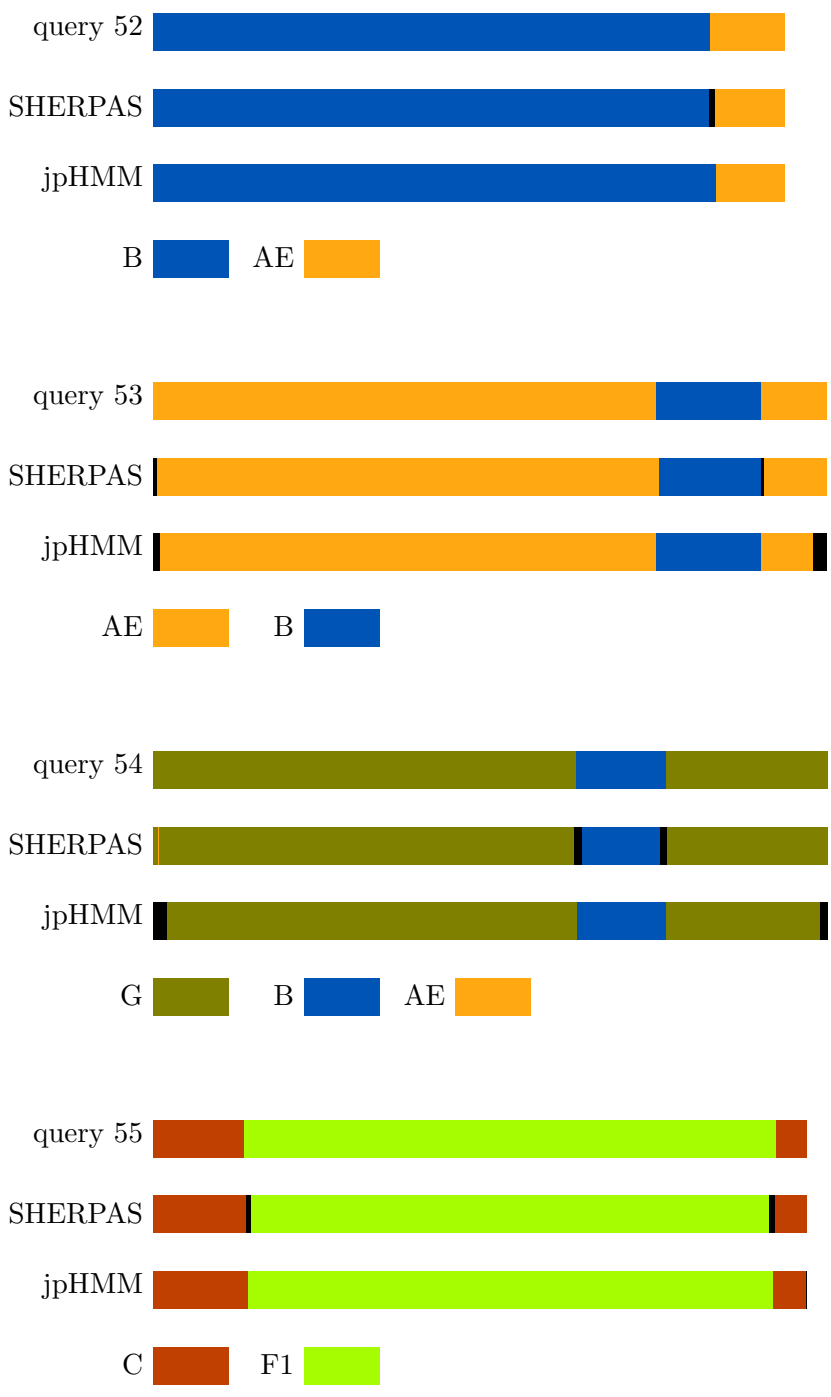
query 52
SHERPAS
jpHMM
B
AE
query 53
SHERPAS
jpHMM
AE
B
query 54
SHERPAS
jpHMM
G
B
AE
query 55
SHERPAS
jpHMM
C
F1

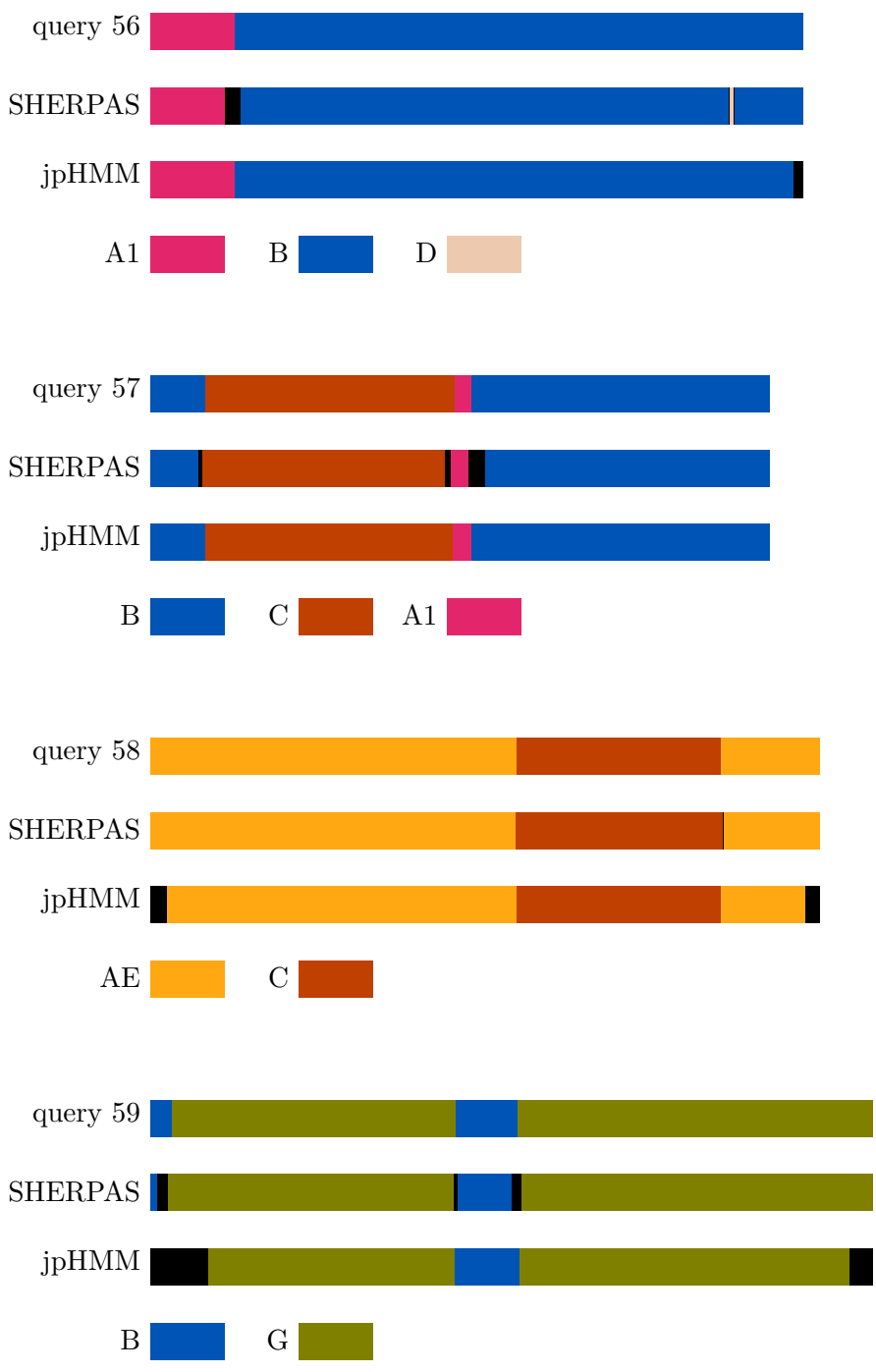
query 56
SHERPAS
jpHMM
A1
B
D
query 57
SHERPAS
jpHMM
B
C
A1
query 58
SHERPAS
jpHMM
AE
C
query 59
SHERPAS
jpHMM
B
G

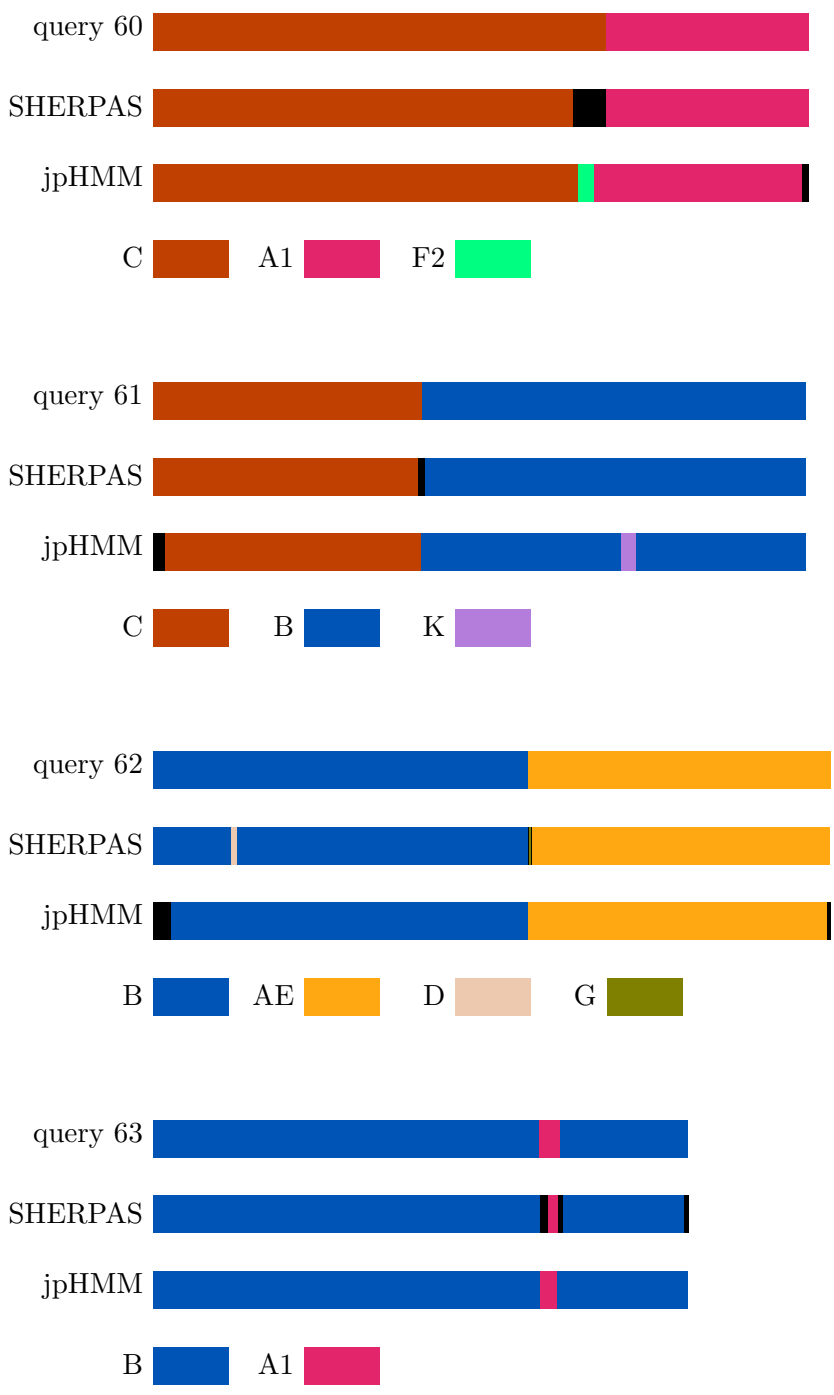
query 60
SHERPAS
jpHMM
C
A1
F2
query 61
SHERPAS
jpHMM
C
B
K
query 62
SHERPAS
jpHMM
B
AE
D
G
query 63
SHERPAS
jpHMM
B
A1

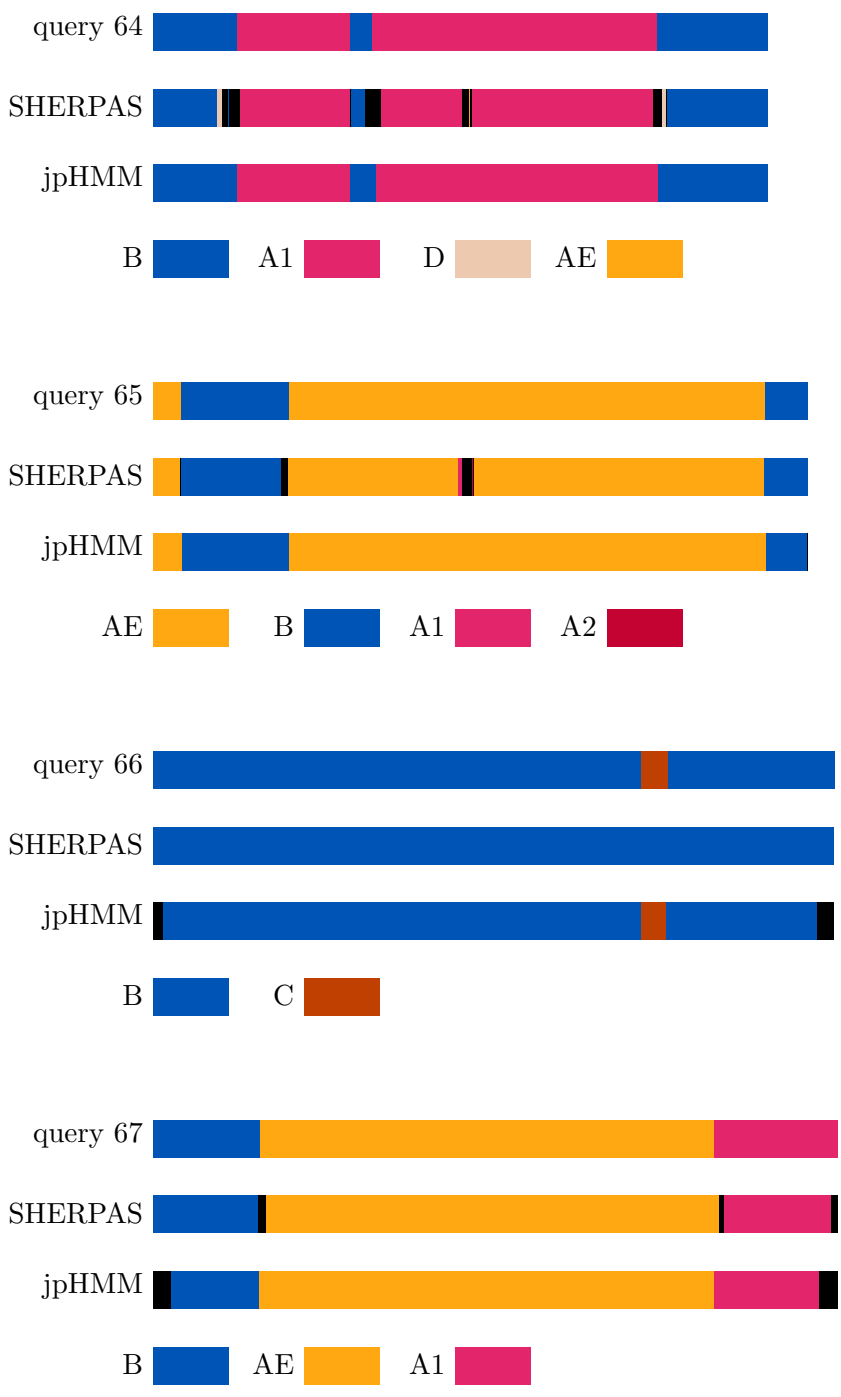
query 64
SHERPAS
jpHMM
B
A1
D
AE
query 65
SHERPAS
jpHMM
AE
B
A1
A2
query 66
SHERPAS
jpHMM
B
C
query 67
SHERPAS
jpHMM
B
AE
A1

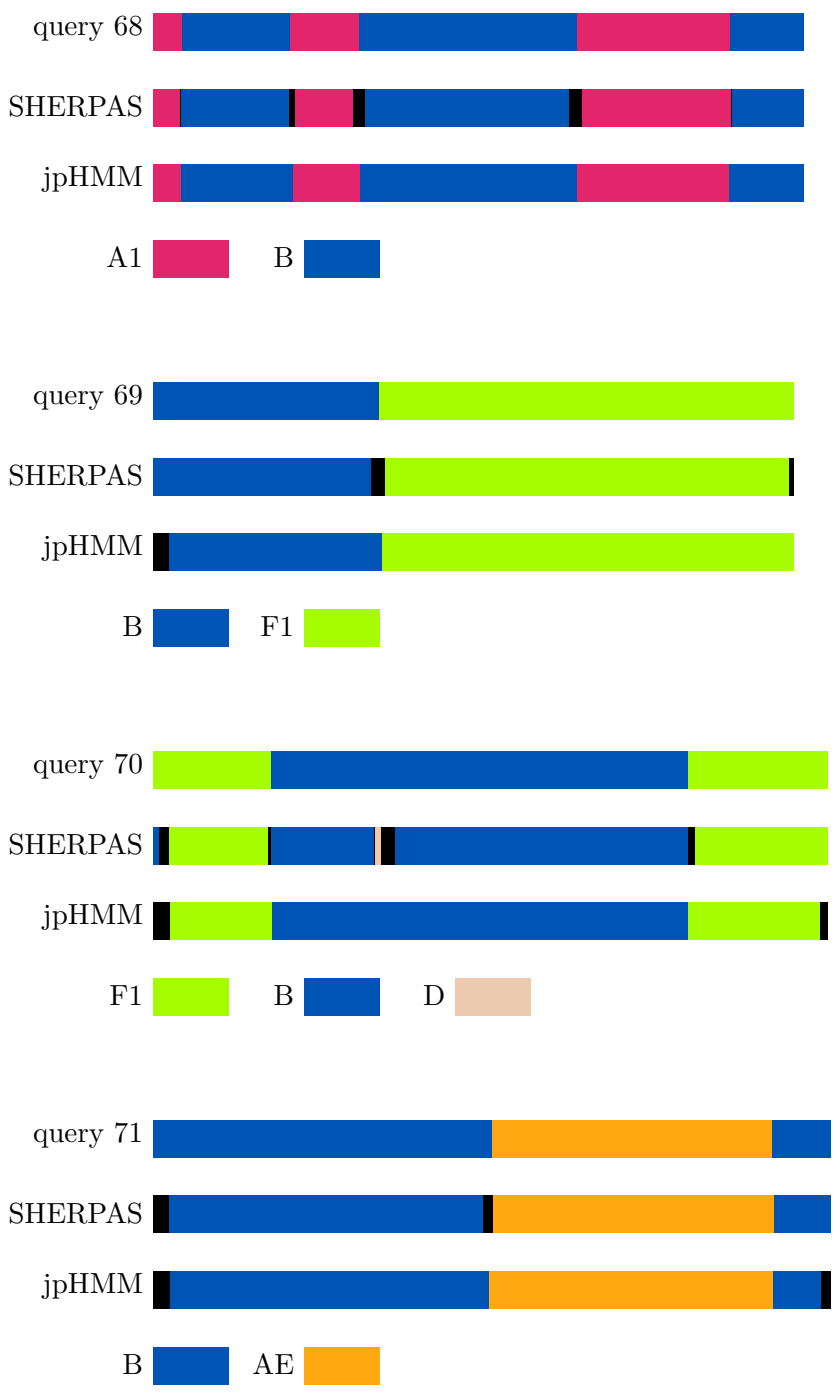
query 68
SHERPAS
jpHMM
A1
B
query 69
SHERPAS
jpHMM
B
F1
query 70
SHERPAS
jpHMM
F1
B
D
query 71
SHERPAS
jpHMM
B
AE

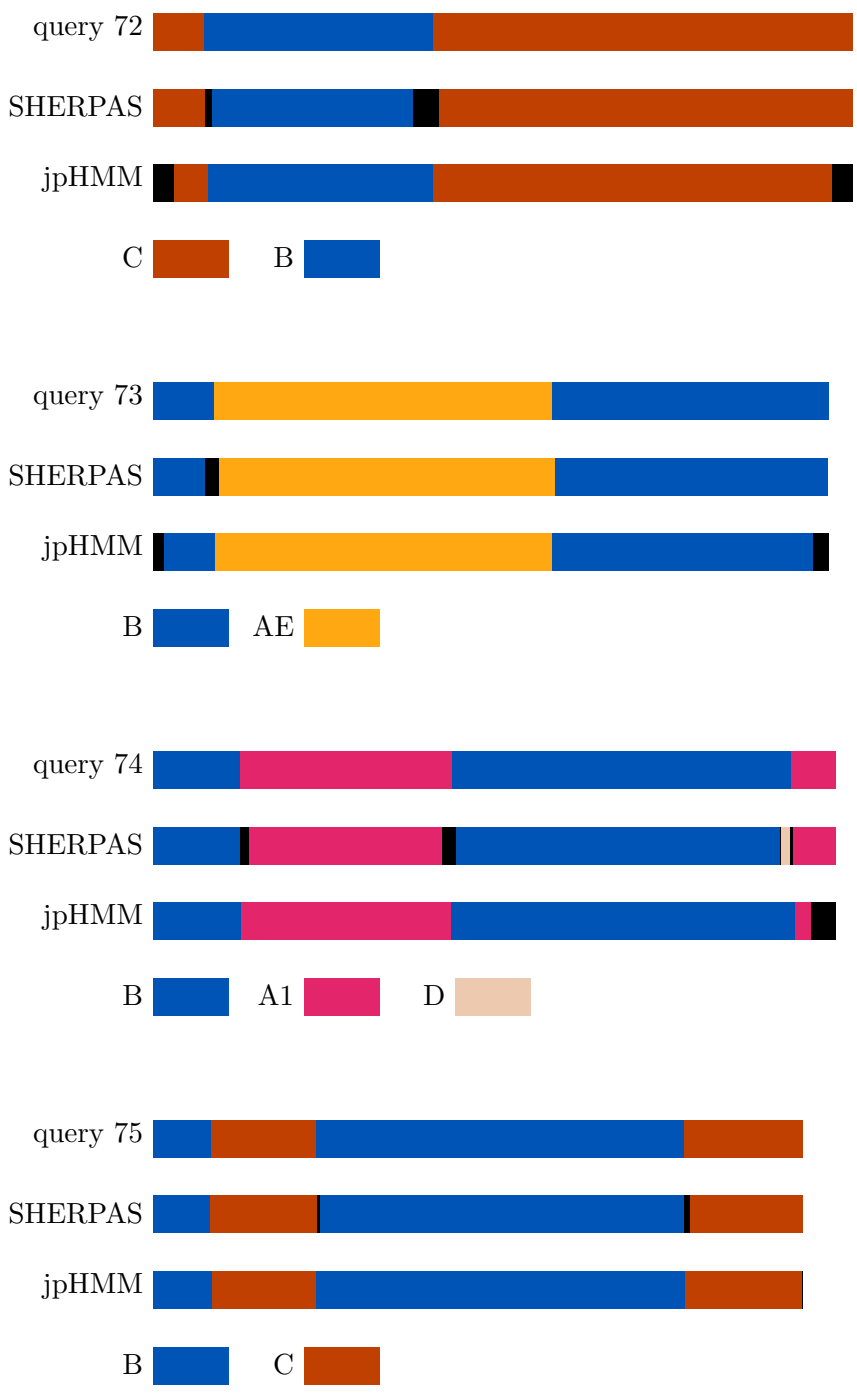
query 72
SHERPAS
jpHMM
C
B
query 73
SHERPAS
jpHMM
B
AE
query 74
SHERPAS
jpHMM
B
A1
D
query 75
SHERPAS
jpHMM
B
C

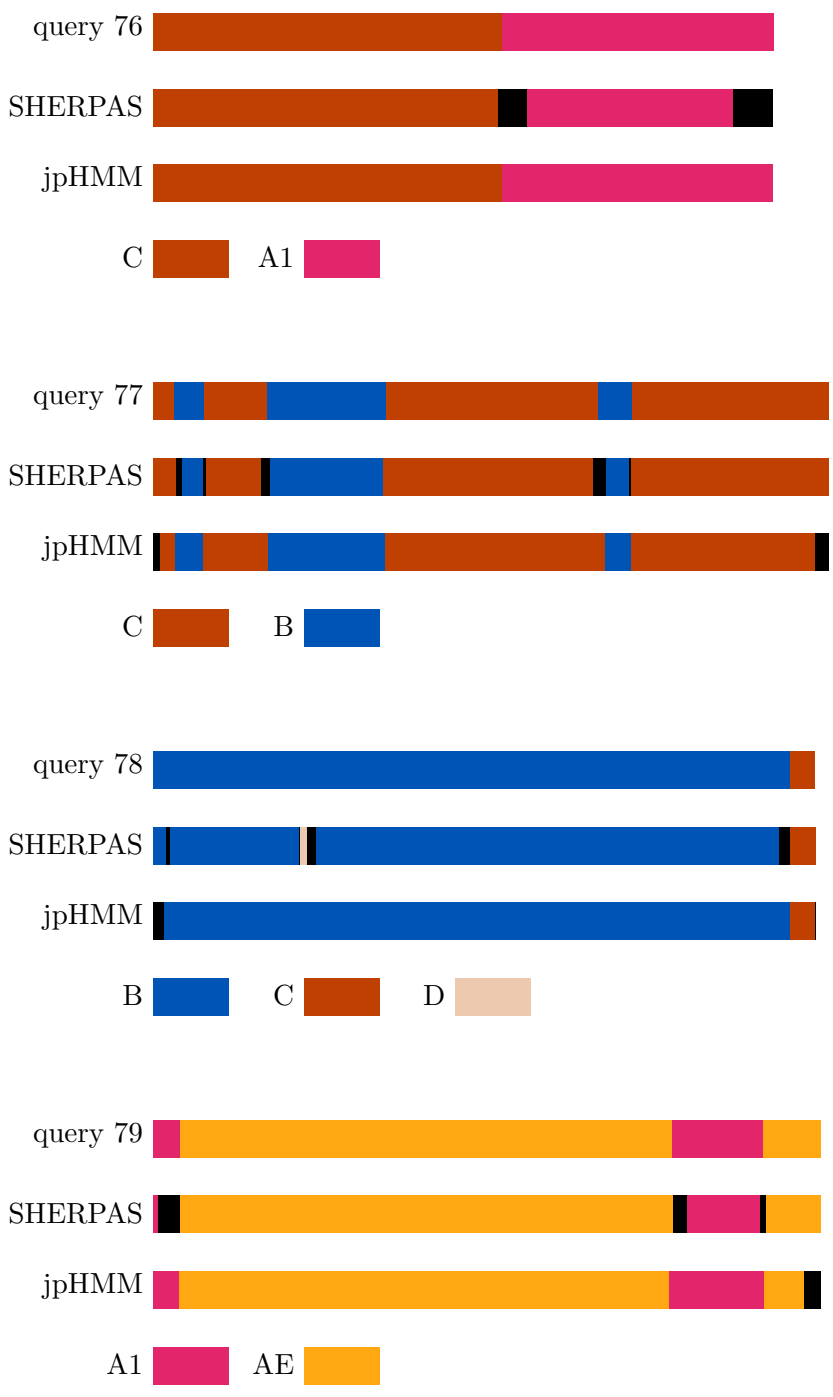
query 76
SHERPAS
jpHMM
C
A1
query 77
SHERPAS
jpHMM
C
B
query 78
SHERPAS
jpHMM
B
C
D
query 79
SHERPAS
jpHMM
A1
AE

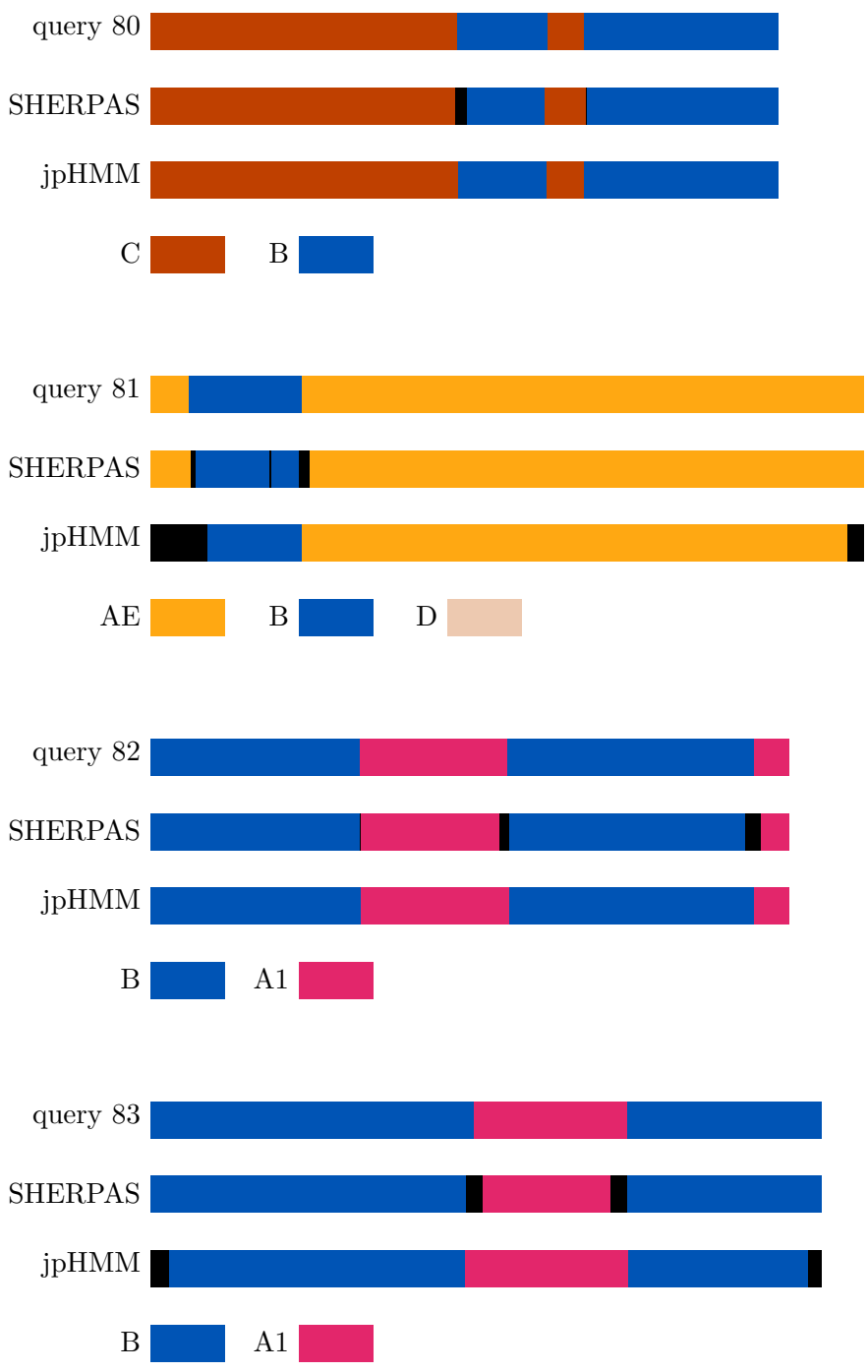
query 80
SHERPAS
jpHMM
C
B
query 81
SHERPAS
jpHMM
AE
B
D
query 82
SHERPAS
jpHMM
B
A1
query 83
SHERPAS
jpHMM
B
A1

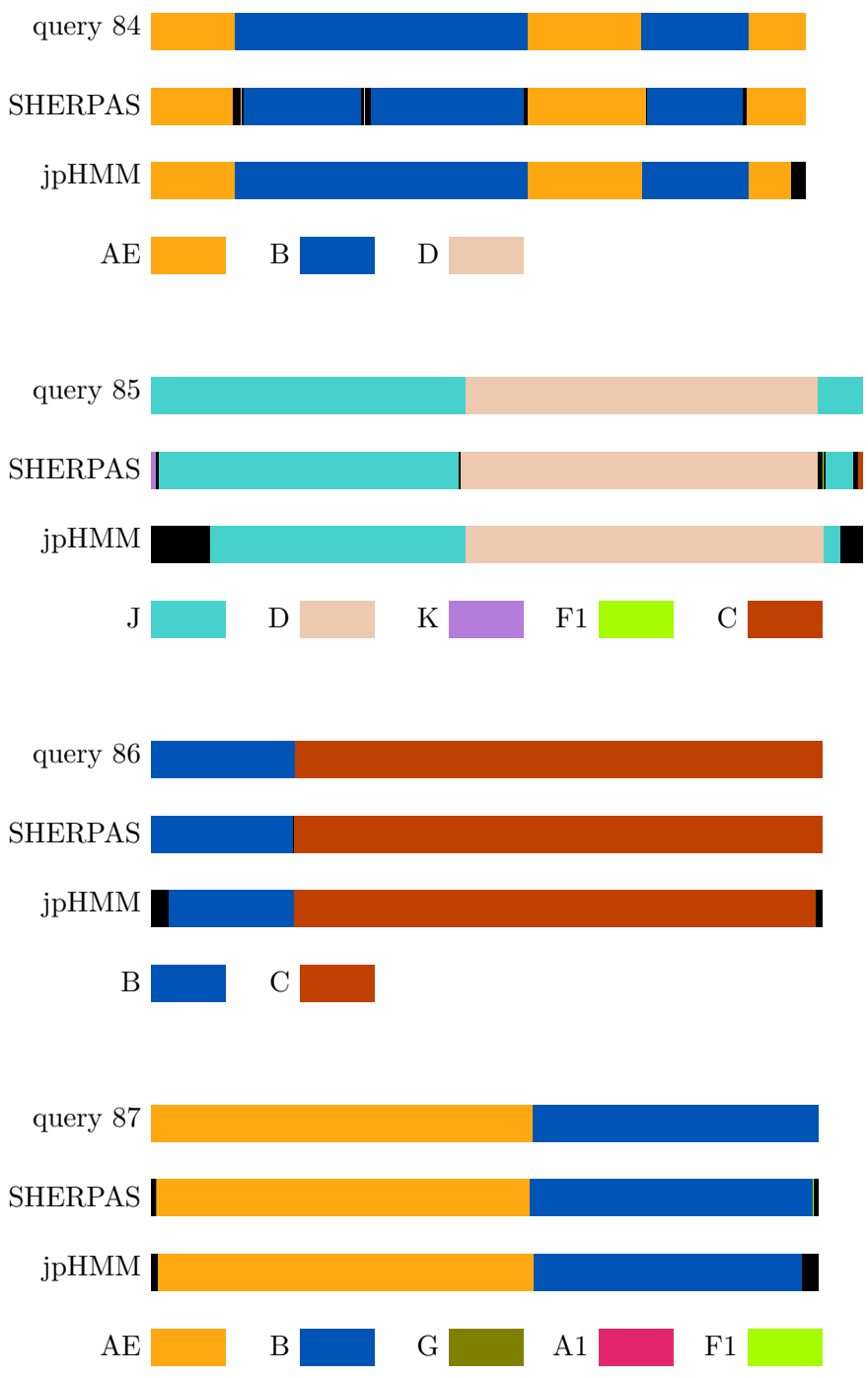
query 84
SHERPAS
jpHMM
AE
B
D
query 85
SHERPAS
jpHMM
J
D
K
F1
C
query 86
SHERPAS
jpHMM
B
C
query 87
SHERPAS
jpHMM
AE
B
G
A1
F1

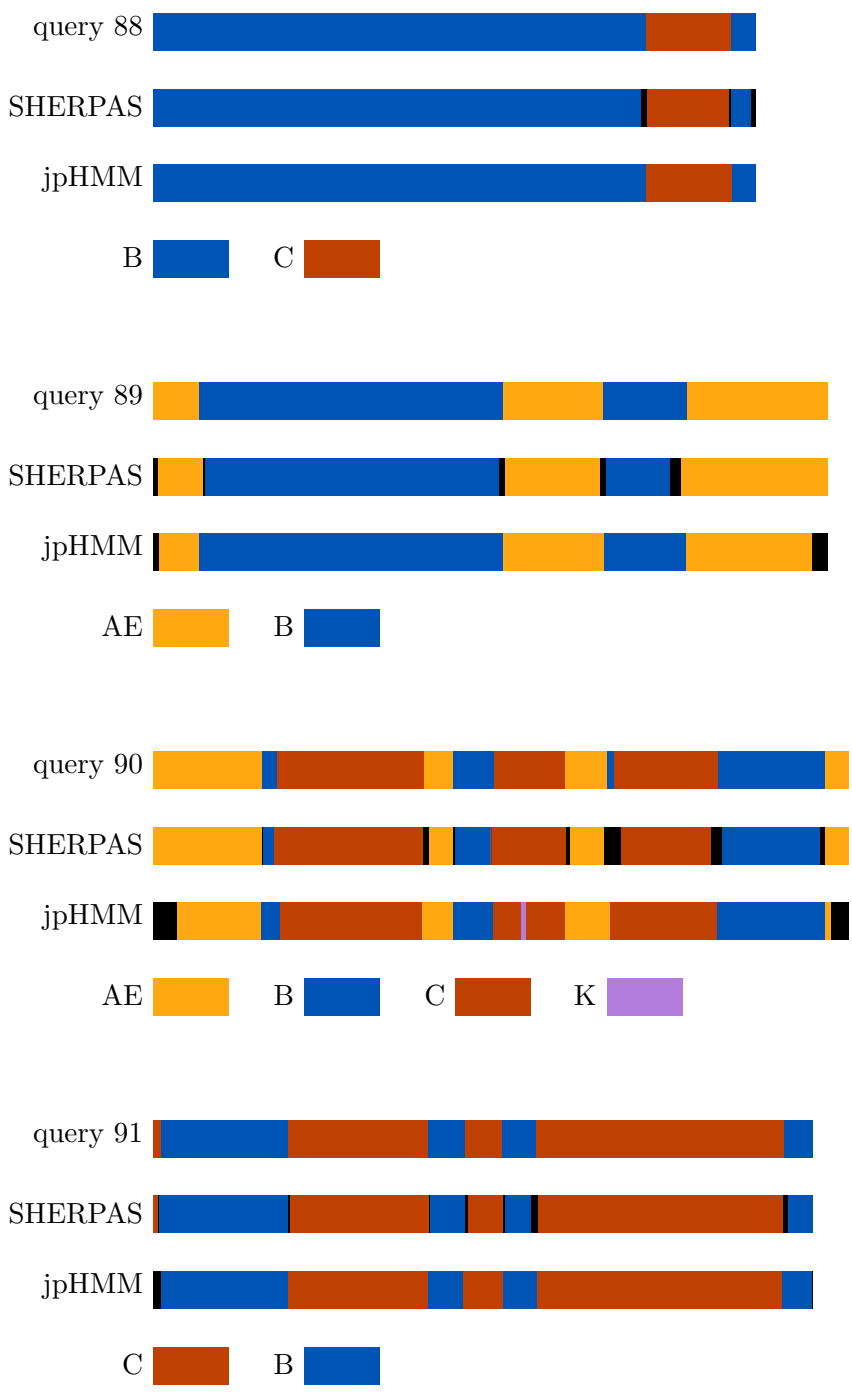
query 88
SHERPAS
jpHMM
B
C
query 89
SHERPAS
jpHMM
AE
B
query 90
SHERPAS
jpHMM
AE
B
C
K
query 91
SHERPAS
jpHMM
C
B

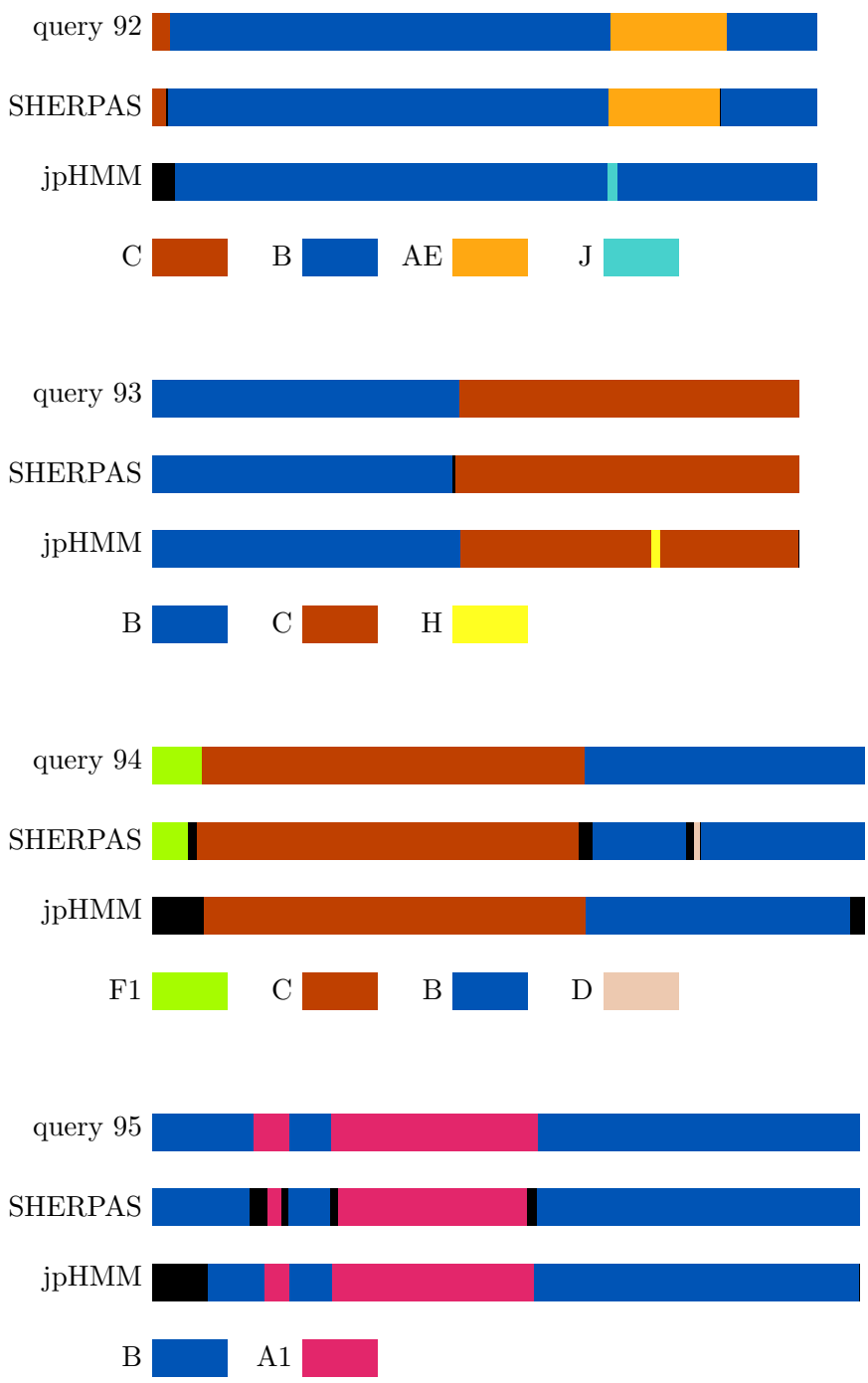
query 92
SHERPAS
jpHMM
C
B
AE
J
query 93
SHERPAS
jpHMM
B
C
H
query 94
SHERPAS
jpHMM
F1
C
B
D
query 95
SHERPAS
jpHMM
B
A1

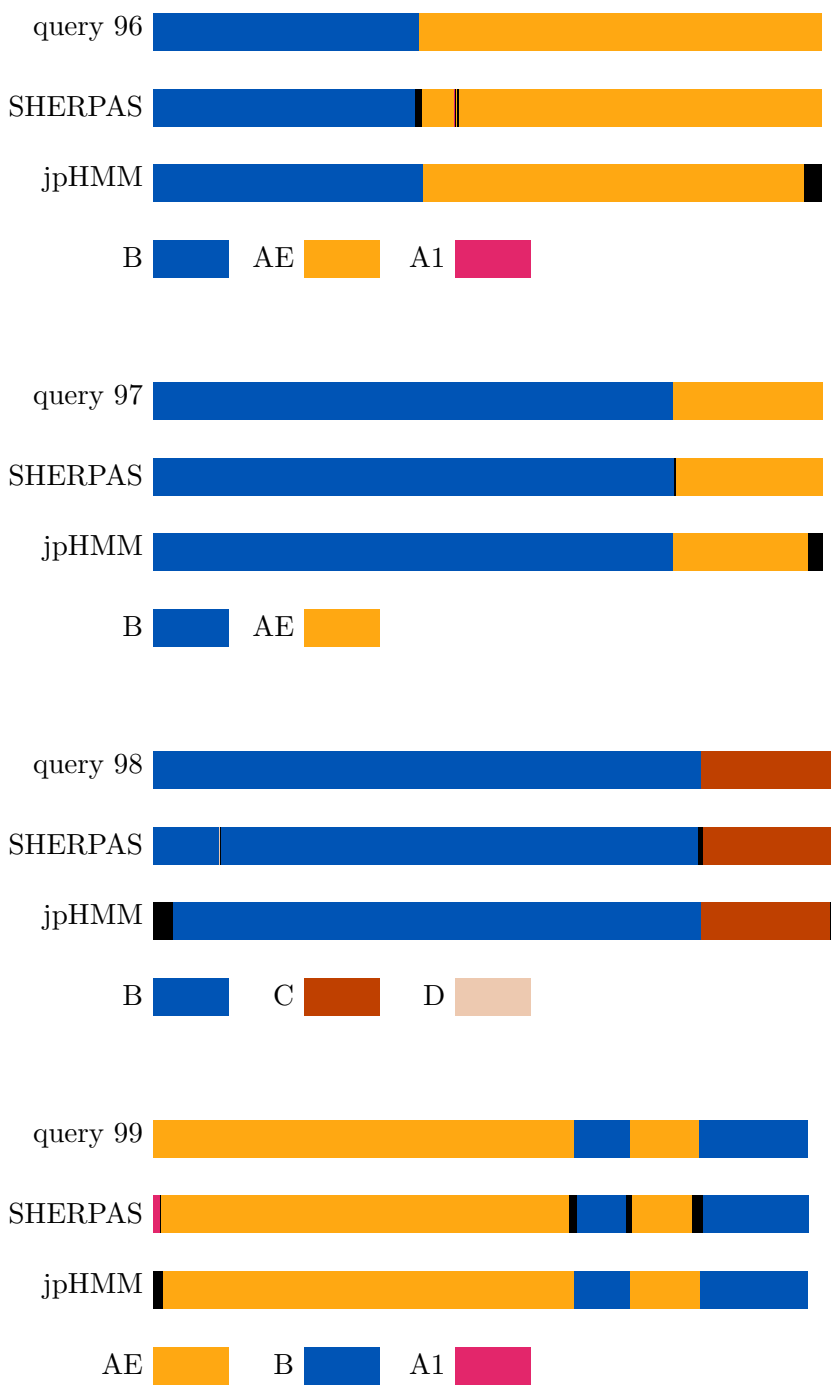
query 96
SHERPAS
jpHMM
B
AE
A1
query 97
SHERPAS
jpHMM
B
AE
query 98
SHERPAS
jpHMM
B
C
D
query 99
SHERPAS
jpHMM
AE
B
A1

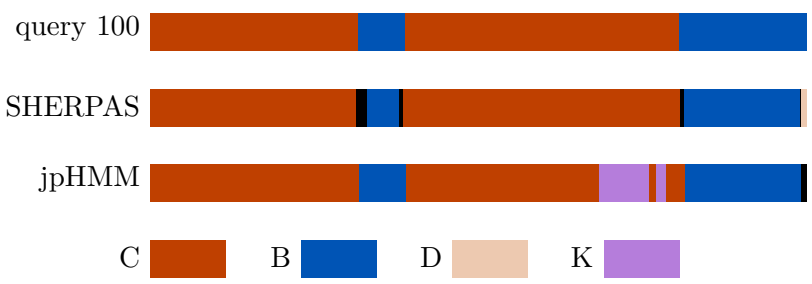
query 100
SHERPAS
jpHMM
C
B
D
K